Schweizerische Eidgenossenschaft
Confédération suisse
Confederazione Svizzera
Confederaziun svizra

Eidgenössisches Departement für
Umwelt, Verkehr, Energie und Kommunikation UVEK

Bundesamt für Energie BFE

Final Report 22.07.2015

High-Ice

System development for high solar thermal gains with ice storage and heat pump

Autoren:

Daniel Philippen, daniel.philippen@spf.ch
Daniel Carbonell, dani.carbonell@spf.ch
Daniel Zenhäusern, daniel.zenhäusern@spf.ch
Martin Granzotto, martin.granzotto@spf.ch
Michel Haller, michel.haller@spf.ch
Stefan Brunold, stefan.brunold@spf.ch
With contributions from Sebastian Sommer, Harini Murali, Philipp Egger, and Arian Causi

Zusammenfassung

Im Rahmen des High-Ice Projektes wurde ein Heizungskonzept untersucht, welches aus Solarkollektoren, einer Wärmepumpe und einem Eisspeicher mit enteisbaren Wärmeübertragern als Hauptkomponenten besteht. Der Einfluss der Komponentengrössen von Eisspeicher und Kollektorfeld auf den Elektrizitätsverbrauch der Heizung wurde mit Simulationen in TRNSYS analysiert. Konzipiert wurde das Heizsystem für den Einsatz in bestehenden Wohngebäuden mit geringer Wärmedämmung. In den Simulationen wurden 2 Einfamilienhäuser mit Energiekennzahlen am Standort Zürich von 60 und 125 kWh/(m^2 a) verwendet. Die Studie hatte zum Ziel, das Heizungskonzept auch unter ökologischen und ökonomischen Gesichtspunkten zu bewerten. Die Ökobilanzen haben gezeigt, dass minimale Umweltwirkungen für die Wärmebereitstellung mit relativ grossen Systemkomponenten erreicht werden. Solange der Einsatz der elektrischen Notheizung verringert werden kann, lohnt es sich gemäss Ökobilanz, ein System grösser zu dimensionieren. Die Wärmegestehungskosten wiederum sind bei gross ausgelegten Heizungen gemäss dem vorgeschlagenen Systemkonzept höher als diejenigen von konventionellen Heizsystemen. Ein weiterer Teil des Projekts war die Entwicklung eines elastischen Wärmeübertragers aus EPDM-Gummi, der durch Aufblasen mechanisch enteist werden kann.

Résumé

Le but du projet High-Ice a été d'étudier un concept spécifique alliant solaire thermique, pompe à chaleur et stockage thermique à glace (solar-ice system). Pour le stockage à glace, une conception avec des échangeurs de chaleur dégivrables a été étudiée. Le lien entre la consommation électrique du système et le dimensionnement des composants principaux (champ de capteurs et stockage) a été analysé au moyen de simulations (logiciel TRNSYS). Le design du système a été mené sur la base de bâtiments existants disposant d'une relativement faible isolation thermique. Deux types de maisons individuelles avec des besoins en chauffage de 60 et 125 kWh/(m^2.a) ont été considérés. L'analyse du concept d'un point de vue environnemental et économique a également constitué un aspect important de cette étude. Une analyse du cycle de vie a montré que pour le chauffage, le plus faible impact écologique est atteint, pour les indicateurs considérés, avec des composants de grande taille. En effet, il a été démontré que l'augmentation de la taille des composants est bénéfique tant qu'elle permet une diminution de l'utilisation de l'appoint électrique. Cependant, l'analyse économique a révélé que les couts de production de chaleur utilisant le système proposé sont supérieurs aux couts engendrés par des dispositifs conventionnel, et ce plus particulièrement pour les systèmes utilisant des composants de grande taille. Par ailleurs, un prototype d'échangeur de chaleur élastique en EPDM permettant un dégivrage mécanique par gonflage a été développé.

Abstract

The objective of the High-Ice project was to investigate a specific concept of a solar thermal and heat pump system with ice storage (solar-ice system). An ice storage design with heat exchangers that can be de-iced was studied. The dependence of the system's electricity consumption on the sizing of the main components (collector field and ice storage) was analysed by means of simulations with the software TRNSYS. The design of the solar-ice system was studied for the use in existing buildings with relatively low thermal insulation. Two types of single family houses with respective space heating demands of 60 and 125 kWh/(m^2 a) in the climate of Zurich were considered. An important additional aim of the study was to analyse the system concept from an environmental and an economic point of view. The life cycle assessment showed that the lowest ecological impact for the heat generation is achieved with relatively large component sizes. It was found that an increase of the component sizes is beneficial as long as it helps to reduce the need for electric backup heating. However, the economic analysis revealed that the heat generation costs, especially for systems with large components, are higher compared to the costs of conventional systems. Further, an elastic heat exchanger plate made of EPDM-rubber that can be de-iced mechanically by inflation, was developed on the laboratory scale.

Contents

1. Introduction

The purpose of this project is the investigation of heating systems for single family houses, that are based on solar thermal heat pump systems and include ice storages. The considered ice storages work with a new type of heat exchanger that can be de-iced. In addition, the benefit of including a waste water heat recovery device is evaluated.

Combined solar thermal and heat pump systems that do not including ice storages became of interest in the last decade, because of their potential to increase the share of renewable energies in space heating and domestic hot water preparation applications. Research on combined solar thermal and heat pump systems has been carried out for many years. However, only recently a significant increase in the number of installed systems could be observed in the European market. Ruschenburg et al. (2013) surveyed about 90 companies and found that the majority of them had entered the market in recent years and that a large number of companies were based in Germany and Austria. A recent example of research done in this topic is a study conducted in the framework of the Solar Heating and Cooling programme (SHC Task 44) and the Heat Pump programme (HPP Annex 38) of the International Energy Agency (IEA). The study entitled "Solar and Heat Pump Systems" is also known under the combined name of T44/A38 (Hadorn, 2015). The related publications provide a good overview of the performance and relevance of these systems.

First attempts to include ice storages in solar thermal heat pump systems were already made in the 1970s (Abrahamsson et al., 1981). However, only in the course of the present decade a number of companies started offering this type of heating system on the market. Concerning the precise system concepts adopted, little information is publicly available. Published values indicate that many of the installed systems can only reach low performance factors, in the range of the values of air-source heat pump systems. A likely explanation of such low performance figures is that for economical reasons many systems are designed with component sizes (collector field area and ice storage volume) that are too small from a system performance point of view.

Although the interest in combined solar thermal and heat pump systems including ice storages ("solar-ice systems") is growing in central Europe, where climatic conditions are appropriate, many questions regarding an adequate system design have not been addressed so far. In particular, further research is needed to increase the reliability of solar-ice systems, being a key to their establishment on the market.

The major goal of the present project is to show how a specific concept of a solar-ice system allows to reach very high yearly performance factors, i.e. a very low electricity demand for the system operation. Besides the focus on the use phase of the heating system, the whole expenditures over the lifetime of the systems are investigated, both in terms of cost and environmental impact. By this approach, the potentially large influence of infrastructure components like the solar collector field and the ice storage can be assessed.

Two kinds of single family houses, which differ in their space heating demand, are considered in the analyses. The specific heating demands are about 60 kWh/m^2a and 125 kWh/m^2a respectively for the climate of the city of Zurich.

An extensive part of the investigations was based on annual system simulations in TRNSYS. In order to establish a reliable simulation set-up, a large effort was dedicated to the development and validation of the coupled models of the ice storage and the ground surrounding it. The mathematical formulation of the two models is presented in Chapter 5. Chapter 6 contains the validation of the models with the help of laboratory measurements in a first step and measurement data from a 75 m^3 ice storage from a pilot plant in a second step. The measurement data of the pilot plant was also used for the validation of the simulation set-up for the complete solar-ice system. The validated simulation deck was then used to optimize the heating system via series simulations (Chapter 7).

In further investigations, the investment and heat generation costs of the different variants of the solar-ice system were derived (Chapter 8), and life cycle assessments were carried out in order to compare the influences of the infrastructure and the use phase of the heating systems (Chapter 9).

An additional aim of the project was the development of a heat exchanger for ice storages that can be de-iced. An elastic heat exchanger that can be de-iced mechanically was developed and experimentally tested (Chapter 10).

2. Ice storages for solar thermal heat pump systems

2.1. Characteristics of ice storages used in heating systems

The expression "ice storage" is used as a common name for a thermal storage that uses the phase change enthalpy of water from liquid to solid as a part of its storage capacity. By freezing water, a high amount of heat can be extracted: per kilogram of water 333 kJ (0.093 kWh) are released during this process. Compared to that, using the sensible heat of water at temperatures above 0 °C, 4.19 kJ (0.001 kWh) can be extracted per kilogram and Kelvin. From these numbers it can be derived that the freezing of 1 kg of water releases the same amount of heat as the cooling of 1 kg of water from 79.5 °C to 0 °C. The high specific storage capacity due to the use of the latent heat of the storage water is an important characteristic of ice storages.

Usually, heat is extracted from ice storages with the help of a heat pump. The heat is extracted via a heat exchanger that can be immersed into the storage water. For operation below 0 °C a mixture of water with antifreeze flows through the heat exchanger. If during the heat extraction the surface temperature of the heat exchanger drops below the freezing point of water, ice can be formed on the heat exchanger. By this process of building up ice, the latent heat of the storage water is extracted. Besides the latent heat, also the sensible heat of the storage water can be used in ice storages.

Ice storages have been used for many decades in the cooling industry and for air-conditioning of buildings (Mehling and Cabeza, 2008). These storages are mostly optimized for the provision of high cooling power to processes and for the dispersal of cooling loads for air-conditioning over the day in order to reduce chiller needs and electricity costs. Different requirements apply when ice storages are used in heating systems for buildings (which may also include a function for cooling the building). Here it is of high importance that the storage has a low cost, is simply mounted, and needs minimal maintenance. In contrast to cooling applications, the reduction of the size of the heat pump and the electricity savings via shaving of peak loads are not relevant.

Characteristics of ice storages that are of interest for solar thermal heating systems are:

- The use of the phase change enthalpy in the ice storage leads to a high volumetric storage capacity, i.e. relatively small-sized ice storages can store a large amount of heat.

- Ice storages have low heat losses during operation at low storage temperatures, and can even gain heat if the storage is colder than the surroundings.

- If the ice storage is installed outside the building (especially if buried in the ground) a thermal insulation may not be necessary.

- The impact on-site is low compared to other heat sources for heat pumps like boreholes or air heat exchangers (no potential restrictions or risks like for boreholes and no visual or acoustic impacts like for air-source heat exchangers).

- Depending on the design of the heating system and thus the temperatures reached in the ice storage in autumn, part of the sensible heat of the ice storage may be used directly in the building (without using the heat pump).

- The regeneration of the ice storage with solar heat at a low temperature level leads to additional solar gains in times during which the solar heat can not be directly used in the building for space heating or domestic hot water preparation.

- Low temperature heat sources like waste heat of e.g. air or waste water can deliver heat for melting the ice.

- If the ice formed in winter is stored until summer or if the building has simultaneous heating and cooling demands, the storage can be used as a heat sink for air-conditioning.

2.2. Heating systems with ice storages: market and research

Already in the 1970ies, solar thermal heat pump systems with ice storages were investigated. An early example of a pilot installation with an interesting system concept is a small local heating grid supplying
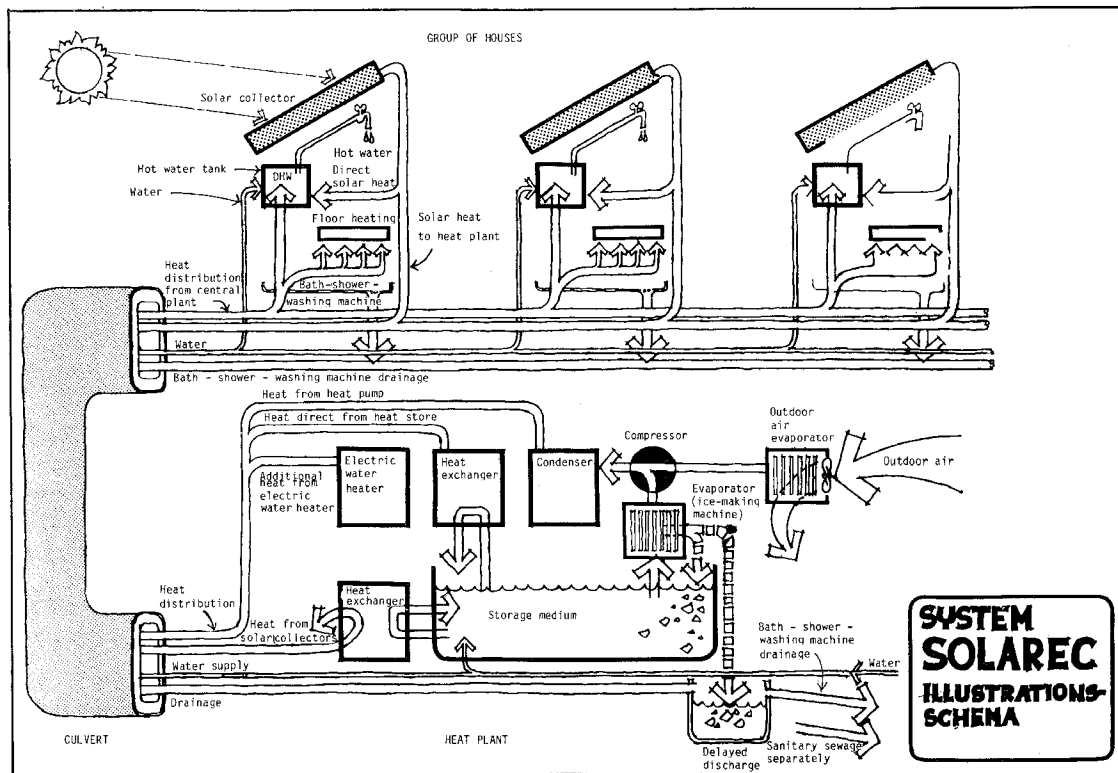
Figure 2.1: Example for an early solar thermal heat pump system with ice storage and waste water heat recovery that has been built 1979 in Sweden (from: Abrahamsson et al. (1981)).

6 single family houses in Sweden, developed by Abrahamsson et al. (1981). There, the ice storage is loaded with solar heat from the collectors and heat from waste water of the houses. The ice storage is unloaded by means of heat exchangers mounted in an ice-machine situated above the storage water. The heat pump can use ambient air or the ice storage as its source. Heat from the solar collectors is also used directly for space heating and DHW-preparation. The energetic efficiency of the heating system in terms of electricity demand was low, with a seasonal performance factor of 1.4. Though, a comparison with today's systems is difficult, because of the technical evolution of different components, like e.g. heat pumps with higher COP.

A detailed review of ice storage systems currently offered on the Swiss market is given in a report of EnergieSchweiz (Minder et al. (2014)). There, the analysed systems are distinguished by the ice storage capacity which varies between several hours up to several weeks when used as single source for the heat pump, considering the same load. Depending on the type of collector used, different temperature levels can be reached, which leads to different concepts for the use of the solar gains. In a system with uncovered non-selective collectors of the company Viessmann/Isocal, the solar heat is only used on the evaporator of the heat pump. In the analysed systems with uncovered selective collectors of Energie Solaire and Consolar the solar gains are also used for space heating. The Solaera system of Consolar uses covered selective hybrid-collectors that can alternatively be used as air-heat exchangers if the included ventilator is switched on. These hybrid-collectors being covered, their solar gains also serve for DHW-preparation. Besides the manufacturers quoted in Minder et al. (2014), there are several small providers of ice storages and/or solar-ice systems in Switzerland and Germany.

Several examples of research work on solar-ice systems can be found. Winteler et al. (2014) have carried out system simulations for the Viessmann/Isocal system using climate data and system boundaries different from the ones used here. For the SFH45 building of Task44/Annex38 a seasonal performance factor of 4.23 is reached. Trinkl et al. (2009) present simulation results for a solar-ice system with different heating loads of the building. The seasonal performance factor there reaches 4.8. A simulation study in which solar-ice systems and waste water heat recovery are analysed was presented by Heinz et al. (2013). For the climates of Strasbourg and Graz high performance factors result for the systems analysed.

2.3. Heat exchangers for ice storages

2.3.1. Overview of heat exchanger types

Several heat exchanger concepts for extracting the latent heat from ice storages are established. Each concept has to ensure that the ice layer on the heat exchanger does not grow too much as this would result in too low source temperatures for the heat pump.

In principle there exist **two strategies for the design of a heat exchanger used in an ice storage**:

(a) **Large heat exchanger, homogeneously distributed** throughout the whole storage volume. Depending on the extraction power of the heat pump and on the specific characteristics of the heat exchanger a maximum ice layer thickness in ranging from several centimetres to a few decimetres is usually allowed, which determines the distribution of the heat exchanger in the storage volume. The following heat exchanger types are commonly used:

- Coils or capillary mats typically made of plastic that are mounted on a supporting structure ("Ice-on-coil type", suppliers are e.g. Viesmann/Isocal, Fafco Switzerland, Consolar, Calmac)

- Flat heat exchanger plates mounted on a supporting structure. Each plate is hollow and brine flows through it. Materials: plastic or stainless steel (supplier e.g. MEFA, BITHERM)

- Spheres made of plastic filled with water (ice balls). The ice storage is filled with the spheres and brine is pumped through the gaps between the spheres (supplier e.g. Cristopia)

(b) **Small heat exchanger in or outside the storage** with prevention of ice formation on the heat exchanger or active removing of ice from the heat exchanger surface:

- Ice slurry machines that can be mounted outside the storage. Here, on a compact heat exchanger either water is sub-cooled and freezes after being released into the ice storage or ice is directly formed on the heat exchanger and continually scraped away by a mechanic device and washed into the storage (e.g. Abrahamsson et al. (1981), Mehling and Cabeza (2008), Mayekawa Intertech)

- Falling water film: the storage water is sprayed over a heat exchanger mounted above an open storage. The storage water freezes on the heat exchanger which is periodically de-iced thermally (Mehling and Cabeza (2008)). This system is know as an ice harvesting system.

- Flat heat exchanger plates made of stainless steel. The plates are mounted vertically at the bottom of the storage and have a low height compared to the water level. The plates are periodically de-iced thermally.

The last concept mentioned above, based on flat heat exchanger plates made of stainless steel immersed in the storage water and de-iced thermally was developed at the SPF Institut für Solartechnik in Rapperswil and is used in this project as the basis for further developments of de-icing concepts as well as for the system simulations.

Several patents can be found on the topic of heat exchangers for ice storages. For example, an early proposal was published by Egli (1944) for a heat exchanger pipe with elliptic cross-section, filled with refrigerant, that can be de-iced by increasing the inner pressure and change the cross-section to a round shape. Schrammel (1986) proposed a concept for heat exchangers for extracting latent heat from surface waters. The heat exchangers are supposed to be de-iced by injecting pressurized air between the heat exchanger and the ice layer or by a mechanical shake. A concept that uses an elastic layer on the heat exchanger surface that can be inflated and thus pushes the ice away is presented in the patent of Hegele (2002). The patent includes also a kind of thermal de-icing with sensible heat from the bottom of the ice storage that is brought into the brine cycle via extra heat exchangers. Senghas (2015) has developed an ice storage with an "ice-in-coil" heat exchanger where water from a separate tank is circulating and freezes inside a coil that is mounted in the ice storage. The ice storage is filled with brine which is pumped towards the heat pump.

An important focus of the project lies on different de-icing concepts. The main aspects of de-icing are discussed in the following sections.

2.3.2. De-icing versus no de-icing

To show the effect of de-icing, the ice-on-coil concept, where ice remains attached to the coil, and the de-icing concept with irrigated heat exchanger plates are compared by calculation. The modelled plate is hollow and brine is flowing through it.

In principle, after ice is formed, the de-icing of the plate can be reached by temporarily heating up the brine flowing through the plate. By melting the ice that is in direct contact with the plate, the adhesion forces between the remaining ice and the plate are annihilated and the ice is detached by the buoyancy forces.

The heat transfer coefficients of two hypothetical heat exchangers – a flat plate made of stainless steel and a coil made of polypropylene – with the same surface area (0.5 m^2) are plotted in Fig. 2.2 as a function of ice thickness. The wall thickness is 0.6 mm for the steel plate and 3 mm for the polymer coil, whose inner diameter is set to 2.6 cm. Icing is done with an inlet fluid temperature of -6 °C. Results are presented for a mass flow of 300 kg/(h m^2), i.e. in this case 150 kg/h, which is a typical value for this application.
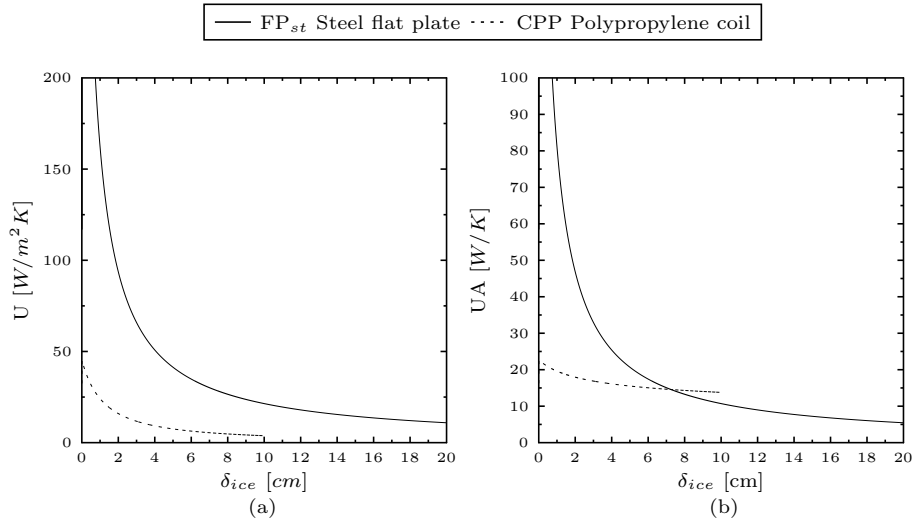
Figure 2.2: Heat transfer coefficient of the heat exchanger between brine and water for a steel flat plate and a polypropylene coil as a function of ice thickness at 150 kg/h mass flow rate (a) U-value (per m^2 of heat exchanger external area, i.e. accounting for growing ice surface area) and (b) UA-value.

The U values of both heat exchangers decrease very fast with time. However, for the coil, the total heat transfer (UA), accounting for the growing ice surface, shows only a small decrease with growing ice thickness. The heat transfer resistance of the growing ice layer is partially compensated by the increased heat transfer area around the coil. In the case of the flat plate, on the contrary, also the UA-value decreases rapidly with growing ice thickness.

The comparison shows that the UA value of the flat plate is higher than the one of the coil for an ice thickness below 7 cm, which corresponds to approximately 13.5 hours of ice-formation under the specific conditions used here. The high decrease of performance for the flat plate is the reason for using the concept of de-icing, which allows to maintain a high performance of the heat exchanger and thus to avoid exceedingly low temperatures at the inlet of the heat pump evaporator. Using de-icing, the performance of the flat plate is better than the one of the polypropylene coil with the same heat exchanger area, if the plate is de-iced before the ice thickness exceeds 7 cm. However, the modelled flat plate is more expensive than the polymer coil as it is made of stainless steel. Therefore, the decrease of performance of the coil could be compensated using a longer coil with a larger total surface.

In a large ice storage of several m^3 the ratio between its volume and the heat exchanger area as well as the spatial distribution of the heat exchanger are of interest. If coils are used, they have to fill up the whole storage volume in order to use all latent heat capacity of the water. If a de-icing concept is applied, heat a few heat exchangers at the bottom of the storage are sufficient to fill up the whole storage with

ice. Therefore, the higher cost per surface area of the stainless steel plates may be compensated by a lower amount of required heat exchanger surface and by lower installation costs.

The following points summarize the most relevant aspects distinguishing the flat plate heat exchangers with de-icing, considered in this project, from the widespread ice-on-coil concept:

- Less heat exchanger area per volume of ice storage is needed, leading to potentially lower material costs.

- Lower installation costs, as heat exchanger plates are only needed at the bottom.

- A strong structure to counteract the buoyancy force of the ice-on-coil heat exchanger when highly loaded with ice is not needed, as the detached ice floats in the water.

- Special design of heat exchangers is needed to ensure that the ice layers can be detached. It has to be avoided, for instance, that ice layers from both sides of the flat plate can grow together or that they grow around other parts like hydraulic connections.

- As the de-icing is an active process, it has to be implemented in the control logic.

- The availability of energy for de-icing has to be ensured. If the energy from the collector field is not sufficient, other sources need to be available, e.g. heat from a combi-storage (from its lowest part that is used for solar DHW-preheating), from waste heat or from an electrical heating rod.

2.3.3. De-icing concepts

There exist different mechanisms for the de-icing of heat exchangers. Besides the ones listed in Section 2.3.1 point (b), other strategies for de-icing can be found. A collection of de-icing strategies, realized and potential ones, are given in Fig. 2.3.

Thermal de-icing

With thermal de-icing (Fig. 2.3, right) the heat exchanger is de-iced before the brine temperatures gets too low for the heat pump. While the heat pump is switched off, the heat exchanger is shortly heated above 0°C. A small amount of ice that is in contact with the heat exchanger is melted, leading to the detachment of the ice layer.

In the case of thermal de-icing the heat exchanger is not treated by any mechanical process and no mechanical devices (moving parts, motors) need to be operated. This can be an advantage for the reliability and longevity of the system.

A disadvantage of thermal de-icing is, that it is only possible while the heat pump is switched off. Thus, the heat pump power and the control logic have to be chosen and designed accordingly. Furthermore, a heat source has to be available for thermal de-icing. If the commonly used heat sources for the ice storage (solar or waste heat) are temporarily not available, de-icing cannot be carried out or has to be done e.g. with an electric rod. Depending on the system, the thermal mass that has to be heated up for de-icing is large (heat exchangers, pipes, etc.) which means that a high amount of heat has to be injected. However, the heat used for thermal de-icing is not lost, since it is at the same time stored in the ice storage. If the solar heat could be used directly in the combi-storage, using it for de-icing presents an exergetic loss, but no energetic loss.

A concept with a heat exchanger immersed in the storage water at the bottom of the casing was developed by our institute. After thermal de-icing, the ice layers separate from the heat exchangers due to buoyancy forces and accumulate at the surface of the water contained in the ice storage. An experimental prototype of a small flat plate heat exchanger with de-icing mechanism was first investigated by Hirsch (2010), a real-scale version was presented in Philippen et al. (2012) and further analysed in Carbonell et al. (2014a). The concept has been successfully used in a pilot plant (Philippen et al., 2014).

Concepts for de-icing of heat exchangers

Mechanical de-icing
- Scraping (ice-slurry)
- Vibration of hx surface
  - Impuls through a hit
  - Ultrasound in water or direct on hx
- Changing the hx shape
  - Bending with bimetallic strip / hx as bimetall
  - Stretching of the hx
  - Inflating the hx
  - Elastic foil on hx's surface

Thermal de-icing
- Heating up brine
  - by heat pump
  - by solar heat
  - by other sources (e.g. waste water)
- Heating up heat exchanger
  - Electric heating wire on hx surface

Figure 2.3: Realized and postulated concepts for the de-icing of heat exchangers for ice storages.

Mechanical de-icing

Mechanical de-icing (Fig. 2.3, left) can in principle be executed while the heat pump is running. This can be of great advantage, because it allows for a simpler control strategy compared to thermal de-icing. Moreover, the mechanical de-icing can be carried out more often, which leads to higher source temperatures for the heat pump and thus higher COPs. Depending on the type of mechanical de-icing, a much smaller amount of energy is necessary for the de-icing process compared to the energy needed for thermal de-icing.

Mechanical de-icing is widely used in ice-slurry machines (types with scraping devices). No concepts other than ice-slurry could be found on the market. A publication of an unexamined application (i.e. in a preliminary stage of a patent application) was found on an elastic pipework element that can be de-iced by mechanical force or deformation (Heilemann et al., 2013). A coating of the element with halogens is also proposed in the publication. The publication was disclosed at the end of 2013, about two years after the start of the High-Ice project. The principle idea of the heat exchangers developed here (see Chapter 10) are somewhat similar to the one in Heilemann et al. (2013).

2.3.4. Characteristics of the analysed mechanical de-icing concept

The collection of existing and potential concepts for de-icing in Fig. 2.3 was used to choose a promising concept at the beginning of the project for the practical development work. The choice fell on mechanical de-icing by changing the shape of the heat exchanger, because this concept doesn't need any moving parts inside the ice storage and hence is likely to lead to a system with high reliability.

The heat exchangers are meant to be installed at the bottom of the ice storage with a heat transfer area appropriate for the extraction power of the heat pump. Depending on the volume and the shape of the ice

storage, the height of the heat exchangers is much lower than the height of the storage water. Therefore, detached ice accumulates in the water section above the heat exchangers. The amount of latent heat that can be extracted from the ice storage, i.e. the maximum amount of water that can be transformed to ice, depends on the ratio of heat exchanger and water heights as well as on the distribution and bulk density of the detached ice-pieces. The bulk density of the ice-pieces, in turn, depends on the shape of the heat exchanger.

Different types of heat exchangers, like e.g. pipes and plates made of different materials, are analysed in the practical part (Chapter 10). The main emphasis is put on mechanical de-icing by inflation of elastic heat exchangers. The inflations is achieved by increasing the pressure of the brine.

3. Description of the analysed heating systems

3.1. General system concept

The ice storage system employed here is based on immersed flat plate stainless steel heat exchangers that can be a de-iced. The de-icing concept serves to improve the heat transfer rate of the heat exchangers while reducing the total heat exchanger area needed in the storage. This system concept has been presented in Philippen et al. (2014, 2012) and Carbonell et al. (2014a,b, 2015). For details on the de-icing concept the reader is referred to Section 2.3.3.

The hydraulic scheme of the complete solar-ice heating system is shown in Fig. 3.1. The main components of the heating system are the collector field, the combi-storage, the heat pump, the ice storage and the waste water heat recovery device.
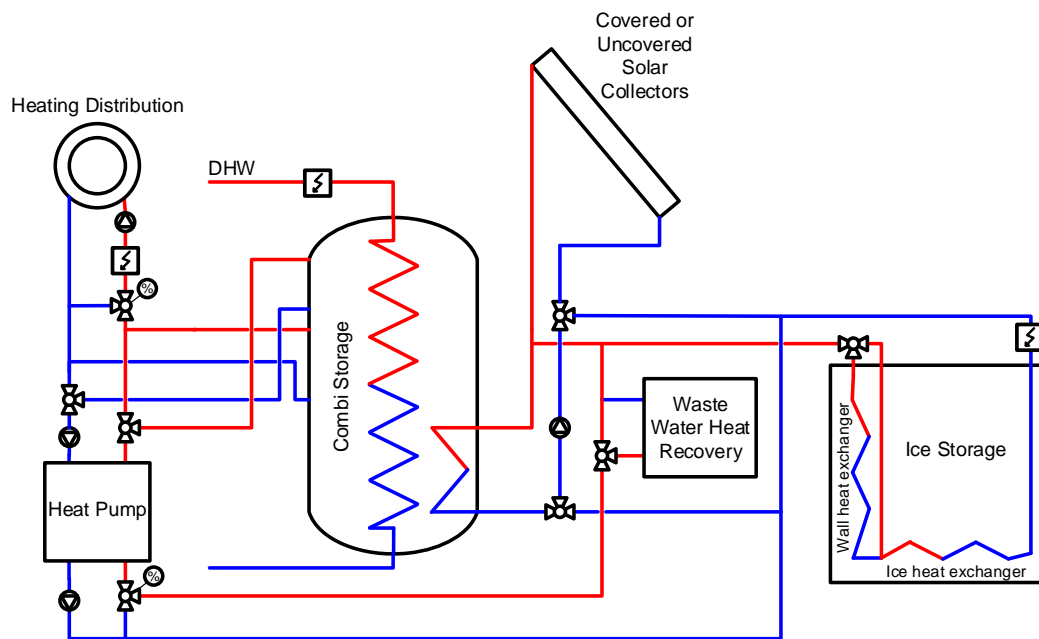
Figure 3.1: Simplified hydraulic scheme of the analysed heating system with device for waste water heat recovery.

The main energy source of the system is the solar irradiation. Some additional energy is extracted from the air, specially when uncovered collectors are used. A part of the total solar irradiation is transformed by the collectors to useful heat for the system. This energy is then transferred, either to the heat pump, to the ice storage or to the combi-storage. When the heat pump is running, two operation modes are possible, depending on whether the collectors are able to provide energy or not: i) the heat pump uses the solar energy directly in a series operation mode or ii) the heat pump uses the ice storage as its source. With the hydraulic set-up proposed here, when the heat pump is running with solar energy as a source, the mass flow from the solar collector field is split: one part of it goes to the heat pump and the other part goes to the ice storage. Therefore, if more energy is available from the collector field than is needed by the heat pump, the ice storage is also loaded while the heat pump is running. On the contrary, if the collector output is lower than the heat pump needs, both, the ice storage and the collector field are used to provide heat to the evaporator of the heat pump. If none of these heat sources are available, which means that the ice storage is full of ice, the solar irradiation is very low or zero (night) and the ambient temperature is very low, too, the temperature of the heat pump evaporator drops below the minimum allowed value and the heat pump stops. In this case, a direct electric back-up is used.

As can be seen in Fig.3.1 the ice storage can have two types of heat exchangers, the ones that can be de-iced (ice-hx) and the wall heat exchangers (wall-hx). These two types of heat exchangers serve different purposes. All of them are fully irrigated flat plate heat exchangers made of stainless steel. The only difference is the special design of the barriers of the ice-hx used to be able to de-ice. The ice-hx are
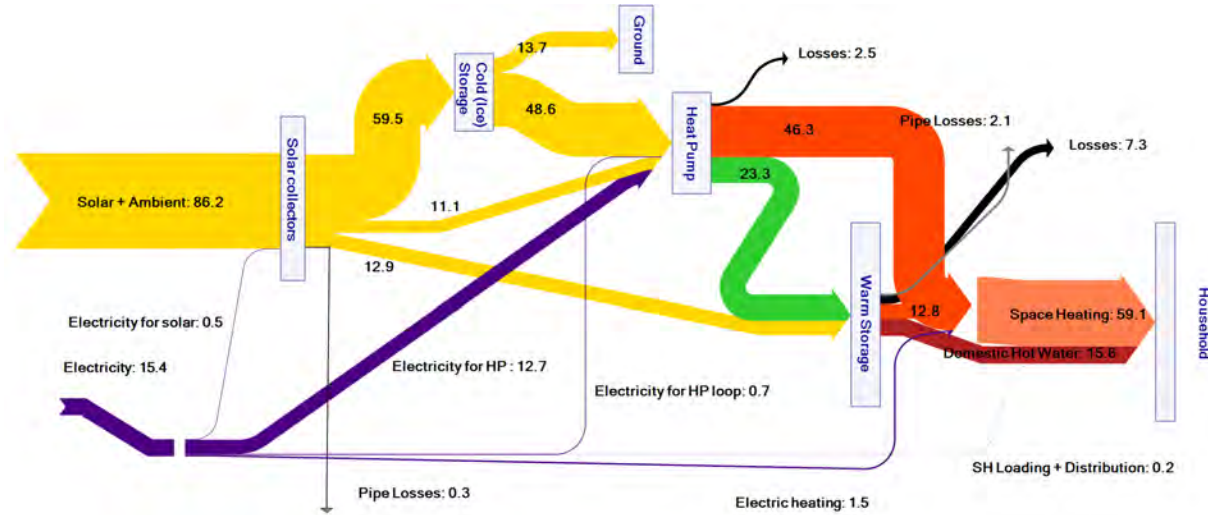
Figure 3.2: Sankey diagrams for $V_{ice} = 15$ m^3 and A_{unc}=25 m^2 with a SPF$_{SHP+}$ of 4.8. Values are in kWh/m^2 of heated building surface area which is equal to 140 m^2.

placed in the lower part of the storage. In principle, the lower the height of the ice-hx the better, since more free space will be available above the ice-hx to store the floating ice layers. The system concept also considers heat exchangers placed along the wall of the storage that, by means of control strategies, are prevented from icing. These heat exchangers mainly serve to use the stored heat, accumulated in summer periods in the upper part of the storage, for space heating (SH) and domestic hot water (DHW) preparation in autumn. Notice that the heat exchangers located at the bottom of the storage cannot access the heat stored in the upper part of the storage directly (provided that temperatures are above 4 °C). The benefits of wall-hx are discussed in Chapter 7.

In Fig.3.1 an optional waste water heat recovery (WWHR) system is located in the source loop of heat pump, before the evaporator inlet. WWHR systems are of special interest in this application due to the low temperature of the ice storage in winter and due to the fact that WWHR provides heat at times when other sources (solar, ambient air) may not be able to provide a significant contribution. Waste water heat recovery is expected not only to increase the system performance, but also to obtain a system, which is more independent on DHW usage. The daily usage of DHW is user dependent and system efficiencies may be highly sensitive on the DHW load profile. With the possibility to recover this heat, the system performance is expected to become less dependent on the amount of DHW consumption. Two different WWHR systems have been analysed in the present study: i) Gravity film heat exchanger (WW$_{GFX}$) and ii) Waste water storage (WW$_{storage}$). Details of the analysed WWHR devices are presented in Section 3.7.

As an illustrative example of energy flows in the solar-ice system proposed in this project, a Sankey diagram for a system with a performance factor SPF$_{SHP+}$ (see Section 4.2 for performance indicator definition) of 4.8 composed of an ice storage of 15 m^3 and 25 m^2 of uncovered selective collectors is presented in Fig.3.2 for the building SFH45* (defined in Section 3.5).

Around 71% of the energy provided by the collector field is transferred to the ice storage. Around 80% of this energy go to the heat pump. This means that approximately 56% of the energy provided by the collector field to the ice storage go to the heat pump. Around 13% of the energy from the collector field go directly to the heat pump and 15% are directed to the combi-storage (warm storage). This approach is conceptually different from other systems, see e.g. Winteler et al. (2014), where most of the energy from the collector field is used directly in the heat pump evaporator.

3.2. System control

The solar-ice system developed in this project requires a controller including functionalities needed for de-icing. In this section, the main control modes applied to the system are explained.

The system has a global control with four main priorities in the following hierarchy:

1. Use of direct solar heat to provide the comfort in the building without switching on the heat pump.

2. Switching on the heat pump when needed in order to provide the comfort.

3. De-icing, if the outlet of the ice storage drops below a defined threshold value, the thermal de-icing operation mode is activated. De-icing also has its priorities: first, it is tried to de-ice with the collectors. If the temperatures are not sufficient, the combi-storage (heat from lowest part that is not loaded by the heat pump) or ultimately direct electric back-up is used.

4. Use solar heat to load storages when the heat pump is off. The control can either decide to load the ice storage or the combi-storage. Different control strategies are used here.

The system part on the secondary side of the heat pump, i.e. the heating distribution and the DHW-preparation, and the heat pump itself are mostly controlled in a standard way. The brine cycle on the primary side, on the other hand, needs some special operation modes and capabilities that allow for de-icing. Also the backup has to be controlled, such that it runs when there is a heating demand in the building and the ice storage is fully iced (no source available for the heat pump). If the ice storage is fully iced also all de-icing programs have to be stopped temporarily. Further season-based prioritizations of storages regarding the use of the solar heat are implemented.

The de-icing program is activated if the outlet temperature of the ice storage drops below a certain threshold. As a first priority, it is then tested whether the thermal collectors can be used to de-ice. As a second priority, the lowest part of the combi-storage [1] is used, if its temperature is high enough. Otherwise, an electric backup is employed to de-ice. The backup is only used if the ice layers on the heat exchangers are getting too thick and run the risk of joining, which would make later de-icing impossible.

The control also has to cope with the fact that the ice storage is a cold sink for a long time during the year. Unless a logic is implemented, that switches to loading of the combi-storage when appropriate, the ice storage would be loaded predominantly. The control mode that actively stops the loading of the cold storage and tries to divert the solar heat on a higher temperature level to the combi-storage is called warm storage priority (**PriorWs**). If PriorWs is not active, the control mode **PriorCs** is on, which mainly loads the ice storage and only loads the lowest part of the warm storage to store some heat for de-icing.

In the case where PriorWs is active, the control also checks if it is possible to do a heat transfer from the cold to the warm storage (**ProgHt**). The program ProgHt can run in early autumn at times during which the ice storage is temporarily on a higher temperature level than the warm storage. The heat from the ice storage can then be used directly in the building without using the heat pump. ProgHt is only activated if wall heat exchangers are installed in the ice storage (see Chapter 3 for details).

3.3. Ice storage and heat exchanger

De-icing is possible by means of heat from the solar collectors or heat from the lowest part of the combi-storage. As mentioned before, when these two sources fail, an electrical rod is employed. The lower part of the combi-storage, which is sometimes used to de-ice, is loaded by the collector field only.

Unless otherwise stated, all calculations in this project are based on flat plate heat exchangers made of stainless steel that are de-iced thermally.

3.4. Collectors

Two different types of collectors, covered (glazed) and uncovered (unglazed), both with selective coating on the absorber, are analysed as components in the solar-ice system. If uncovered collectors are used below ambient temperature, they are able to extract a considerable amount of heat from the ambient air, that can be used as source for the heat pump or stored in the ice storage. The decrease of spectral selectivity, which appears when the uncovered collectors are used below dew point and water condensates on the absorber surface, is taken into account in the collector model (for details about the physical phenomenon see Haller et al. (2014a)).

---

[1] The part that is used for DHW-preheating and that is only loaded with solar heat

3.5. Buildings

Three buildings are simulated within the project. Their definitions are based on the IEA SHC Task44 /Annex38 boundary conditions (see Dott et al. (2012) and Haller et al. (2012) for details). Buildings SFH45 and SFH100 are taken from there, and, as an additional variation, SFH100 with floor heating is considered.

In the Task44/Annex38 definition "SFH" stands for Single Family House, and the numbers correspond to the yearly energy demand for space heating in units of kWh/m² (per heated area) in the city of Strasbourg. In Zurich, the same buildings have a larger heating demand, as shown in 3.1. In order to remind of the fact that the simulations in this project are not done for the climate of Strasbourg, the energy demands in the building's names are marked with an asterisk *. The buildings SFH100* with radiators or floor heating are distinguished by the indices HT and LT (for High respectively Low Temperature heat distribution system). To summarize, in this report the simulated buildings are denominated **SFH45***, **SFH100$^*_{HT}$** (which both follow the Task44/Annex38 definitions), and **SFH100$^*_{LT}$** (where floor heating is assumed).

Table 3.1: U-Values of the external building walls and windows (with frame), and space heating demand for the three simulated buildings in Zurich. (SFH100$^*_{LT}$ has a slightly higher heating demand compared to SFH100$^*_{HT}$ because it has more losses to the ground due to the floor heating system).

	Space heating demand kWh/m^2a	U-Value external wall W/m^2K	U-Value ground floor W/m^2K	U-Value window W/m^2K
SFH45*	59	0.286	0.173	1.5
SFH100$^*_{HT}$	124	0.667	0.278	3
SFH100$^*_{LT}$	128	0.667	0.278	3

Buildings with very low heating demand (e.g. passive houses), were not simulated because the solar-ice concept presented here is expected to be too expensive for such buildings. In fact, the solar-ice system is rather meant to be used to retrofit heating systems of existing buildings. Here, the system is expected to significantly reduce the electricity demand for the heat pump and, as the heat demand is high, to deliver the heat with moderate heat generation costs.

In buildings SFH45* and SFH100$^*_{LT}$ the low temperature heat distribution system has flow and return temperatures of 35 and 30 °C respectively at nominal conditions. Building SFH100$^*_{HT}$ has radiators and needs a heat distribution on the temperature level 55/50 °C. The simulated buildings have a heated surface area of 140 m², distributed on two floors, as shown in Fig. 3.3. The length of the building is 10.6 m and its width 7.6 m with a total window area of 23 m². Important values of the building are given in Table 3.1 (more details can be found in Dott et al. (2012)). The set room temperature is 20 °C and is controlled to ± 0.5 °C during the heating season.

Figure 3.3: Schematic view of the building (showing south and west façades). The south roof is inclined 45 ^{o}. (Dott et al., 2012)

3.6. Loads

Domestic hot water (DHW)

The domestic hot water (DHW) tapping profile is obtained from Task44/Annex38 (Haller et al., 2012), the DHW set temperatures are 45 °C and 55 °C respectively and the cold water temperature is set to 10 °C. The average tapping amount is 140 l/d. This corresponds to 2133 kWh/a or 15.2 kWh/a per m^2 of heated building area. Fig. 3.4 shows the daily energy distribution of the DHW profile.
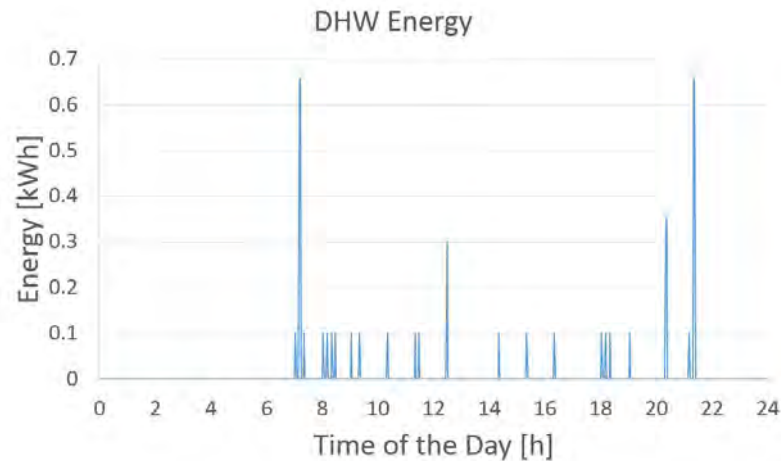
Figure 3.4: Thermal energy profile of the provided DHW.

Other loads

For ventilation losses a constant air exchange rate of 0.4 h^{-1} is considered as fresh air demand of the building. Also a freely driven night ventilation with tilted windows is considered in order to simulate passive cooling. For shading all windows are equipped with Venetian blinds and are simulated with a constant factor of 0.25. Shading is activated automatically if all of the following three conditions hold (off-values in parentheses):

- horizontal, global irradiation greater than 300 (200) W/m^2
- room temperature greater than 23.8 (22.8)°C
- 24 hour moving average ambient temperature greater than 12 °C

Also internal gains due to inhabitants and gains from electric equipment are considered. The underlying profiles have a time resolution of 1 hour. Gains caused by inhabitants are 60 W. For the assumed 4-person household, these gains sum up to 9 kWh/m^2a. Thermal gains caused by electric equipment are in total 13.4 kWh/m^2a. The time profiles and the calculation base for all internal loads are presented in Dott et al. (2012).

3.7. Waste water heat recovery (WWHR)

Heat recovery systems can be classified into retentive and not retentive systems, and into active and passive systems (Heinz et al., 2013, van Velsen and Benz, 2013). In non retentive systems, the heat has to be extracted at the time when waste water is available.

Retentive systems, on the other hand, are able to store the grey water (black water is not considered) to be used when needed. If the heat of the waste water can be used in a passive way, there is no need to run an additional circulation pump.

Waste water storage:

An indoor storage is used to collect grey water[2]. In this study, a waste water storage with a volume of 130 litres and an incorporated spiral heat exchanger made of steel was simulated. The stored heat can either be used on the evaporator of the heat pump or in the ice storage. The tree way valve switches if the temperature of the waste water in the storage is at least 5 K higher than the temperature of the brine coming from the ice storage. It switches back if this Δ T is less than 4 K. The minimum allowed average temperature in the waste water storage was set to 4 °C. If this value is undershot, the heat exchanger in the storage is bypassed as shown in Fig. 3.1. The waste water heat exchanger can be operated by the pump of the primary heat pump loop. The main advantage of this system is the temporal flexibility to use the waste heat. Most of the collected heat can be used even with low heat transfer rates after fouling occurred. Disadvantages of this system are a large space requirement and possibly large maintenance demand. If the storage only allows the usage of grey water, the waste water streams have to be separated.

Gravity film heat exchanger (GFX):

A GFX is composed of a central pipe with a wound, soldered pipe on its outside, as shown in Figure 3.5. Both pipes are made of copper. The central pipe is integrated into the buildings sewer. The brine on its way from the ice storage to the heat pump flows trough the wound pipe. The GFX has an inner diameter of 100 mm. The diameter of the wound pipe is 12 mm and reaches from the bottom to the top of the 2 m long GFX. For the recovery of waste water heat with the GFX, two cases were defined. If the heat pump is running, the tree way valve switches over to increase the temperature of the brine cycle, if the waste water temperature is at least 5 K higher than the temperature of the brine coming from the ice storage. The tree way valve switches back, if this temperature difference is drops below 4 K. The second case is, that the heat pump is off and waste water heat is available. The brine loop pump is turned on to transfer heat from the GFX to the ice storage, if the waste water temperature is 5 K higher than the temperature at 20 % relative height in the ice storage. The brine loop pump is turned off, if the temperature difference drops below 4 K. An advantage of this system is its low space demand. Moreover, the system can use the energy of both black and grey water. A disadvantage of a GFX is the fact, that waste water heat will only be recovered, if the heat pump is running or if the brine cycle pump is turned on, when the waste water flows through it. Further, there is only a very short time for the heat exchange from waste water to the hx wall. The usage of a GFX requires more sensors and a quick control. In any event, warm water taps with a short residence time inside the GFX can not be exploited fully.
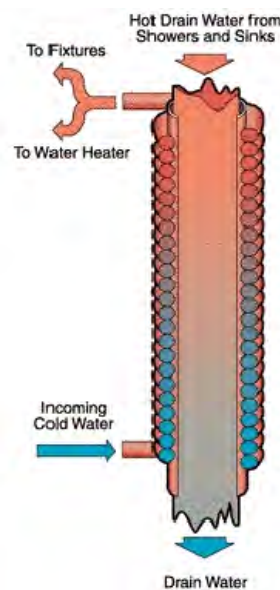

Figure 3.5: Operating principle of a GFX. Gfxtechnology (2015)

---

[2]"Grey water" denotes waste water from the bath (without toilet) and from the washing machine. "Black water" is the total mixed waste water from a building.

Waste water profile

The average water consumption in western Europe amounts to 130 – 150 litre per day and person. Thereof, 90 litre are cold water, which enters on a temperature level of 8 – 11 °C and leaves the house with 14 – 19 °C (mean 16 °C). The rest is hot water, which leaves the house with an average temperature of 22 °C (Heinz et al. (2013)). The measurements of Heinz et al. have shown that the water consumption and the temperature level vary only little over the year. The same authors found out that it could be useful to separate the waste water stream into grey water and black water, because grey water (23 °C) has a higher temperature level than the total waste water stream (16 °C). Approximately 77 % of the total input energy of warm and cold water are flushed away in the waste water. Almost half of this energy is from the bath. In order to create a waste water profile, TU Graz measured the amount of DHW, black and grey water(Heinz et al. (2013)). In the simulations, however, the DHW profile defined in IEA SHC Task 44 was used. The DHW amount defined in IEA SHC Task 44 is 1.4 as high as the value proposed by TU Graz. To have the same DHW amount in both files, all values (DHW, black and grey water) in the file of TU Graz were multiplied by a factor 1.4. For all simulations the newly created profile of grey water was used. The amount of grey water in this file is 300 kg per day with an average flush rate of 3.7 kg/min and an average temperature of 23 °C. If all this grey water can be cooled down to 5 °C, this corresponds to 8 kWh of useful energy of per day. Figure 3.7 shows the hourly energy of the used two week waste water file.
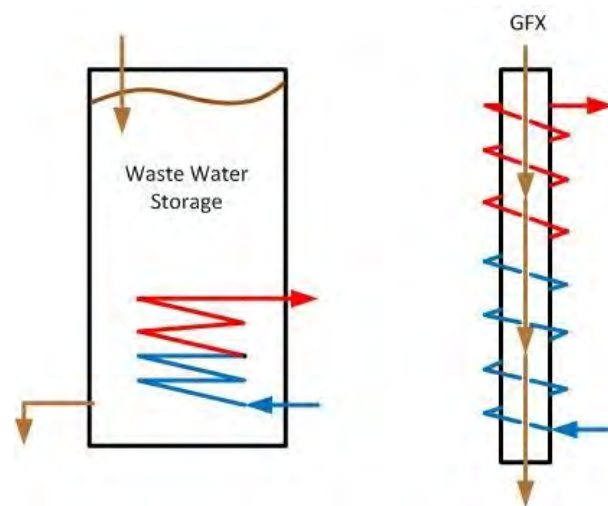
Figure 3.6: Schemes of WWHR systems (left: Waste Water Storage,right: Gravity Film Heat Exchanger (GFX). Brown dyed is the Waste Water Stream, blue is the cold brine side and red the warm brine side.

3.8. Climates

Three locations in Switzerland were used to map the Swiss climate. Zurich is used as "standard climate" for the simulations, because it is a typical location for the Swiss midland climate, where most of the Swiss buildings are located. This region usually has not too cold but foggy winters, which leads to a decreased regeneration of the ice storage in winter. For simulations in an alpine region with very cold but sunny winters, the climate of Davos was chosen. Locarno on the south of the Alps was chosen as a third location. There, winters are relatively mild and sunny and the irradiation over the year is very high, as shown in Fig. 3.8

Table 3.2: Extract of the used weather data for the simulations METEOTEST (2012)

	Mean temperature (Year)	Mean temperature (Nov - Feb)	Monthly mean global irradiance (Year)	Monthly mean global irradiance (Nov - Feb)
	$°C$	$°C$	kWh/m^2	kWh/m^2
Zurich	7.8	1.5	98	50
Davos	1.7	-2.3	143	117
Locarno	10.2	3.6	117	84
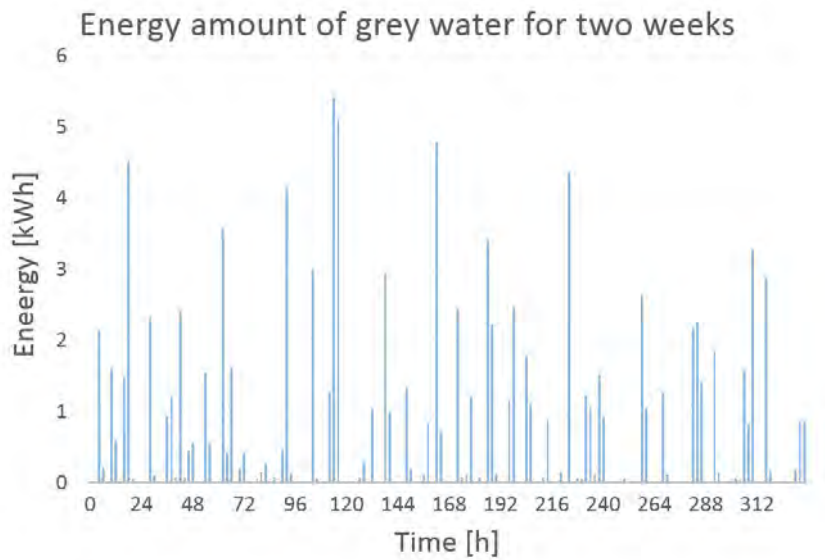
Figure 3.7: Thermal energy of the used grey water file for two weeks. The energy is calculated with the temperature difference from 5 °C to the waste water temperature.
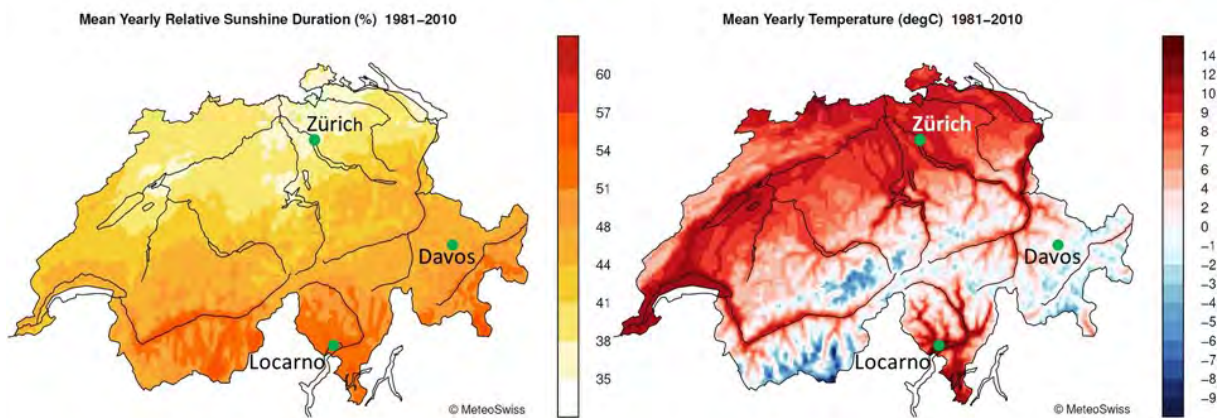
Figure 3.8: Mean yearly relative sunshine duration in % (share of the maximal possible sun shine duration from sunrise to sunset) and mean yearly temperature in °C (average from 1981 - 2010). MeteoSchweiz (2015)

4. Methodology

4.1. Transient system simulations

Energy simulations were conducted with the simulation environment TRNSYS-17 (Klein et al., 2010). The detailed energy system simulation model of a solar thermal heat pump system implemented in a single family house from the SFOE-project "SOL-HEAP" (Haller et al., 2014a) was used as a base. The system set-up was changed to the demands of this project, i.e. different hydraulics, implementation of ice storage coupled with the ground, and new system control.

The basic components to model a solar-ice system are: collectors, heat pump, ice storage, sensible thermal storage, building, climate and control. In this project as optional components also waste water heat recovery devices are included.

The time step of yearly simulations is set to 120 seconds. As a verification process several systematic checks are done for all simulations. Heat balances are checked in all individual components, hydraulic loops and also from the system perspective. The convergence criteria from TRNSYS is set to 5e-4, which allows to achieve heat imbalances always below 0.5% in respect to the total demand. Iteration problems are also checked for all simulations and are always below 50 time steps per year simulated. In most cases iteration problems are in the order of 10 - 20 per year. Once this verification process is fulfilled and the numerical errors are solved, validations of the whole system is necessary. For this purpose, results from the validation procedure for the whole system, using monitored data from a pilot plant, are presented in Section 6.2.

4.1.1. Collector model

Collectors, both covered and uncovered, are modelled with TRNSYS Type 832 (Haller et al., 2014b). This model is based on the type described in Perers and Bales (2002), with the extension to several control volumes in the fluid flow and the consideration of latent gains. The fluid flow discretization is used to overcome the problems of using only one control volume, as described for example in Carbonell et al. (2013). The model is based on the following energy balance equation:

$$\dot{q}_{out} = F'(\tau\alpha)K_b I_b + F'(\tau\alpha)K_d I_d - c_{wF'}u_w(I_b + I_d) + C_{IR}(I_{IR} - \sigma T_{amb}^4) \tag{1}$$

$$- a_1\Delta T_{amb} - a_2|\Delta T_{amb}|\Delta T_{amb} - c_{w,hl}u_w(\Delta T_{amb}) + \dot{q}_{lat} - C_{eff}\frac{\partial T_m}{\partial t} \tag{2}$$

with $\Delta T_{amb} = T_m - T_{amb}$, $u_w = wf \cdot u_{w,o}$ and $I_{IR} = rf \cdot T_{IR,0} + (1 - rf)\sigma T_{amb}^4$

In the above equation, $\dot{q}_{out}$ is the heat output of the collector and $\dot{q}_{lat}$ the latent (condensation and sublimation) heat gains per unit area; $F'(\tau\alpha)$ is the zero loss efficiency (η_0) under no wind conditions; K is the incidence angle modifier, and I the incident radiation on collector plane, where the subscripts b and c refer to beam and diffuse respectively; $c_{w,F'}$ is the factor for a wind dependency correction; u_w is the wind speed parallel to the collector plane; a_1 and a_2 are the first and second order heat loss coefficients; T_m is the arithmetic mean of the collector temperature; T_{amb} the ambient temperature at location of collector field; $c_{w,hl}$ the wind speed dependency of heat losses; c_{IR} the long wave irradiation dependency of heat losses (or gains); I_{IR} the long wave irradiation on collector plane; σ is the Stefan Boltzmann constant; t the time and C_{eff} the effective thermal capacitance of the collector.

4.1.2. Heat pump model

The heat pump is calculated using the parameter fit model presented in Afjei and Wittwer (1995). This model has been extensively used in the last years, and besides the validation provided in the original work, it has been recently validated in several other works: e.g. Carbonell et al. (2012) compared the model in steady state with experimental data under non standard conditions, i.e. high source evaporator temperatures and low temperature difference between evaporator and condenser. It was concluded that provided the data used to fit the coefficients included the non-standard conditions, predictions of the

model were not bad. Recently Paerisch et al. (2014) validated the model also in non stationary conditions and proposed improvements for non-standard mass flow rates.

The heat pump model is a black-box model based on quasi steady state performance maps. The mathematical formulation is simplified to a two-dimensional polynomial plane able to describe air and water/brine source heat pumps. This model is based on a biquadratic polynomial fit of the condenser heat power Q_c and the compressor work W_{cp}:

$$Q_c = bq_1 + bq_2\bar{T}_{e,in} + bq_3\bar{T}_{c,out} + bq_4\bar{T}_{e,in}\bar{T}_{c,out} + bq_5\bar{T}_{e,in}^2 + bq_6\bar{T}_{c,out}^2 \tag{3}$$

$$W_{cp} = bp_1 + bp_2\bar{T}_{e,in} + bp_3\bar{T}_{c,out} + bp_4\bar{T}_{e,in}\bar{T}_{c,out} + bp_5\bar{T}_{e,in}^2 + bp_6\bar{T}_{c,out}^2 \tag{4}$$

where $T_{e,in}$ is the fluid inlet temperature in the evaporator and $T_{c,out}$ the fluid outlet temperature in the condenser. The normalized temperature $\bar{T}$ is obtained from $\bar{T} = T[^oC]/273.15 + 1$. For the solution of the system of equations the brent solver is used. The polynomial coefficients bq_i and bp_i are calculated using the multidimensional least square fitting algorithm of Scipy (Jones et al., 2001) in Python.

4.1.3. Sensible thermal energy storage model

The thermal energy storage (TES) model used for the combi-storage has been developed at our Institute. The model is an extension of the Plug Flow model presented in Kleinbach et al. (1993). The storage is modelled in two steps. First the direct ports are solved in the so-called plug flow model and afterwards the unsteady heat conduction equation inside the storage, considering the source terms of the heat exchangers, is solved.

The plug flow model part is direct and very fast, but it has some limitations, e.g. small time steps should be used (in the range of a few minutes). The second part of the model solves the heat conduction process iteratively. The heat exchangers are solved using an step-by-step model (Carbonell et al., 2013) considering the transient term. Afterwards the energy introduced in each plug of the storage is calculated. This energy is considered as a heat source term in the one-dimensional unsteady heat conduction equation of the storage. This process is repeated until convergence.

4.1.4. Building model

Two TRNSYS types have been used based on different building models. The first type is the standard TYPE 56 from TRNSYS. This detailed building model is described in TRNSYS 17 documentation. What is important to mention is that TYPE 56 is a detailed building model where different zones and many data can be defined. Therefore it takes a while to set-up a specific building and it is not so easy to modify it in order to achieve a specific heating demand. For these reasons a simplified building model has been used as well.

The employed simplified model computes the heat transfers in the building according to ISO 13790:2008 (D) standard. This model has been implemented as a TRNSYS TYPE 5897 by Leconte et al. (2014). In order to account for short time-scale dynamics, the model has been extended in the present project including the thermal mass of the air inside the building. While this thermal mass can be neglected in hourly simulations, it's effects play an important role in modelling the response of the room temperature on changes in the heating power at shorter time-scales. Therefore, the additional capacity C_{air} has been added at the air node of the model. The corresponding changes were made in the source code of TYPE 5897. The heat transfer in the building is mathematically described using the mass temperature θ_m, the room/air temperature θ_{air}, and the star node temperature θ_s, that is introduced by a Y-Δ transformation. A scheme of the complete, extended building model is shown in Figure 4.1. The thermal balance equations at the three temperature nodes are:

$$C_m\frac{d\theta_m}{dt} = H_{tr,em}(\theta_a - \theta_m) + H_{tr,ms}(\theta_s - \theta_m) + \Phi_m \tag{5}$$

$$H_{tr,ms}(\theta_s - \theta_m) + H_{tr,w}(\theta_s - \theta_a) + H_{tr,is}(\theta_s - \theta_{air}) = \Phi_{st} \tag{6}$$

$$C_{air}\frac{d\theta_{air}}{dt} + H_{ve}(\theta_{air} - \theta_{sup}) + H_{tr,is}(\theta_{air} - \theta_s) = \Phi_{ia} + \Phi_{sh} \tag{7}$$
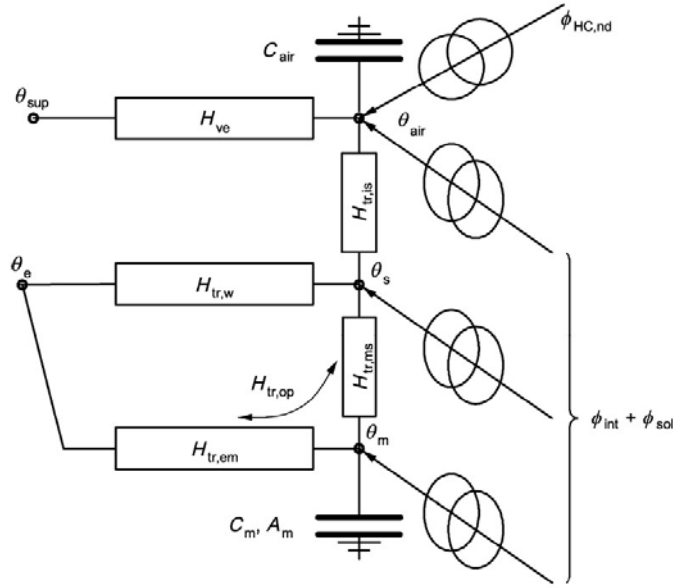
Figure 4.1: Scheme of the ISO building model extended with the thermal mass of the air (Figure modified from (ISO 13790:2008 (D))).

where Φ_{sh} is the power from the space heating system; the heat sources Φ_{ia}, Φ_{st} and Φ_m denote the fractions of internal and solar gains to the air, to the star node and to the mass temperature node respectively. The heat capacities C_m and C_{air} represent the thermal mass of the building walls and the air inside the rooms. The terms $H_{tr,w}$ and $H_{tr,op}$ represent thermal conductance of the windows and walls respectively. The building's ventilation system is represented equivalently by a conductance H_{ve} that connects the room temperature with the ventilation supply temperature θ_{sup}. The other parameters are a result of the Y-Δ transformation. The conductances $H_{tr,is}$ and $H_{tr,ms}$ describe the equivalent heat conductances between the star node, the air, and the mass node respectively. Default values for $H_{tr,is}$ and $H_{tr,ms}$ are given by the ISO model standard.

4.1.5. Gravity film heat exchanger (GFX) model

The GFX is modelled using TYPE 878, which was developed in the framework of the project WRGpot of Heinz et al. (2013). The model is based on the one-dimensional solution of a pipe, considering the heat transfer resistivity of the fouling layer. The heat exchanger is calculated using the Logarithmic Mean Temperature difference (LMTD) method. The U value is obtained considering the resistivity of both fluids, pipe and fouling layer, using variable fluid properties and the increase of the fouling layer thickness.

4.2. Performance indicators

The main performance indicator for the systems is the System Performance Factor calculated as described in Malenkovic et al. (2012):

$$SPF_{SHP+} = \frac{Q_{DHW} + Q_{SH}}{P_{el,T}} = \frac{Q_D}{P_{el,T}} \tag{8}$$

Q is the yearly heat load energy and $P_{el,T}$ the total yearly electric energy consumption. The subscripts SHP, DHW, SH and D stand for solar and heat pump, domestic hot water, space heating, and total demand respectively.

The total electricity consumption is calculated as:

$$P_{el,T} = P_{el,pu} + P_{el,hp} + P_{el,cu} + P_{el,aux} + P_{el,pen} \tag{9}$$

where the subscripts *pu*, *hp*, *cu*, *aux* and *pen* refer to circulation pumps, heat pump, control unit, auxiliary and penalties respectively. The symbol "+" in the $SHP+$ from Eq. 8 refers to the consideration of the heat distribution circulating pump in the electricity consumption. Therefore, the system performance indicator used in this work includes all circulation pumps of the system and also all thermal losses/gains from storages and piping. Penalties for not providing the heating demand at the desired comfort temperature are calculated according to Haller et al. (2012). $P_{el,aux}$ is an auxiliary electric heater used when the heat pump is not able to deliver the heating demand. This is the case when the ice storage is full of ice and the collector field is not able to provide enough heat for the heat pump evaporator.

4.3. Validations with measurement data of a pilot plant

For the validation of the developed models and the whole system simulation, measurement data of a pilot plant is used. The pilot plant is a solar-ice system with heat pump and has been designed, supervised, and monitored by our institute (Philippen et al., 2014). One year of operation has been chosen for the validation (1st February 2013 until 31th of January 2014).
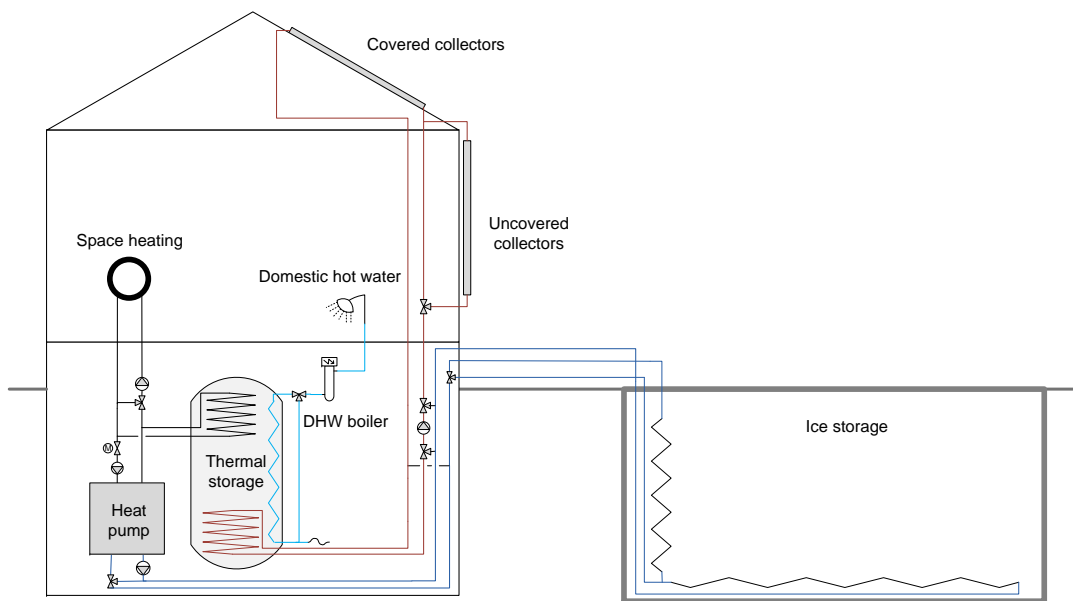
Figure 4.2: Simplified hydraulic scheme of the pilot plant used for validation of the energy simulations.

A simplified hydraulic scheme of the pilot plant is shown in Fig. 4.2. The building which is supplied by the pilot plant is a kindergarten with a yearly demand of around 35 MWh for space heating and a very low domestic hot water demand. The pilot plant started to operate in February 2013.

Main components of the pilot plant are:

- An ice storage with around 75 m^3 storage water volume which is buried in the garden of the building.

- 50 m^2 of covered selective collectors (Bruderus Logasol SKS 4.0 w), oriented south with and inclination of 40°.

- 14 m^2 of uncovered selective collectors (Energie Solaire SA), oriented west with an inclination of 90° mounted at the façade.

- Sensible thermal storage of 3.5 m^3 (FSave GmbH) with three heat exchangers. One for loading from the collector field in the bottom part, one for loading with the heat pump in the upper part, and the last one to provide or to pre-heat domestic hot water.

- Brine to water heat pump (Lexeta SI 18 TU) with 17 kW at B0/W45 with a COP of 3.6.

- Brine made of de-mineralized water and mono-ethylene-glycol with a concentration of 34% (Osterwalder Freeze Protection).

To calculate the energy flows of all relevant system components their volume flows and in- and outlet temperatures were measured. Also important temperatures like the ground temperature around the storage at several locations were monitored (Fig. 4.3(a)). Temperatures were measured with Pt100 4-wire-sensors calibrated in pairs where necessary for accuracy, or with Pt1000 sensors. Volume flows were measured with magnetic inductive flow meters (Endress + Hauser Promag). Solar irradiation was monitored per collector field with Pyranometers (Kipp & Zonen CM-5). Long wave radiative exchange was monitored with a Pyrgeometer mounted in the plane of the uncovered collector field (Kipp & Zonen CGR 4). Also ambient temperature and relative humidity were measured. The measurement data was recorded with a high temporal resolution of 1 second if needed with data acquisition devices (Yokogawa DA100-1, WAGO 750-352). The data was averaged every minute for the simulations and for the calculation of energy outputs.

The ice storage of the pilot plant is a rectangular box made of concrete with the following inside dimensions: $L = 9.2$ m length, $W = 4.4$ m width and $H = 2.11$ m height; with a total water volume of 74.6 m^3. A scheme of the ice storage buried in the ground is shown in Fig. 4.3a (cross section with $W \cdot H$). A photograph taken inside the ice storage is presented in Fig. 4.3(b), where several heat exchangers can be seen in the bottom part with horizontal flow direction and at the background on the wall with vertical flow direction.
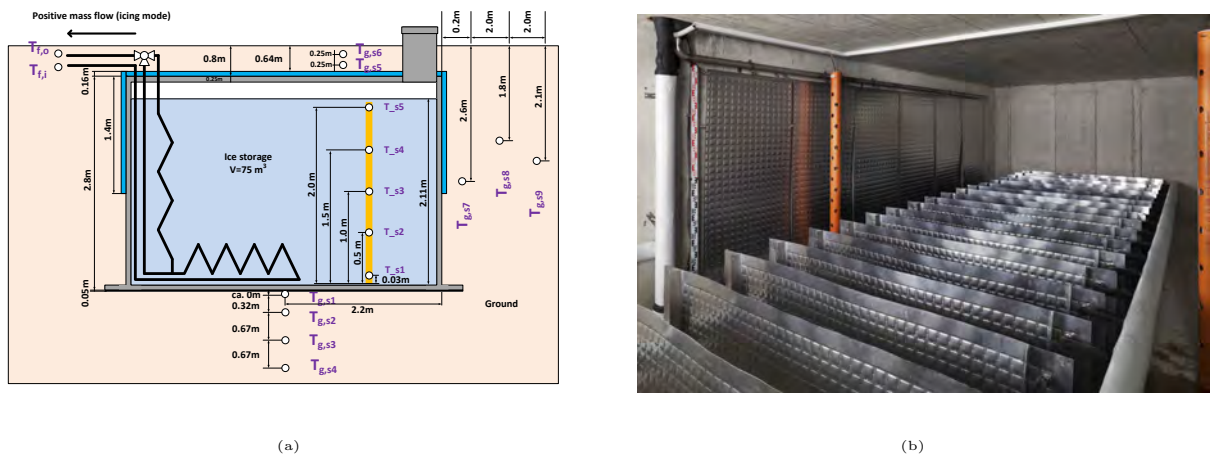
Figure 4.3: Pilot plant: (a) scheme of the buried ice storage in the ground with geometry, sizes and temperature sensor positions (purple markings) and (b) view into the ice storage before filling it with water.

The heat exchangers on the bottom are used to build ice and can be de-iced thermally. 24 hx are used in parallel, each with an area of 2.10 m^2 (area including both sides of the heat exchanger). The positions of the hydraulic connections relatively to the ice storage height are 4% and 26%.

At one wall of the storage 6 parallel hx of 3.23 m^2 each are connected in parallel. Height of the connections is 14% and 92%. The heat exchangers on the wall serve for stratified loading and unloading of the ice storage with sensible heat. They are not allowed to build up ice and are bypassed in case the brine is below 0°C. If the ice storage temperature is above the needed temperature for heating (e.g. >30°C, at the beginning of the heating season) the stored sensible heat can be used directly via the wall heat exchangers without the heat pump.

Several temperature sensors are placed in and around the ice storage (Fig. 4.3a). The storage water temperature is measured at five evenly distributed heights (1%, 25%, 48%, 71%, and 96% relative to the storage height[3]). Nine different sensors are located in the ground around the storage: four below, two above and three on the side of the storage (side with $L \cdot H$).

For validating the ice storage model together with the ground model, measured inlet temperatures and mass flow rates of the heat exchangers, the initial temperatures of the ground and climate data (solar irradiation and ambient temperature) are used. The amount of ice in the storage was not measured as this measurement is difficult to carry out due to the fact that the ice is floating and the level of the water for this case is independent from the amount of ice inside the storage.

---

[3] Bottom of storage: 0% height; Surface of the water: 100% height

For the validation of the whole transient energy simulations the heating system and also the building were set-up and validated using initial values from the measurement and climate data from the entire year that was looked at. In this period a sensor for the mass flow of the building system was deteriorated. Therefore constant mass flows based on measurements of the following years when the sensor was replaced have been used for calculating the heating demand of the building. Moreover during the year considered some small changes in the control strategies have been done in order to improve the performance and to fix errors. In the simulation the same control over the year without applying the changes was used.

4.4. Laboratory measurements

For validating the ice storage model with heat exchangers that can be de-iced thermally and also for the development of heat exchangers for mechanical de-icing an ice storage was used in the lab.

The shape of the storage is rectangular with a volume of 1 m^3. A figure of this ice storage is shown in Fig. 4.4a. For measuring temperatures Pt100 4-wire-sensors were used that were calibrated in group (accuracy $\pm$ 0.04 K). The temperature of the fluid was measured at the inlet and outlet of each heat exchanger. For the validation of the heat exchanger model the surface temperature near the hydraulic connections of one heat exchanger was monitored. Conditioning of the brine was done with a thermostat (Lauda RP 855). As heat transfer fluid a mixture of 67% of water and 33% of mono-ethylene-glycol (Clariant Antifrogen N) was used. The mass flow of the fluid was measured with a magnetic inductive flow meter (Krohne IFS 5000, accuracy $\pm$ 0.5%). The temperature of the storage water was measured at four different heights: 5%, 35%, 65% and 95% relative to the storage height. During the experiments measurements were recorded every two seconds. Values for data processing and simulations were averaged for every minute.

Experiments for the validation of ice storage and heat exchanger models

The experimental set-up consists of several heat exchangers connected in series (Fig. 4.4b). Two of them are on the wall of the storage (hx_1 and hx_2 respectively), referred to as wall-hx, and the heat exchanger where ice is formed is located at the bottom of the storage tank (hx_3), referred to as ice-hx. During icing the flow is circulating only through the ice-hx at the bottom. All heat exchangers used for the validation are flat plate fully irrigated heat exchangers made of stainless steel (details of heat exchangers are provided in Table 4.1).

(a)   (b)
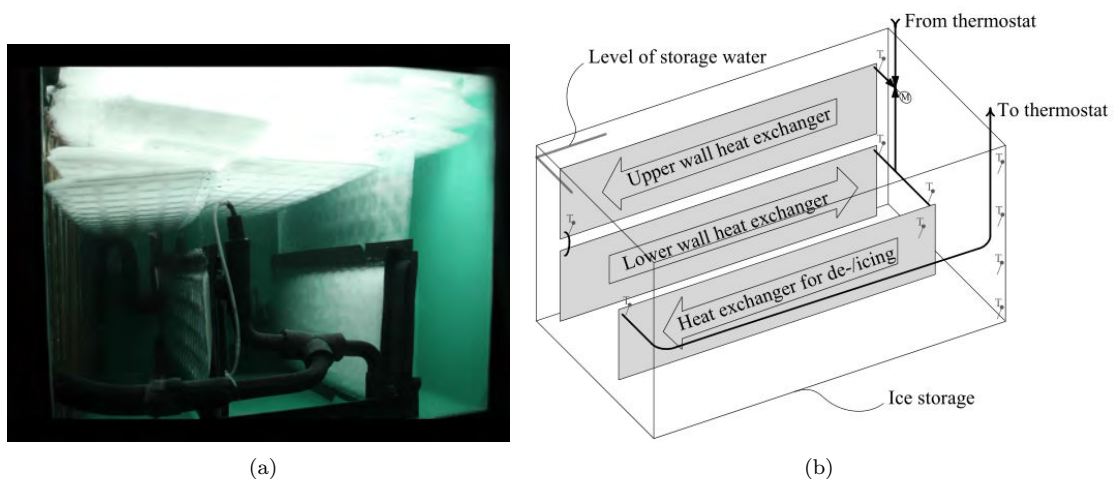
Figure 4.4: (a) Side view into the laboratory sized ice storage during de-icing (bright: ice plates on hx and floating in water) and (b) scheme of experimental set-up for the validation of the ice storage model.

Ice storages may be used not only for icing, but also as a long term sensible storage tank. Therefore it is necessary to validate the model not only for icing and de-icing, but also for heating and cooling with natural and forced (via heat exchangers) convective heat exchange processes. Moreover, the formation

Table 4.1: Characteristics of the heat exchangers for validation in lab. Length L_{hx}, height H_{hx}, and area A_{hx} of the steel plates with thickness of 6 mm, wall thickness δ_p of 0.9 mm, and conductivity λ_p of 15.3 W/mK. z_{in} and z_{out} are absolute input/output heights of the connections (values in parentheses are relative to tank height).

Heat Exchanger	L_{hx}	H_{hx}	A_{hx}	z_{in}	z_{out}
	m	m	m^2	m	m
wall-hx$_1$ (hx$_1$)	0.90	0.29	0.522	0.70 (100%)	0.41 (59%)
wall-hx$_2$ (hx$_2$)	0.93	0.29	0.539	0.41 (59%)	0.12 (17%)
ice-hx (hx$_3$)	0.90	0.30	0.507	0.10 (14%)	0.40 (57%)

and melting of ice also has to be validated in order to predict the time the ice storage will be full of ice. The following modes were used in the experiments to gather data for the validation:

- **Natural Cooling (NC)**. Cooling down the storage starting at 40 °C by losing heat to the ambient during approximately three days without using the heat exchangers.

- **Forced Heating (FH)**. The storage tank was heated from ambient temperature up to 50°C using all heat exchangers connected in series.

- **Natural Melting (NM)**. Around 70 kg of ice were formed in the storage tank via the heat exchangers before starting the test. After the icing process was finished, the ice was melt due to heat gains of the store from the ambient. However, the mass flow through the ice-hx was circulating with a low inlet temperature not able to produce ice. This procedure was chosen in order to validate simultaneously the heat exchanger heat transfer at low temperatures without producing ice and the melting of ice.

- **Continuous Icing (CI)**. A relatively constant inlet temperature of the heat exchanger at -5 °C was imposed and the ice layer grew at the surface of the heat exchanger continuously. This experiment is of relevance because the thickness of the ice layer was measured and compared to numerical results.

- **Icing and De-Icing (IDI)**. The sequence consists in cooling down to -5°C the inlet temperature of the heat exchanger during one hour. In this period ice was formed on the surface of the heat exchanger. After one hour, a heating period of 15 min was imposed with around 10 °C inlet temperature. During this sequence the ice was melted at the surface of the heat exchangers and the ice plates were detached from the heat exchanger surface when the melted ice layer was thick enough.

- **Icing and De-Icing until Fully iced storage (IDI-F)**. The sequence of IDI was used until the ice storage was full of ice. Two ice-hx were used at the bottom part of the storage. This test is used to check whether the model is able to predict the physical phenomena when the storage is full of ice and ice layers can not detach from the heat exchangers.

It is important to remark that the mass of ice was measured only twice in the experiments NM and IDI, once at the beginning and once at the end of the test. The reason for this is that every time the mass of ice is measured the system is modified considerably. The storage tank is opened and all ice is weighted with a net on top of the storage. In this process the ice layers are broken increasing the contact area between the ice and the liquid water and therefore accelerating the melting process of the coming periods. Moreover, in order to take the ice out of the storage, the water is mixed with the movement of the hands inside the storage affecting the temperature profiles. Obviously, it is possible to measure the ice with more advanced methods, but for the purpose of the analysis this method was considered to be sufficient. Notice that with floating ice the water level can not be used to measure the mass of ice unless all ice plates are forced to be underwater. The mass of ice is needed to estimate the time when the storage will be full of ice and until this point, results of heat exchanger performance are not significantly affected by the mass of floating ice.

4.5. Calculation of costs

For all analysed heating systems investment costs and heat generation costs for Swiss prices of 2013/2014 are calculated. The comparison of cost is used to find both system designs that have a good efficiency and possibly a good value for money.

The investment costs of the solar-ice systems are based on real costs that were gathered during the realization of a demonstration plant (Philippen et al., 2014). The costs were used to derive cost functions per component. The cost functions are then used to calculate investment costs per specific system size simulated. Investment costs for a ground source heatpump (GSHP) system that is used as a reference are based on two offers of Swiss sellers for a GSHP system that supplies a single family house with heat (Causi, 2014). The cost functions were derived from average costs of the two offers. All received cost functions were verified by a Swiss seller of heating systems in terms that they represent actual average market prices. A table with cost functions of the solar-ice system is given in Appendix A.

For each system the present value of costs and the annuity are calculated as shown in the following using the methodology of VDI (2012) and Bangerter (1985) with some simplifications. Main assumptions for the economic analysis are given in Table 4.2. The electricity prices are taken from the price list of a regional Swiss utility and represent typical prices for small customers. The increase of electricity cost is based on the assessment of this utility.

Table 4.2: Assumptions for calculation of heat generation costs.

Rate of interest	2.0 % p.a.
Analysis period	20 years
Yearly Maintenance	0.25 % of investment costs
Lifetime ice storage casing and bore holes	50 years
Electricity costs (incl. VAT)	Fixed costs: 171 Fr. per year
	Variable costs: 0.13 Fr. per kWh
Increase of electricity costs	1.5 % p.a.

To receive the present value of the total system PV_{System} the present values of costs for electricity used by the heating system (PV_{Elec}), for maintenance (PV_{Main}), and residual values of components (PV_{ResVal}) are added to the total investment costs (I):

$$PV_{System} = I + PV_{Elec} + PV_{Maint} - PV_{ResVal} \tag{10}$$

The costs of electricity is calculated assuming a fixed yearly increase c of the energy price. The present value of electricity costs is:

for $r \neq c$:

$$PV_{elec} = E_0 \cdot \frac{1}{r-c} \cdot \left(1 - \left(\frac{1+c}{1+r}\right)^T\right) \tag{11}$$

for $r = c$:

$$PV_{elec} = E_0 \cdot \frac{T}{1+r} \tag{12}$$

where r is the rate of interest per annum (e.g. 2 % p.a.); c the yearly price change rate of electricity ($c = 1.5\%$ p.a. assumed); E_0 the electricity costs in year 1 and T the observation period in years.

The yearly maintenance costs are derived from the investment costs I by a cost factor m. As simplification it is assumed that part of the maintenance costs is allocated to replacement procurements for pumps, brine, etc. A relatively high maintenance factor m of 0.25 % is therefore chosen. The present value of maintenance costs is:

$$PV_{Main} = I \cdot m \cdot b \tag{13}$$

with:

$$b = \frac{(1+r)^T - 1}{(1+r) \cdot r} \tag{14}$$

where m is the yearly maintenance costs factor related to the total investment I.

Only residual values from ice storage casing and from boreholes (for the reference system GSHP) are taken into account as these components consist of very robust materials (concrete, plastics) and their lifetime therefore is much longer than the observation period of 20 years. A life time of 50 years is assumed for these two components. With a simple approach for the residual value RV the present value PV_{ResVal} is gained by:

$$PV_{ResVal} = RV \cdot (1 + r)^{-T} \tag{15}$$

with:

$$RV = I_{Comp} \cdot \frac{T_{lifetime} - T}{T_{lifetime}} \tag{16}$$

where I_{Comp} is the investment costs of the specific component and $T_{lifetime}$ the lifetime of the specific component.

The annuity of the heating system A_{System}, i.e. the yearly payment of equal amount over the observation period T, is calculated by multiplying the present value with the annuity factor a:

$$A_{System} = a \cdot PV_{System} \tag{17}$$

with:

$$a = \frac{1}{b} \tag{18}$$

The heat generation costs are obtained by dividing annuity and present value by the yearly amount of heat delivered by the heating system or respectively, by the amount of heat delivered over the observation period:

$$HGC_A = \frac{A_{System}}{kWh_{HeatYear}} \tag{19}$$

$$HGC_{NPV} = \frac{NPV_{System}}{kWh_{HeatObservPeriod}} \tag{20}$$

4.6. Life cycle assessment

In order to provide an additional basis for the comparison of different system concepts, we quantify their environmental impacts by means of a life cycle assessment (LCA) (for an introduction see e.g. Frischknecht (2005)).

An environmental impact always needs to be related to a functional unit, which is the basis for comparing the impacts of different products or processes. For the comparison of heating systems the functional unit is chosen to be the providing of 1 MJ of useful heat.

A life cycle assessment study consists of two main stages. First, a life cycle inventory (LCI) is established. In the LCI all relevant materials and processes needed to provide the functional unit are recorded. Hereby, contributions from all life cycle stages, i.e. production, use and disposal of the product are taken into account. In a second step, the ecological impact of the product, i.e. of the functional unit, is determined based on a specific impact assessment method. This second step is referred to as the life cycle impact assessment (LCIA).

For the LCI's in the present study, background data is taken from the database Ecoinvent v3 (EI3) (Weidema et al., 2013). Whenever possible, datasets specific for Switzerland are chosen. Regarding allocation, the "recycled content" system model is adopted, corresponding to the approach used by Ecoinvent version 2. Foreground data is either collected from manufacturers, based on experience gained from the construction of the Kindergarten pilot plant or estimated. The new datasets are established according to the methodology of EI3.

The impact assessments are established with the following three methods: Cumulative Non-Renewable Energy Demand version 1.09 [CED_{nre}] (Hischier et al. (2010), Pré Consultants (2014)), Ecological Scarcity 2013 [Umweltbelastungspunkte (UBP)] (Ahbe et al. (1990), Frischknecht et al. (2009), Pré Consultants (2014)) and IPCC 2013 [Global Warming Potential (GWP)] (IPCC (2007), Pré Consultants (2014)). CED_{nre} and IPCC 2013 are so-called single issue methods. The CED_{nre} quantifies the total use of non-renewable primary energy throughout the life cycle of a product in units of energy. The IPCC 2013 method quantifies the global warming potential (GWP) associated to the life cycle of the product in units of [kg CO2-equivalent] within a certain time horizon. In the present study a horizon of 100 years is chosen. The Ecological Scarcity method aims at a more comprehensive assessment of the ecological impact. It contains 19 impact categories (like e.g. energy resources, land use, water pollutants). All impacts are quantified in units of "Umweltbelastungspunkten" (environmental load points) [UBP, Pts] and can be aggregated to a single score.

The system boundary for the LCA is defined such that it includes all components of the heat providing system (including circulating pumps) except for the distribution systems for space heating and domestic hot water. In the inventory, the infrastructure of the circulating pump for space heating and of the electric back-up is neglected. The transport of the system components from the factory to the building site is also neglected, except for the transport of the concrete for the ice storage casing. The transport of the excavated earth is included.

The compilation of the LCI data as well as the evaluation of the impact assessment methods are carried out with the software SimaPro version 8 (Pré Consultants (2014)).

5. Mathematical formulation of new system components

In order to simulate the solar-ice system, several new models were developed. The models developed are: i) ice storage ii) ground surrounding the ice storage and iii) master control of the complete system. They are described in the following sections.

5.1. Literature review

An ice storage model for solar-ice applications needs to have features like consideration of stratification effects, coupling with heat exchangers, losses to the surroundings, and temperature inversion algorithms from standard sensible storage tanks as described e.g in Kleinbach et al. (1993), Newton et al. (1995), Drück (2007) and Cadafalch et al. (2015). Moreover, the ice storage model needs to handle the phase change phenomena, see e.g. Drees and Braun (1995), Jekel et al. (1993), Lee and Jones (1996).

The following features distinguish the modelling of ice storages for solar-ice concepts from the modelling of ice storages for cooling applications:

- The ice tank may be buried in the ground and therefore needs to be coupled to a ground model. The coupling between the ice storage tank and the ground is studied in section 6.1.2.

- The ice storage in a solar-ice system may benefit from stratification effects in warm periods. Therefore, a one control volume approach, as is commonly used for ice storages in cooling applications, may not be accurate enough for solar-ice systems.

- The melting process (charging of the ice storage) is effected by means of heat exchangers and not by direct water circulation in the storage. Hence, in a solar-ice system there is no forced convection in the bulk water of the storage. As a consequence, also the heat transfer coefficients for ice melting are different.

Besides these differences, for the ice storage concept presented here, the de-icing mechanism needs to be modelled, which is not considered in any of the models found in the literature. To the authors' knowledge, all other solar-ice concepts for heating applications that are on the market or in the demonstration stage use ice-on-coil, and de-icing is not possible (see Chapter 2.2).

5.2. Mathematical formulation of the ice storage

The mathematical model for the ice storage is based on the solution of the energy conservation law applied to the water of the storage:

$$\rho \frac{\partial h}{\partial t} + \rho \vec{v} \cdot \nabla h = -\nabla \cdot \vec{q} \tag{21}$$

where h is the specific enthalpy, $\dot{q}$ is the heat in W/m^3, t is the time, $\vec{v}$ is the velocity and ρ the density.

Neglecting the radiative heat transfer, the term $\nabla \cdot \vec{q}$ can be split into the conductive heat transfer between fluid control volumes $\nabla \cdot (\lambda \nabla T)$, the heat exchanged from the surroundings through the wall surfaces $\dot{q}_{ext}$, and the heat delivered by the heat exchangers $\dot{q}_{hx}$. Eq. 21 can be then expressed as:

$$\rho \frac{\partial h}{\partial t} + \rho \vec{v} \cdot \nabla h = \nabla \cdot (\lambda \nabla T) + \dot{q}_{ext} + \dot{q}_{hx} \tag{22}$$

The model neglects the forced convection heat transfer between control volumes because no direct charging or discharging that would lead to a net mass flow from one control volume to the next is possible for this storage. Therefore, the action of the body forces is the only mechanism able to create fluid movement. As typically done in storage tank models (see for example Newton et al. (1995)), a reversion elimination algorithm is used to account for the mixing of layers when the vertical density gradient is positive. With these simplifications and assuming a one dimensional behaviour along the height of the storage y, Eq. 22 can be simplified:

$$\rho \frac{\partial h}{\partial t} = \frac{\partial}{\partial y}(\lambda \frac{\partial T}{\partial y}) + \dot{q}_{ext} + \dot{q}_{hx} \tag{23}$$

Assuming that the solid phase will always remain at the same temperature, the enthalpy of a phase change as a function of temperature can be derived:

$$h = \int_{T_{ref}}^{T} c_p dT + f_l h_f \tag{24}$$

where h_f is the enthalpy of fusion of water and f_l is the liquid fraction which can be obtained with the following expression:

$$f_l = 1 - \frac{M_{ice}}{M} \tag{25}$$

M being the mass of water. Introducing Eq. 24 and Eq. 25 into Eq. 23 one obtains:

$$\rho c_p \frac{\partial T}{\partial t} - \frac{h_f}{V} \frac{\partial M_{ice}}{\partial t} = \frac{\partial}{\partial y}(\lambda \frac{\partial T}{\partial y}) + \dot{q}_{ext} + \dot{q}_{hx} \tag{26}$$

where V is the water volume in the storage tank. The second term on the left side of Eq. 26 is the heat of phase change $\dot{q}_{ice}$, which can be split into the formation of ice on the heat exchanger $\dot{q}_{ice,hx}$ and the melting of floating ice $\dot{q}_{ice}^{m}$:

$$\dot{q}_{ice} = \frac{h_f}{V} \frac{\partial M_{ice}}{\partial t} = \dot{q}_{ice,hx} - \dot{q}_{ice}^{m} \tag{27}$$

Introducing Eq. 27 into Eq. 26:

$$\rho c_p \frac{\partial T}{\partial t} = \frac{\partial}{\partial y}(\lambda \frac{\partial T}{\partial y}) + \dot{q}_e + \dot{q}_{hx} + \dot{q}_{ice} \tag{28}$$

The first term of Eq. 28 represents the accumulated sensible heat of the fluid. The first term on the right side of Eq. 28 is the heat of conduction between control volumes and it is calculated using the conductivity of water at the specific temperature multiplied by the effective conductivity factor $\lambda_{eff} = \lambda_w(T) r_{eff}$ in order to account for conduction in the walls of the storage. The last three terms are explained in the following sections.

5.2.1. Losses to the surroundings

The second term on the right side of Eq. 28 represents the heat losses to the surroundings through the external surface area of the storage tank A_{ext}. It is calculated assuming a constant heat transfer coefficient U_{ext} for each control volume j as:

$$\dot{Q}_{e,j} = U_{ext,j} A_{ext,j} (T_j - T_{ext,j}) \tag{29}$$

where $\dot{Q}_{e,j} = \dot{q}_{e,j} V$ and T_{ext} is the temperature of the surroundings, which can be either the ground or the air room temperature, depending on whether the ice storage is underground or not. The heat loss coefficient is provided as an input of the model for several surfaces, i.e. top, bottom and lateral side. The latter is split into two values, one for the upper and one for the lower half of the lateral sides.

5.2.2. Heat exchangers

A constant heat transfer coefficient along the fluid path is assumed for the heat exchangers. With this assumption, an analytical solution of the fluid temperature in the heat exchanger can be obtained:

$$T_{f,o} = T_{sk} + (T_{f,i} - T_{sk}) e^{\frac{-U A_p}{\dot{m} c_p}} \tag{30}$$

where $\dot{m}$ is the mass flow rate, T_f is the fluid (brine) temperature of the heat exchanger and the subscripts o, i and sk refer to outlet, inlet and sink respectively. When ice is formed, T_{sk} is defined as the freezing temperature T_{fr} and only one control volume is assumed for the heat exchanger. When there is no ice, the heat exchanger is discretized into several control volumes, if the fluid path is parallel to the normal vector of the plane between different control volumes of the storage tank. In this case the sink temperature T_{sk}

for each section of the heat exchanger is equal to the storage water temperature T_j of the corresponding control volume. If the flow goes perpendicular to the normal vector of the plane between control volumes, a volume averaged temperature of the storage is used as T_{sk} and a single control volume is used. The global heat transfer coefficient is defined as:

$$U = \frac{1}{\frac{1}{\alpha_i} + \frac{\delta_p}{\lambda_p} + \frac{1}{\alpha_o}} \tag{31}$$

where α_i is the internal heat transfer coefficient of the heat exchanger, δ_p and λ_p are the thickness and conductivity of the plate.

In order to calculate α_i standard equations for corrugated plates are used (Cooper and Usher, 2002). The heat transfer coefficient between the flat plate and the storage water α_o is calculated in two ways, depending on if there is ice on the surface of the heat exchanger or not. When ice is present:

$$\alpha_o = \frac{\lambda_{ice}}{\delta_{ice}} \tag{32}$$

and when ice is not present, the natural convection heat transfer coefficient is calculated using the Nusselt number obtained from the generic expression prosed by Morgan (1975) :

$$Nu = C(Ra)^c \tag{33}$$

where Ra is the Rayleigh number and C and n are empirical coefficients that can be adjusted for specific conditions. Common values of C and n from Eq. 33 for a vertical plate are $C = 0.59$ and $n = 1/4$ for laminar flow and $C = 0.1$ and $n = 1/3$ for turbulent flow. An equation for the entire regime of Ra was proposed by Churchill (2002). Nevertheless, in this work, the expression of Eq. 33 is used, as it allows an easy fitting when necessary.

Once the outlet temperature is known, the heat transfer to the storage can be calculated:

$$\dot{Q}_{hx} = -\dot{m}c_p(T_{f,o} - T_{f,i}) \tag{34}$$

The averaged fluid temperature used to calculate α_i can be obtained from:

$$T_{f,av} = T_{f,in} - \frac{\dot{Q}_{hx}}{A_{hx}} \frac{1 - F_{PP}}{\alpha_o F_R} \tag{35}$$

where A_{hx} is the heat exchanger area under consideration and F_R is the removal factor calculated as in Duffie and Beckman (2006):

$$F_R = \frac{\dot{m}c_p}{A_{hx}\alpha_o}\left(1 - e^{\frac{-A_p U}{\dot{m}c_p}}\right) \tag{36}$$

The flow factor F_{PP} is obtained from:

$$F_{PP} = \frac{F_R}{F_P} \tag{37}$$

where F_P is the efficiency of the heat exchanger, obtained as the ratio between the actual amount of useful heat transferred and the amount of heat which would be transferred if the outer surface resistance of the heat exchanger were zero (Logie and Frank, 2013):

$$F_P = \frac{U}{\alpha_o} \tag{38}$$

The temperature of the external surface of the heat exchanger plate, used to calculate α_o, is obtained from:

$$T_{hx,s} = T_{f,in} - \frac{\dot{Q}_{hx}}{A_p} \frac{1 - F_R}{\alpha_o F_R} \tag{39}$$

The surface temperature is also used to predict when ice is formed on the surface.

Because $T_{f,av}$ is used to calculate α_i and $T_{hx,s}$ to calculate α_o, an iterative procedure is needed to solve the heat exchanger model.

### 5.2.3. Ice formation and melting on the heat exchanger

For a time step Δt, the heat of solidification $\dot{q}_{ice,hx}$ can be discretized as:

$$\dot{Q}_{ice,hx} = \frac{h_f \rho_{ice} \Delta \delta_{ice} A_p}{\Delta t} \tag{40}$$

where A_p is the surface area of the flat plate heat exchanger. The term $\Delta \delta_{ice}$ represents the distance by which the solid phase interface moves during the time Δt. The mathematical model for solidification is based on the quasi steady state approximation presented in Baehr and Stephan (2010). It includes the assumption that the capacity of the ice solid layer can be neglected. It is further assumed that the interface layer between the ice and the storage water is at the freezing temperature. Therefore, when ice is formed, the heat transfer coefficient between the external surface of the ice and the storage water is not needed. When the ice layer is growing at the external surface of the heat exchanger, the conductive heat $\dot{Q}_c$ at the interface between the ice and the storage water is equal to the heat of solidification $\dot{Q}_{ice,hx}$ (see Fig.5.1):

$$\Delta \delta_{ice} = \frac{\dot{Q}_c \Delta t}{h_f \rho_{ice} A_p} \tag{41}$$

The conductive heat at the interface is calculated as the heat delivered by the heat exchanger with a negative sign ($\dot{Q}_c = -\dot{Q}_{hx}$).
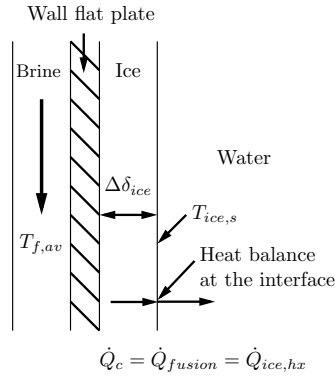
Figure 5.1: Heat balance at the interface between ice layer and water for the solidification model following Baehr and Stephan (2010).

When heat is added while the heat exchangers are covered by an ice layer, ice is melted at the surface in contact with the heat exchanger and $\Delta \delta_{ice}$ is negative. In this case the ice thickness is not used in Eq. 32 and therefore $\alpha_o = 0$.

When the reduction of the ice thickness reaches a critical value $\Delta \delta_{ice,crit}$, the rest of the ice layer is assumed to detach from the surface of the heat exchanger and float up to the surface of the ice storage. After this process, ice layers are rearranged from top to bottom. Since ice layers are arranged chaotically and some water remains between the different layers, only a certain mass of ice is allowed in each storage control volume, which is defined as a parameter. The mass of ice on the heat exchangers is subtracted from the mass of water for each control volume. Total mass and volume are conserved for each control volume, i.e. the expansion of the ice is neglected. Melting of the ice plates on the surface in contact with the heat exchangers is only possible with heat coming from the heat exchanger. Melting of ice plates on the surface in contact with the storage water is not considered. This assumption is valid, because ice plates are not expected to remain on the surface of the heat exchangers for long periods, due to the applied de-icing concept.

As soon as the volume above the heat exchangers is filled with floating ice plates, ice layers are assumed to stick to the surface of the heat exchangers and de-icing is no longer possible, until some ice is melted in

the upper part of the storage. The ice storage volume corresponding to the height of the heat exchangers can also be partially filled with floating ice before de-icing is blocked.

5.2.4. Melting of the floating ice

When the ice layers detach from the heat exchangers, they float up to the water surface at the upper part of the storage, where they can be melted. The calculation of the melted floating ice for each control volume j is simplified assuming a global heat transfer coefficient:

$$\dot{Q}_{ice,j}^m = \alpha_j^m A_{ex,j}(T_j - T_{fr,j}) \tag{42}$$

where α_j^m is the heat transfer coefficient between the ice plates and the water. This coefficient is calculated using the generic Eq. 33 with coefficients from the heat transfer between a colder upper plate and a warmer fluid below the plate (Incropera et al., 2006), i.e. $C = 0.15$ and $n = 1/3$. The temperature of the ice $T_{fr,j}$ is assumed to be 0 °C. The area of exchange A_{ex} between ice and water from Eq. 42 is obtained from:

$$A_{ex,j} = \frac{M_{ice,j}}{\rho_{ice}\Delta\delta_{av}} \tag{43}$$

where the average thickness of the ice plates $\Delta\delta_{av}$ is assumed to be 1cm.

5.2.5. Temperature inversion algorithm

A temperature reversion elimination algorithm that forces fluid temperatures of the different layers to increase with height allowing for stratification effects has been implemented (see e.g. Newton et al. (1995)). When the storage tank is heated at a position other than the top, a positive vertical density gradient provokes a fluid instability, which in turn causes a mixing process due to natural convection. This process ends up with higher and uniformly mixed temperature in the upper layers. A volumetric infinitely fast mixing model was assumed. The model developed here also considers that at 4°C the density of water is at its maximum, i.e. stratification for temperatures below this value is always with the coldest temperature at the top. During icing, it is common to have 0°C at the top and 4°C at the bottom.

5.3. Mathematical formulation of the ground model

The ground model is solved using the transient heat conduction equation in cylindrical coordinates with a heat source term $\dot{q}_v$, which represents the heat coming from the ice storage:

$$\rho c_{p,g} \frac{\partial T_g}{\partial t} = \frac{1}{r}\frac{\partial}{\partial r}(\lambda_g r \frac{\partial T_g}{\partial r}) + \frac{\partial}{\partial y}(\lambda_g \frac{\partial T_g}{\partial y}) + \dot{q}_v \tag{44}$$

where r and y are the radial and axial coordinates and the subscript g refers to the ground.

Different boundary conditions are used for the ground model. The ground model is solved assuming axial-symmetry with null gradients at the axes ($r = 0$) and at the end of the domain in the radial coordinate. At the bottom boundary ($y = 0$) a fixed temperature equal to the undisturbed ground temperature, calculated as the average of the monthly ambient temperatures over the year, is used. The boundary surface between the ground and the air is simulated using a heat flux with heat transfer losses to the ambient air:

$$-\lambda_g \frac{\partial T_g}{\partial y} = \alpha_{g,air}(T_g - T_{air}) - \dot{q}_{sol} \tag{45}$$

where the coefficient $\alpha_{g,air}$ is the heat transfer between ground surface and air considering convection and thermal radiation. The solar gains q_{sol} are calculated considering the absorptivity of the ground, defined as an input parameter. Shadows on the ground surface that could, for instance, be caused by neighbouring buildings are not considered in the term $\dot{q}_{sol}$.

5.4. Numerical implementation of the coupled ice-ground model

The partial differential equations of the ice storage Eq. 28 and of the ground Eq. 44 are discretized over control volumes using a fully implicit scheme with a first order time derivative. For the diffusion term a second order central difference scheme is employed. The ice storage is solved one dimensionally along the axial coordinate y with equally distributed control volumes. The discretized form of Eq. 28 is expressed in the form (Patankar, 1980):

$$A_P T_P = A_S T_S + A_N T_N + B \qquad (46)$$

where the subscript P refers to the nodal value of the control volume under consideration j, and N and S represent the nodal values for North and South nodes respectively. The terms Q_{hx} and Q_{ice} are fully included in the term B. The resulting discretized equation is solved using the tridiagonal matrix algorithm (TDMA, see e.g. Patankar (1980)), which is a direct solver for this case.

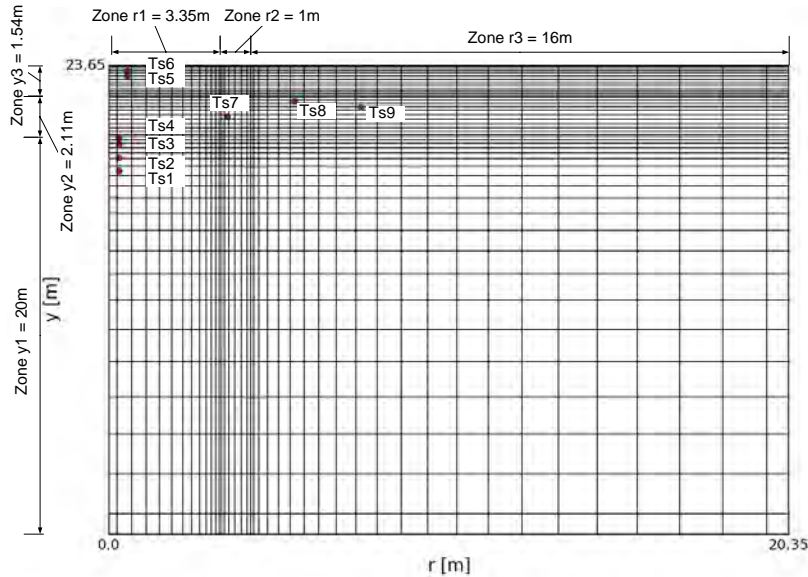The discretized equations of the ground model derived from Eq. 44 are expressed in the form:

$$A_P T_P = A_E T_E + A_W T_W + A_S T_S + A_N T_N + B \qquad (47)$$

where the subscripts E and W represent the nodal values for East and West respectively. Considering that the indexes i and j represent radial and axial coordinates, one can see that, for example $T_E = T_{i+1,j}$ and $T_N = T_{i,j+1}$.

The discretized equation in two dimensions expressed as Eq. 47 is solved using a line by line method combining the TDMA and a Gauss-Seidel iteration.

The discretized ground domain that belongs to the ice storage is considered as an internal boundary condition in the ground model and thus is not solved. At the interface between the ice storage and the ground a Newman boundary condition is defined with the heat flux calculated in the ice storage as heat losses to the exterior (term Q_e in Eq. 28).

The discretized mesh in all the physical domain is shown in Fig.5.2 with three different zones for both r and y axes.

Figure 5.2: Example of a cylindrical axial-symmetrical discretization of the ground around the ice storage with the different discretized zones in r and y axes. Red dots are the positions of the sensors used to compare numerical results with the experiments (see Chapter 6.1.2).

The ground domain can be divided in different zones where ground properties and number of control volumes can be defined separately. The three zones in r direction, r_1, r_2 and r_3, are defined with sizes of 3.35 m (ice storage radius), 1 m and 16 m length respectively. The zone r_1 is linked with the ice storage

volume, so it is adapted when the ice storage volume is changed. The numbers of control volumes for these zones are $3 \cdot n_{mesh}$, $2 \cdot n_{mesh}$ and $5 \cdot n_{mesh}$, where n_{mesh} is an integer that defines the mesh density. Three zones are defined in the y direction, with 20 m, 2.11 m (ice storage height) and 1.56 m hight. They have $5 \cdot n_{mesh}$, $3 \cdot n_{mesh}$ and $3 \cdot n_{mesh}$ control volumes respectively. Each zone has its own number of control volumes n_{cv} with their own concentration scheme and ground properties. As can be observed in the graph, regions with higher gradients, close to the ice storage, have a denser discretization. The discretized mesh shown in Fig. 5.2 corresponds to $n_{mesh} = 3$ and was used in all simulations, unless otherwise stated.

The algorithm for solving the system of equations of the ice storage is shown in Fig.5.3. Several iterative loops are needed in order to properly solve the ice storage for each time step. When coupled with the ground model, several iteration loops between the two models are needed to reach global convergence. The ground and the ice storage are coupled via the ground temperature at the interface boundaries from the ground to the ice storage and via heat losses from the ice storage to the ground. TRNSYS was used to couple both models. The two models were implemented in FORTRAN 90.
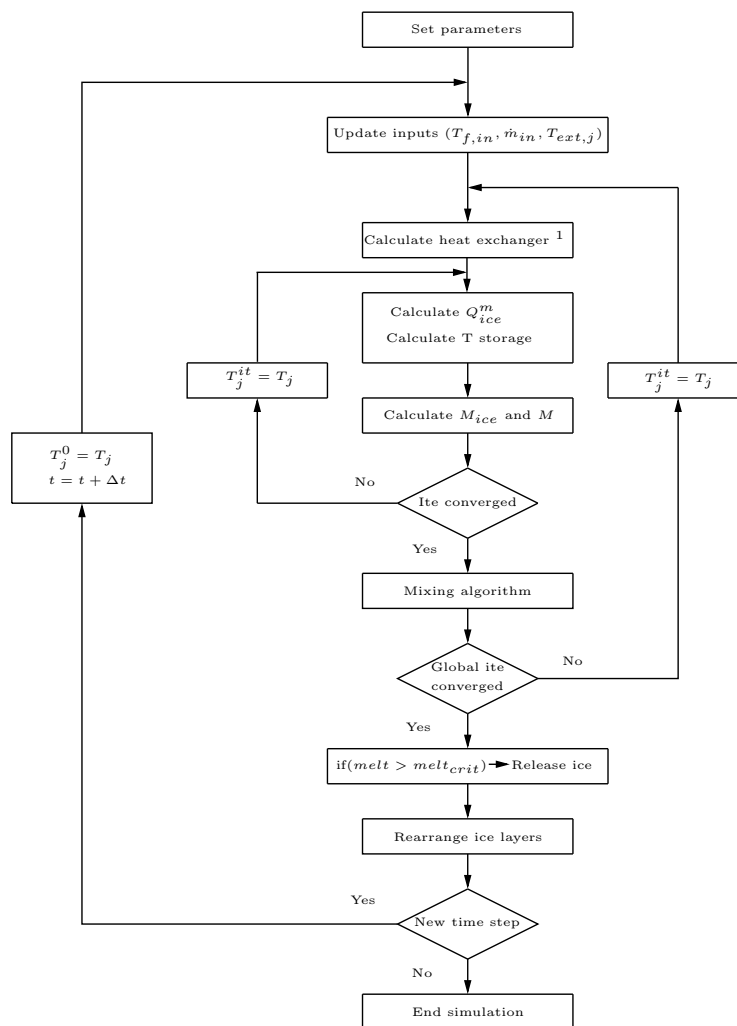
Figure 5.3: Numerical algorithm for the ice storage model. [1]The solution of the heat exchanger also needs an iterative loop.

6. Numerical validation of component models and the system

The key components of solar-ice systems are the solar collectors, the heat pump, the thermal sensible storage, the ice storage and the ground that surrounds the ice storage. At the beginning of the project models were available for solar collectors, heat pump and thermal storage. Models have been developed for the ice storage and the ground. The mathematical formulation of those models has been presented in Chapter 5. The ice storage has been validated in two phases. In the first one presented in Section 6.1.1 a validation is provided using laboratory experiments for an ice storage of 1 m^3. In a second phase the coupled ground and ice storage models were validated using experimental data from a pilot plant with an ice storage size of 75 m^3. These results are presented in Section 6.1.2. The same pilot plant has been the used to validate the whole system (see Section 6.2).

6.1. Validation of the ice storage model

The ice storage model has been validated for a rectangular storage casing using experiments from a 1 m^3 ice storage build in the laboratory and also using monitoring results from a pilot plant installation with 75 m^3 ice storage volume. The experimental set-up for the laboratory scale ice storage is described in Section 4.4. A brief description of the pilot plant used to further validate the ice storage and the whole system is given in Section 4.3.

6.1.1. Validation of a rectangular ice storage tank with laboratory measurements

A validation process with comparisons between numerical calculations and experimental data of a laboratory scale ice storage of 1 m^3 is provided. Six cases of interest, namely NC, NM, FH, CI, IDI and IDI-F, explained in section 4.4, are used for the validation process. As explained in section 4.4 monitored data was processed and used for simulations using a one minute time step resolution. Nevertheless, for a better visualization, experimental results are shown in the figures with less data points.

Natural cooling (NC)

The first case analysed is the natural cooling process. In this case only the storage temperatures are compared with the experiments since there is no circulating flow through the heat exchangers. This is the easiest case modelled and it is used to calculate the effective conductivity λ_{eff} and the heat loss coefficient to the surroundings U_{ext}. Results for storage temperatures at four different heights are presented in Fig.6.1(a). When the above mentioned values are adjusted, results match very well with experiments. In this case λ_{eff} was set to 2.5 times the water conductivity evaluated as a function of the temperature. The heat transfer coefficient U_{ext} was estimated as 1.4 for top cover, 0.9 for bottom and 1.1 W/m^2K for lateral sides.

Natural Melting (NM)

In this test a nearly natural melting process is investigated. The first part of this validation consist in analysing the heat exchanger performance. The energy extracted from the storage predicted by the model has been compared with the experimental data with very good results (not shown here). The ice-hx was the only hx used for this comparison.

In Fig. 6.1(b) the storage temperatures at different heights (left axis) and the mass of ice in the storage (right axis) are plotted along the time. The storage temperatures are predicted with relatively good precision for all heights. The lower temperature analysed at $z = 5\%$ increases with time due to heat gains from the ambient and the temperature difference with respect to the experiments is small. The upper layers are full of ice and therefore they are at more or less constant temperature. On the right y-axis of Fig. 6.1(b) the mass of ice has been plotted. In the experiments only two measures were taken at the beginning and at the end of the experiment in order to avoid human interference in the results. The prediction of ice melting is in good agreement with respect to the experimental data.
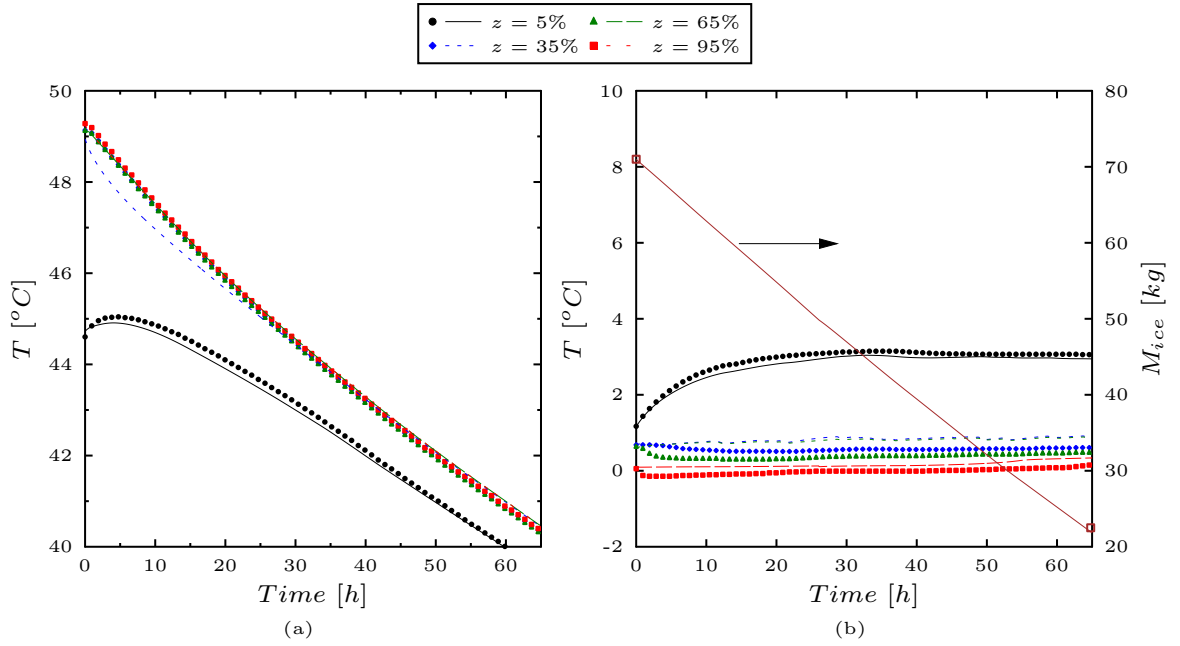
Figure 6.1: Comparison between experiments (symbols) and numerical calculations (lines) for the storage tank temperatures at four different heights of the storage (left axis) in (a) NC and (b) NM along with the mass of ice (right axis).
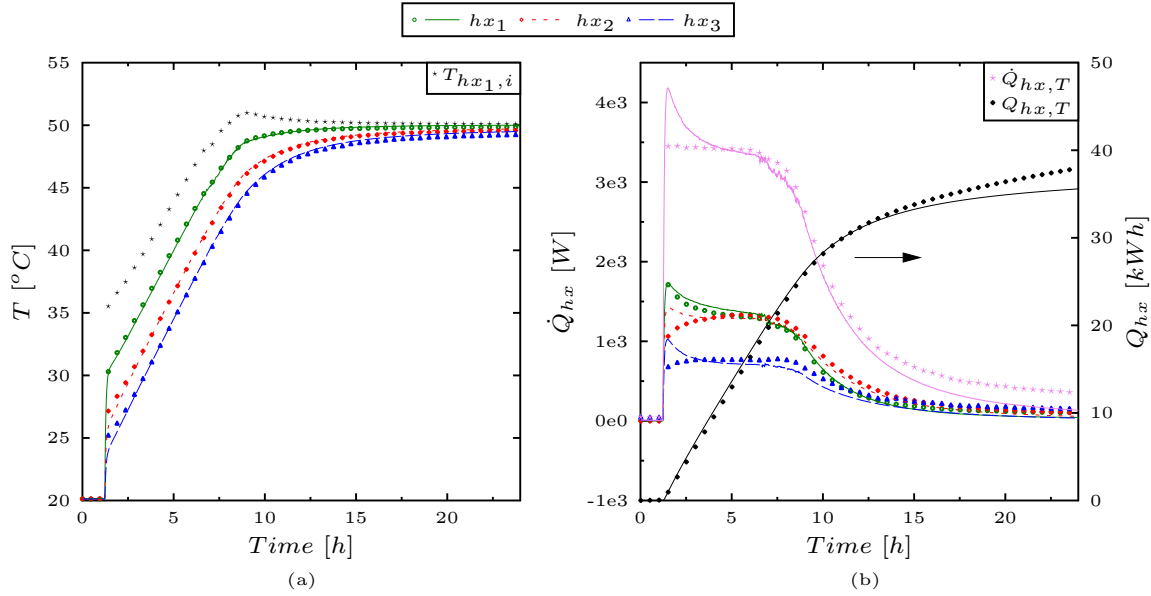
Forced heating (FH)

The forced heating case has been measured in order to validate the heat exchangers performance. The heat exchangers are connected in series from hx_1 to hx_3 (see Section 4.4 and Fig. 4.4 for details). Besides the serial mode, the model also allows a parallel mode with independent inputs for each heat exchanger. The parallel mode is employed to fit the parameters of the heat transfer coefficients for each heat exchanger individually (n value from Eq.33). The series calculation is used for system simulations when the inlet temperature for each heat exchanger is unknown. After the fitting procedure, the series method is used in the results presented in this section. The outlet temperature for each heat exchanger is presented in Fig. 6.2(a) for experiments and numerical calculations along with the inlet temperature of hx_1. In general, temperature predictions are quite precise except at the beginning of the heating period were the transient analysis, that has been neglected in the present model, is of importance.

The assumption of steady state leads to an over-prediction of the heat exchanger performance providing more heat than in the experiments when heating starts (see Fig. 6.2(b)). The peak at the beginning of the heating period is only observed experimentally in the first heat exchanger. In the rest the sharp increase of inlet temperature is relaxed by the thermal capacity of the heat exchangers. The sum of power of all heat exchangers ($\dot{Q}_{hx,T}$) is also presented in Fig. 6.2(b). Comparing this value with experiments it can be observed that simulations over-predict heat exchanger performance for around 4 hours and afterwards under-estimated values are obtained. The energy provided by each heat exchanger and the sum of all of them have been calculated. The total value ($Q_{hx,T}$) is presented in the right axis of Fig. 6.2(b). Predictions tend to under-estimate the energy provided at long term. Differences are larger in the region where the temperature difference between inlet and outlet for each heat exchanger is small.

Continuous icing (CI)

The test started without any ice in the storage and on the heat exchangers. A flow of around 200 kg/h was imposed during 15 hours with T_{in} = -4.5 ºC allowing the ice layer to increase continuously on the ice-hx. The wall-hx were not used in this experiment. After approximately 15 hours four measurements of the ice thickness were taken, two on each side of the heat exchanger. One of the sides has a barrier (side$_{w-b}$) to protect the hydraulic connections to ice. The side without barriers is labelled as side$_{w/o-b}$.

Figure 6.2: Comparison between experiments (symbols) and numerical calculations (lines) for case forced heating. Heat exchangers (a) outlet temperature and (b) power provided to the storage tank.

In the $\text{side}_{w/o-b}$ of the heat exchanger two measurements of 54.7 mm and 50.8 mm at beginning and end sections of the heat exchanger were obtained. In the side_{w-b} the measurements were 41.5 mm and 41.3 mm. The average of all four is 46.5 mm. Results of ice thickness are presented in the left axis of Fig. 6.3 and the total energy extracted by the ice-hx is shown in the right axis of Fig. 6.3. The ice thickness at the end of the experiment is very similar to the measured one at the $\text{side}_{w/o-b}$. In the model it is assumed that the ice is formed equally in both sides of the heat exchanger, but this is not observed in this experiment and less ice is formed on the side_{w-b}. Therefore a global over-prediction of the ice formation is obtained with the model. This explains why the energy transferred to the storage is lower in the numerical model, since more ice layer represent a higher resistivity of the ice and therefore a lower heat exchanger efficiency. In the experiments, some energy is used to cool down the ice. This thermal capacity of the ice has been neglected in the model. However, this is not relevant under this specific conditions where the T_{in} is not too far from the freezing point.

Icing and de-icing (IDI)

An icing and de-icing sequence has been imposed in the experiments in order to validate the model under these conditions. In this case only the ice-hx is used (bottom hx of Fig. 4.4). With the IDI sequence almost all examined phenomena take place. Experiments and simulations are presented in Fig. 6.4 and Fig. 6.5.

The outlet heat exchanger temperature is reasonably well predicted. The experimental surface temperature presented is the average of the two surface sensors (see Section 4.4). In the model the surface temperature of the heat exchanger is calculated by Eq.39. When ice is attached to the surface the average between the $T_{hx,s}$ and T_{fr} is presented in the results as $T_{hx,s}$. When there is no ice on the heat exchanger surface, the presented $T_{hx,s}$ is weighted with the storage temperature of the corresponding control volume T_j as $T_{hx,s} = 0.8 T_{hx,s} + 0.2 T_j$. The only relevant case in which $T_{hx,s}$ plays a role is when there is no ice attached to the surface because this value is used as an indicator of the time when ice is formed. When the $T_{hx,s}$ is below a certain threshold, usually lower than 0 ^{o}C due to sub-cooling, water starts to solidify. The need of using a weighted value with the temperature of the storage instead of the value calculated with Eq.39 for $T_{hx,s}$, suggest that the generic expressions used for corrugated plates for the internal heat exchanger coefficient α_i may not be very precise for this heat exchanger and under the conditions imposed here. Nevertheless, the experiments performed in this work are not sufficient to develop an accurate Nusselt expression.

The thickness of ice is shown in the right axis of Fig. 6.4. The ice layer grows until approximately 1.4 cm
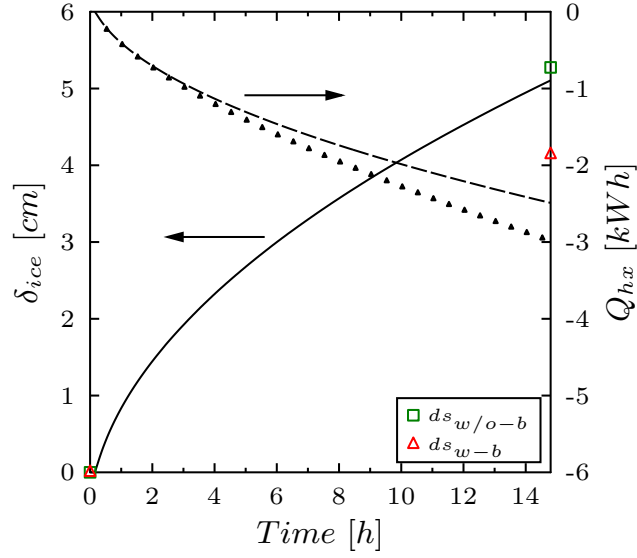
Figure 6.3: Comparison between experiments (symbols) and numerical calculations (lines) for case of continuous icing. Ice thickness (left axis) and energy extracted by the heat exchanger to the storage (right axis). Measurements are shown for the surface with and without barriers, ds_{w-b} and $ds_{w/o-b}$ respectively.
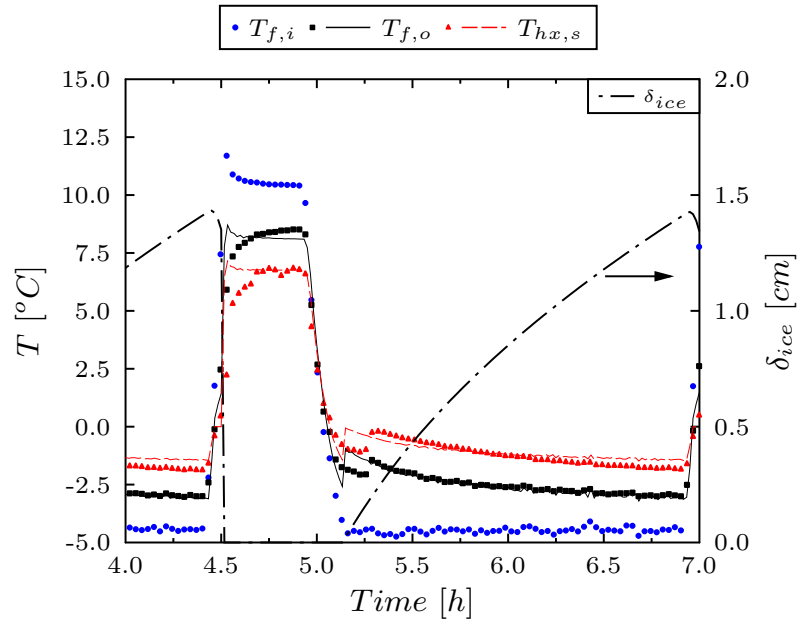
Figure 6.4: Comparison between experiments (symbols) and numerical calculations (lines) for case of IDI. Inlet, outlet and surface temperatures of the heat exchanger in the left axis and ice thickness in the right axis.

in the cooling cycle. When the heating cycle starts and a small ice thickness is melted, the ice layer detaches from the heat exchanger and the ice thickness is zero. As it can be observed the ice formation starts earlier in the simulations with a rapid increase of the surface temperature from the sub-cooled to the freezing state. From these results one can see that simulations react too fast on changes of inlet temperature, which suggest that the consideration of the capacity terms in the heat exchangers may improve the numerical results.

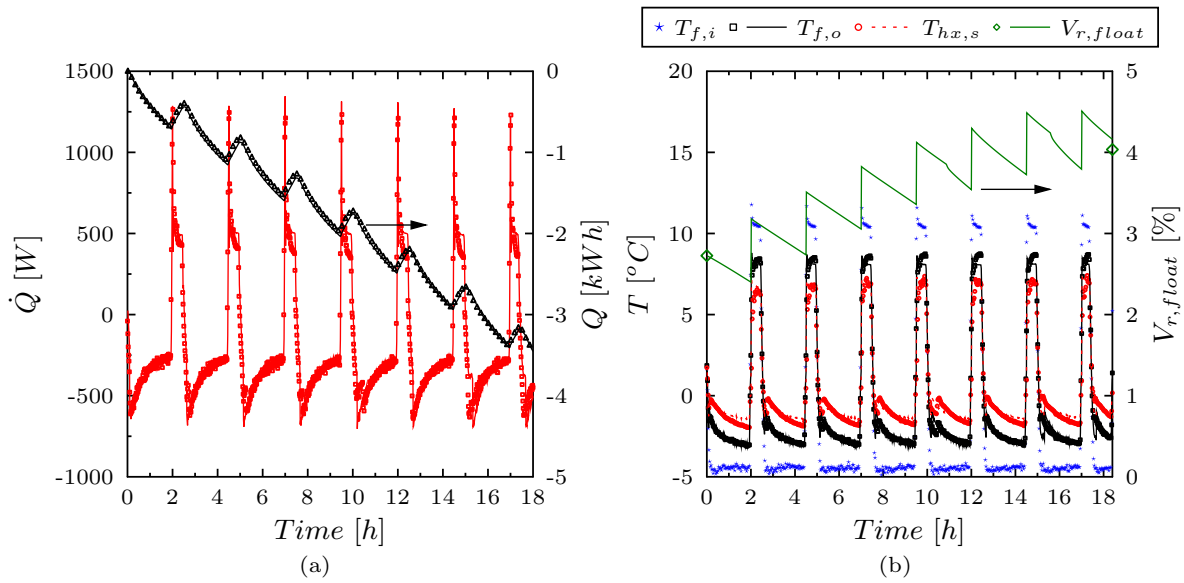In Fig. 6.5(a) power and energy provided by the heat exchanger are shown. Both power and energy

Figure 6.5: Comparison between experiments (symbols) and numerical calculations (lines) for the case of IDI. (a) Power (left axis) and energy (right axis) provided by the heat exchanger to the storage and (b) heat exchanger outlet and surface temperatures (left axis) and ratio of floating ice volume (right axis).

extracted of the heat exchanger presented in Fig.6.5(a) show very good agreement with experimental data. In Fig. 6.5(b) the relevant temperatures of the heat exchanger for the whole experiment are presented along with the ratio of floating ice (right axis). Predictions for this value are in relatively good agreement with the measurements with an over-prediction of the mass of ice. This slight over-prediction may be attributed to the results shown in CI results, where the ice formation is over-predicted because the two sides of the heat exchanger are assumed to ice identically. Another reason may be that the ice starts to form earlier in simulations and therefore the icing process last longer compared to experiments due to the not precise predictions of the temperatures.

Icing and de-icing until saturation (IDI-S)

The cumulated energy provided by the heat exchangers, along with the heating and cooling parts of it, are shown on the left axis of Fig. 6.6(a) for the whole test. As it can be observed, the cooling process is reasonably well predicted along the whole test, but predictions of the heating process show larger discrepancies. At the end of the test after 94 hours, the difference of total energy is in the order of 11%.

The maximum volume allowed in each ice storage control volume is a parameter set to 60%. This value has not been measured and it has been estimated based on a visual monitoring. Nevertheless this value can not be extrapolated to a real scale ice storage because it depends, among other factors, to the ratio between the heights of the heat exchangers that can be de-iced and the upper part of the storage.

The ratio of ice volume is shown in the right axis of Fig. 6.6(a). When a certain volume of the storage above the hx is filled with ice, the model assumes that ice plates can not be detached from the heat exchangers because they can not float up. The simulated ice volume ratio $V_{ice,r}$ increases up to 18% where it stabilize with some fluctuations. Under these conditions in the laboratory-sized storage, ice plates are blocked on the heat exchanger surfaces and the total mass of ice grows slower compared to when de-icing is possible.

This case of icing and de-icing until saturation conditions is a complex case where a lot of uncertainties that affect the dynamics of the process exist. Ice plates can detach or not depending on the positions of the other ice plates that are chaotically floating in the storage. Therefore the goal of this comparison was not to exactly match the experiments but to analyse how the model behaves under these conditions and understand the dynamics of the process to predict the time when the ice storage is full of ice. The uncertainties depend, among other factors, on the ice storage geometry, size and heat exchangers distribution on the lower part.
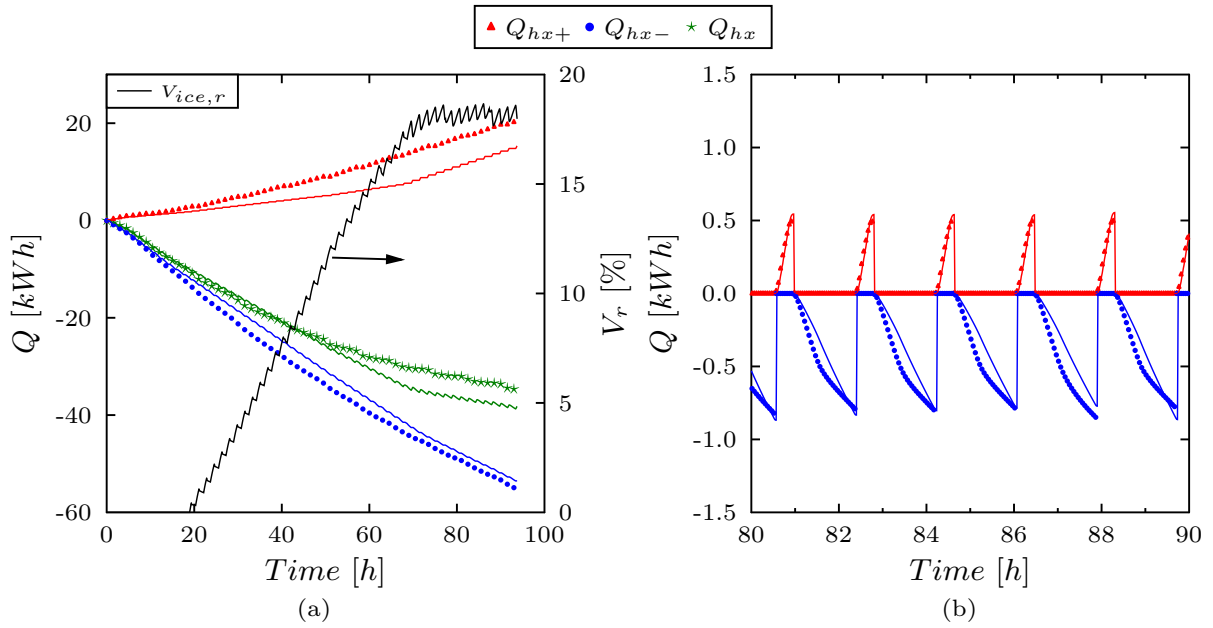
Figure 6.6: Comparison between experiments (symbols) and numerical calculations (lines) for case IDI-S. (a) Cumulated energy provided by the heat exchangers (Q_{hx}) split in heating ($Q_{hx,+}$) and cooling ($Q_{hx,-}$) terms in the left axis and ratio of ice volume in the right axis. (b) Cumulated energy provided by the heat exchangers ($Q_{hx,+}$ and $Q_{hx,-}$) for each heating and cooling cycle. $V_{ice,r}$ is the volume ratio between ice and storage.

6.1.2. Validation of coupled models of ground and ice storage

A validation of the developed models of an ice storage and the ground that surrounds the buried storage with measurement data from a pilot plant is presented in the following. The ice storage from the pilot plant with the positions of the sensors and the monitored values has been described in Section 4.3.

One simplification used here is that the ground model assumes the interface to the ice storage to be of cylindrical shape, even though the ice storage model itself is solved with the real rectangular shape. Otherwise the ground would need to be solved in three dimensions with the increased computational time. The cylindrical interface encloses the same corresponding volume and the same height of 2.11 m as the rectangular storage. The error of this assumption is not expected to be large on a monthly time scale basis.

Ice storage temperatures and ice volume ratios

Simulated and experimental averaged ice storage temperatures are plotted in the left axis of Fig. 6.7a. Numerical calculations correspond very well with monitored data along the whole year.

In the right axis of Fig. 6.7a the simulated ratio between the volume of ice and the total volume of the storage V_r is shown. The pilot plant started to operate in February of 2013 and therefore the mass of ice at that time was zero. Ice is produced until approximately beginning of April (day 90) and at the 5th of May the ice is completely melted (day 125). Ice starts to build again at the 12th of December (day 346), which means that the ice storage is big enough to provide sensible heat, stored in summer period, for the heat pump during October, November and mid December.

Temperatures at three different relative heights of the ice storage have been plotted in Fig. 6.7b. The temperature around the center of the storage (z = 47.6%) is very well predicted. However, temperatures at the lower part (z = 1.4%) are over-predicted and temperatures at the upper part (z = 95.7%) under-predicted. Simulations predict temperatures with lower stratification than the one observed in real conditions. This stratification effect is related, among other factors, to the losses to the surroundings which basically depend on heat transfer coefficients and ground temperatures (see Eq.29) and on the heat exchanger model.
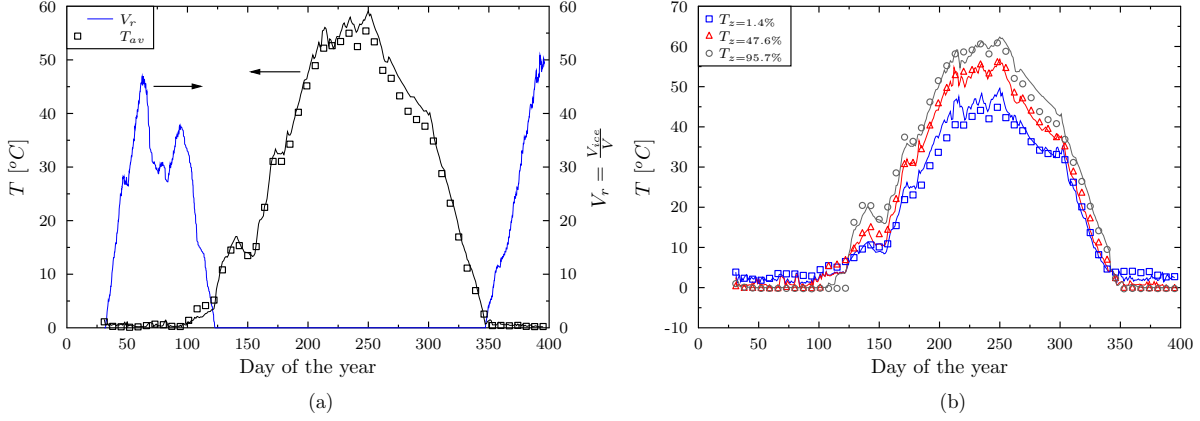
Figure 6.7: Comparison between experiments (symbols) and simulation (lines) for (a) average ice storage temperature (left axes) and ice ratio volume (right axes) and (b) temperatures at different relative heights z of the storage.

Heat exchangers

An important value of interest in the ice storage modelling is its capacity to predict energy flows at monthly and yearly bases. The accumulated energy delivered by the heat exchangers Q_{hx} has been compared with monitored data and it is shown in Fig. 6.8.
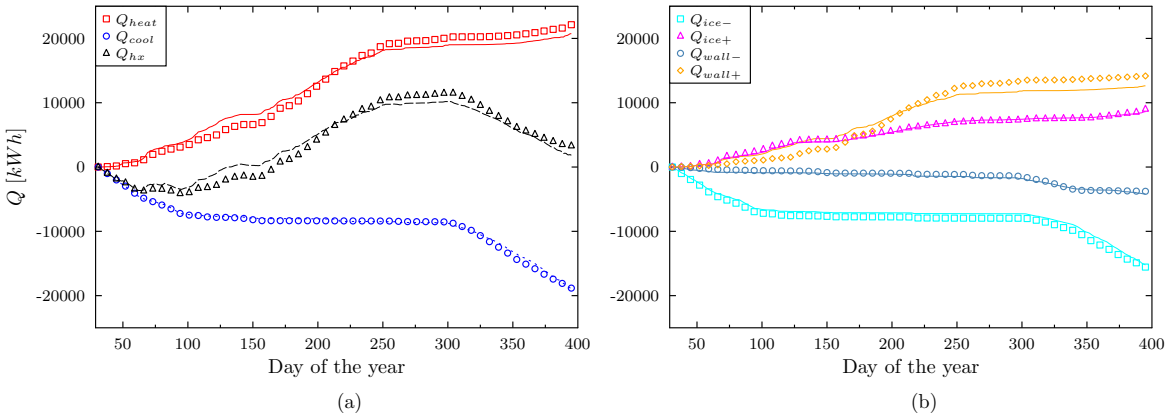
Figure 6.8: Comparison between experiments (symbols) and simulations (lines) of accumulated heat input (+), heat extraction (-) and total energy (Q_{hx}) for the heat exchangers of the ice storage considering: (a) all heat exchangers together and (b) energy split for each heat exchanger

In Fig. 6.8a the term Q_{hx} has been separated into heat input (Q_{heat}) and heat extraction (Q_{cool}). Results match quite well with monitored data, specially for heat extraction. In Fig. 6.8b the energy exchanged has been split in the two heat exchanger types, i.e. wall and ground mounted heat exchangers. In this graph, it is clear that the wall heat exchanger during heating is the cause of the main differences. In particularly, it seems that the accumulated energy $Q_{wall,+}$ deviates from monitored data until day 250 ($\sim$ 9th of September) where simulated and monitored values seem to go parallel, meaning that calculations are accurate again.

Ice storage

Simulated monthly energy fluxes are presented in Fig. 6.9. In this figure, the sensible energy exchanged by the heat exchangers Q_{hx} has been split in heating (+) and cooling (-). The positive heat provided to the storage from the heat exchangers Q_{hx+} represents the heat provided by the solar collectors, and the negative fluxes Q_{hx-} the energy extracted from the heat pump to provide heating demand. The term Q_e is heat the exchanged with the ground which is positive in winter (the ground heats up the ice storage) and negative in the other months. The term Q_a is the accumulated sensible heat (first term of
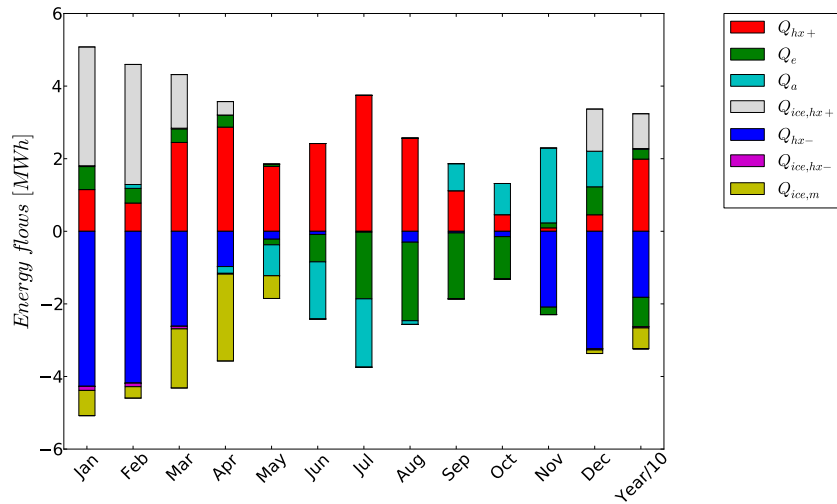
Figure 6.9: Simulated monthly and yearly energy flows in the ice storage (for year: values divided by 10) . All heat fluxes are explained in the text except Q_a which refers to the accumulated sensible energy in the storage.

Eq. 28) which represents both the release of sensible energy from the storage in the positive axis and the accumulation of heat in the negative axis.

Sensible heat is accumulated in May, June and July and it is released in September, October, November and December.

Notice that in this kind of system the collector field is largely oversized for summer periods. Therefore losses to the ground can easily be compensated with solar energy that otherwise would not be used and would increase the risk of reaching stagnation.

The latent energy included in the ice on the surface of the heat exchangers $Q_{ice,hx}$ has also been separated in two terms for ice formation (+) and for ice melting (-). The term $Q_{ice,m}$ refers only to the melting of the floating ice. Ice is produced from December to April, as can be observed with the contributions of the term $Q_{ice,hx}+$. In those months the floating ice is also melted (see $Q_{ice,m}$), but the total mass of ice increases in those months because $Q_{ice,hx}+ > Q_{ice,m}$. In April, this tendency is changed and the melting of ice is higher than the production of it and therefore, it is the month where the total mass of ice starts to decrease.

Ground temperatures

Nine different sensors, shown in Fig. 4.3a are used to compare numerical simulations of the ground model with experiments. Simulation and experimental results are presented in Fig. 6.10. The simulated domain in the vertical y-direction extends to 23.65 m (as described in Fig. 5.2) but not all the domain are shown in Fig. 6.10. The positions of the sensors in the simulated ground discretization mesh are shown in Fig. 5.2.
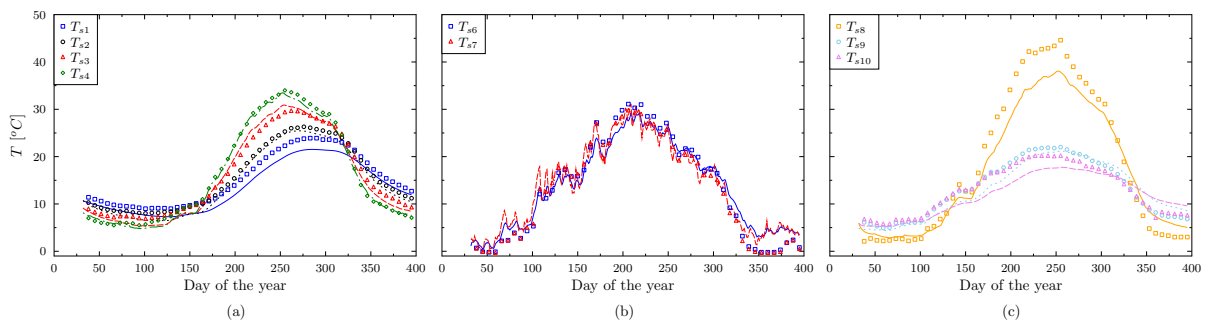
Figure 6.10: Comparison between experiments (symbols) and simulations (lines) of ground temperatures: (a) below , (b) above and (c) at the sides of the ice storage.

Predictions of the sensors below the ice storage (Fig. 6.10a) match qualitatively well with experiments. Predictions tend to cool down the ground too quickly in winter. In spring period, when the ground is heated up, predictions match very well with experiments except for T_{s1}, which is the lowest positioned sensor. After reaching the maximum temperatures around September ($\sim$ day 250), the simulation tends to under-predict temperatures in the cooling process of the ground. One of the main reasons for differences between calculations and experiments is assumed to be the existence of ground water flow, which is quite common in the region where the ice storage is located. Ground water flow has not been considered in the model of the ground. Besides the ground water flow, other phenomena such as e.g. rain penetration effects, grass or other materials on the surface between the ground and the air, shadows on the ground due to nearby buildings, etc. have been neglected.

Temperature of the sensors above the ice storage are shown in Fig. 6.10b and show a good match between predictions and experimental data. Some discrepancies are observed after beginning of December ($\sim$ day 340) when simulations tend to over-predict experimental data. In this graph the influence of the weather on ground temperatures can be seen, since fluctuations of temperatures are much larger compared to temperatures below the ice storage. The monitored data is only plotted every week and therefore some fluctuations may not show.

Results for sensors at the side of the storage are shown in Fig. 6.10c. Predictions are qualitatively good for sensors 9 and 10, but not for sensor 8, which is close to the ice storage. The large discrepancy in T_{s8} can be explained with the simplification of using cylindrical coordinates for a rectangular ice storage. The sensor 8 is at 20 cm from the largest side surface of the rectangular ice storage.
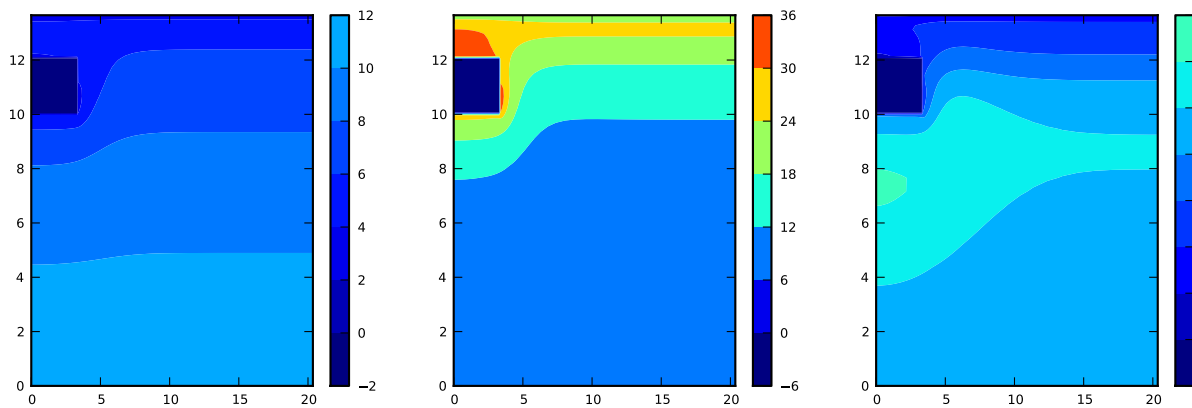
Figure 6.11: Numerical ground temperature at three different time periods of the year: left 1-4-2013, mid 30-7-2013 and right 27-2-2013.

Simulated ground field temperature profiles for three different times of the year are shown in Fig. 6.11. In this figure the ice storage is located in the dark blue rectangle situated on the left side (for plotting purposes, the ice storage is always at a temperature of -1°C, temperatures of the ice storage are not solved in the ground model).

6.2. Validation of the whole system

The building where the pilot plant is installed in is a kindergarten with a low insulation standard and a yearly heat demand of around 35 MWh. Radiators are used in the heat distribution system, which is not very convenient for combined solar thermal and heat pump systems. The domestic hot water demand is very low and has been neglected in the study.

The hydraulic set-up of the installation along with the monitored sensors in the whole system, ice storage, and the ground that surrounds the ice storage are shown in Fig. 4.2 and Fig. 4.3. The description of the pilot plant is provided in Chapter 4. For the simulation of the building the extended version of the ISO model described in Section 4.1.4 is used.

Fitting the building demand

In order to validate the whole solar-ice system a fitting of the simulations results to the real heating demand and to the flow and return temperatures of the heating distribution system is necessary. The building model was parametrized accordingly. Fitting of the monthly energy demand is also desired but sometimes difficult to achieve. Notice that the validation of the building and the radiators models is not possible with the data available.

The parameters of the ISO building model were first based on physical aspects and afterwards modified to fit the yearly and monthly heating demand of the monitored data. Monthly and annual results for the heating demand are presented in Fig. 6.12a (annual results are scaled down by a factor of 10). The total annual heating demand is in good agreement with the monitored values. However, the monthly distribution shows larger differences.
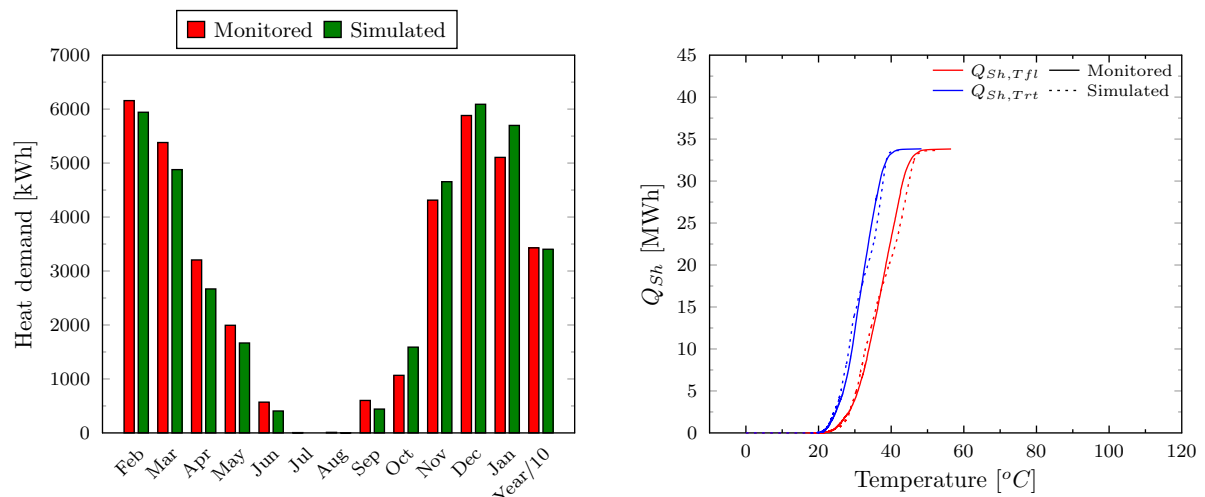
Figure 6.12: Comparison between monitored data of the pilot plant and simulations for (a) space heating demand and (b) flow and return temperatures to/from the radiator.

The cumulated heat provided to the heat distribution system has been plotted as a function of the flow and return temperatures in Fig. 6.12b for both simulation and experiment. This kind of comparison was suggested in Haller (2012) for comparing simulations from different modelling platforms. Differences in the supply and return temperatures of the heating system are expected to have a significant effect on the performance of both, solar collectors and heat pumps. Values from simulation and experiment match well. However, in the simulation roughly one half of the energy is provided at lower temperatures levels and the other half at higher temperatures than in the experiment.

Collector field

The monthly solar irradiation on the collector planes and the averaged ambient temperatures measured in the pilot plant are shown in Fig. 6.13a. This data is used as an input for the system simulation. The monitored and simulated monthly energy fluxes from the collector field to the different components heat pump (Hp), thermal energy sensible combi-storage (Tes), and ice storage, are shown in Fig. 6.13b. Simulated annual solar gains provided to the heat pump and ice storage presented in the last column are quite similar to the measured ones. Nevertheless the energy provided to the combi-storage is over-predicted. Besides this difference, some monthly values differ substantially. Some differences can partially be explained by non-identical system control. Even though experiment and simulation use a similar system control concept, the way they are implemented are not exactly the same.

Balance of thermal storages

The energy flows in and out the combi-storage for both monitoring (left column) and simulation (right column) data are shown in Fig. 6.14a. The energy input to the combi-storage is provided by the collector
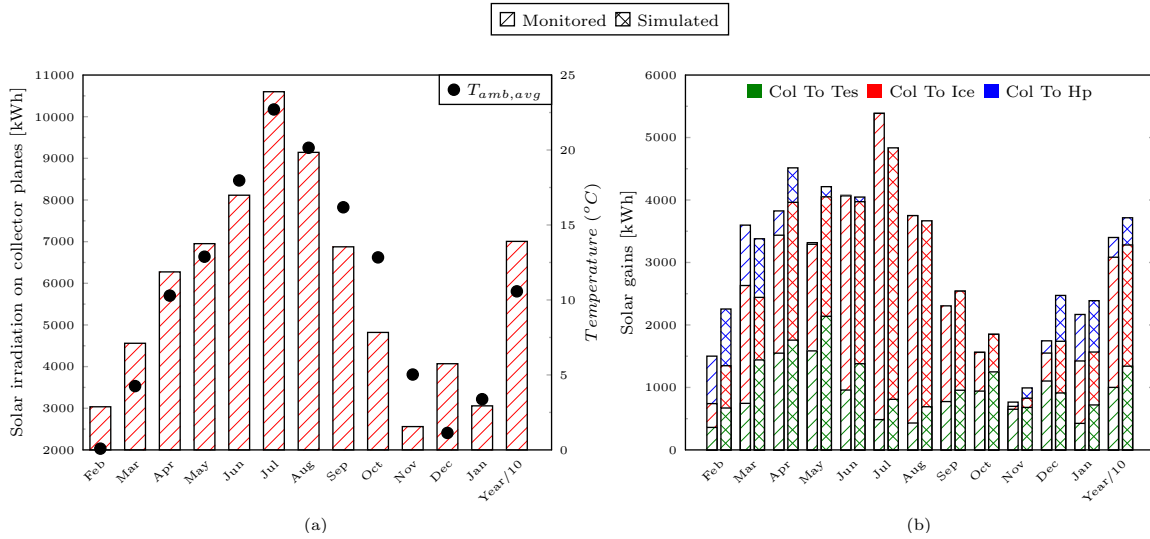
Figure 6.13: (a) Solar irradiation an collector plane (left y-axes) and ambient temperature (right y-axes) for the pilot plant and (b) comparison between monitored data and simulation for solar heat provided for the heat pump, and for thermal (sensible) and ice storage.

field (Col to Tes), the ice storage (Ice to Tes), and the heat pump (Hp to Tes). The negative energy flows are those extracted for space heating (Tes to Sh), ice storage (Tes to Ice) and thermal losses (Tes Losses).
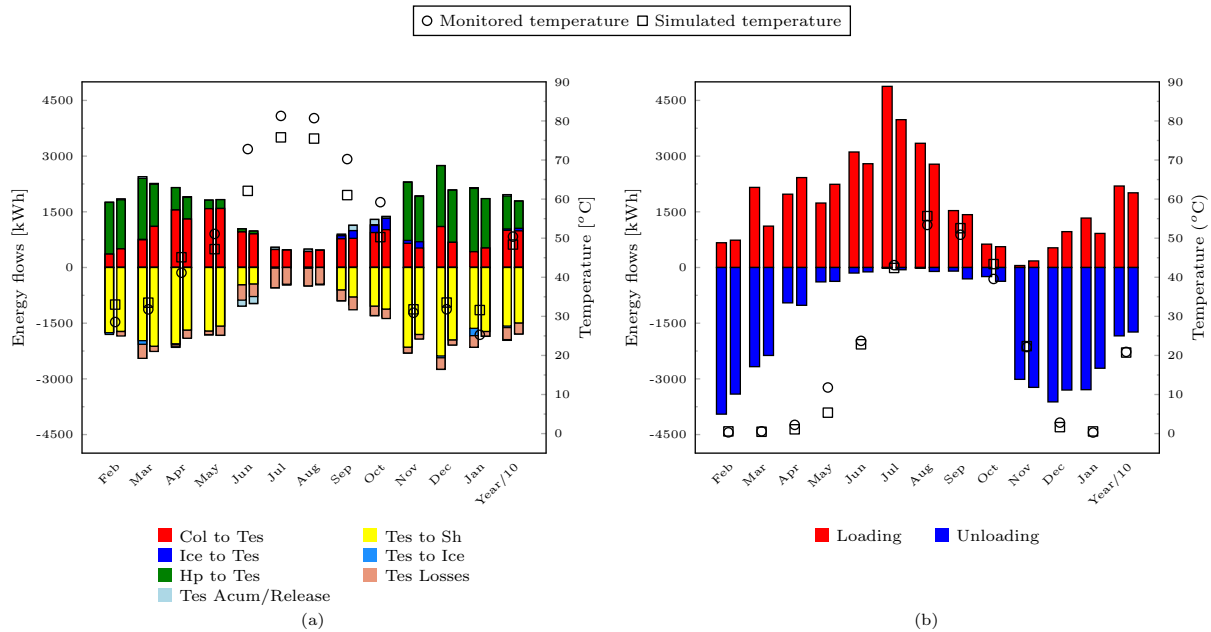
Figure 6.14: Comparison between simulation (left column) and numerical calculations (right column) for the energy flows and averaged storage temperature for (a) sensible thermal storage and (b) ice storage.

All energy flows are obtained directly from the monitoring system except the accumulated/released energy and storage losses. The sensible energy accumulated or released in the combi-storage (Tes Acum/Release) has been calculated using four sensors at different heights of the storage using a volume weighted average. Storage losses are then calculated with the heat balance of the storage. Yearly simulated energy flows in and out of the combi-storage are in relatively good agreement with the monitored values. The real storage gets more energy from the heat pump and provides more energy to the building compared to the simulation. The average storage temperature is shown in Fig. 6.14a. Averaged temperatures of the storage are usually under-predicted in warm periods and over-predicted in cold months which could

explain why the simulated heat pump needs to provide less energy to the combi-storage. This temperature over-prediction could be due to control differences and/or due to different heat losses in the combi-storage. The heat loss coefficient of the combi-storage has not been analysed in detail. Although the combi-storage was build on-site, typical values from other similar storages have been used for the heat loss coefficient of the storage and also for the heat transfer values of heat exchangers in the simulation.

The energy flows for the ice storage are presented in Fig. 6.14b along with the averaged temperature in the ice storage. Yearly heating and cooling energy flows are in relative good agreement with monitored data. However both heating and cooling energy flows are under-predicted. The average temperature in the ice storage is well predicted, better than that of the combi-storage. In the ice storage case, however, a specific fitting of the heat losses of the storage was done in the validation of the ice storage presented in Section 6.1.2.

Overall system performance

Overall energy fluxes in the whole system are shown in Fig. 6.15. The energy balance in the overall system includes as inputs to the system: energy from the collector field to the heat pump (Solar to Hp), ice storage (Solar to Ice) and to the combi-storage (Solar to Tes); the electricity to run the heat pump and the heat from the ice storage (From Ice storage). Energy outputs of the system are the space heating demand, the losses in the combi-storage (Losses TES), the losses in the piping (only included in simulations) and the energy delivered to the ice storage (To ice storage). The energy from the ice storage includes sensible heat release and ice formation, while the energy to ice storage includes accumulation of sensible heat and ice melting. The predicted yearly energy flows of the system shown in the last column of Fig. 6.15 are in very good agreement with the monitored values.
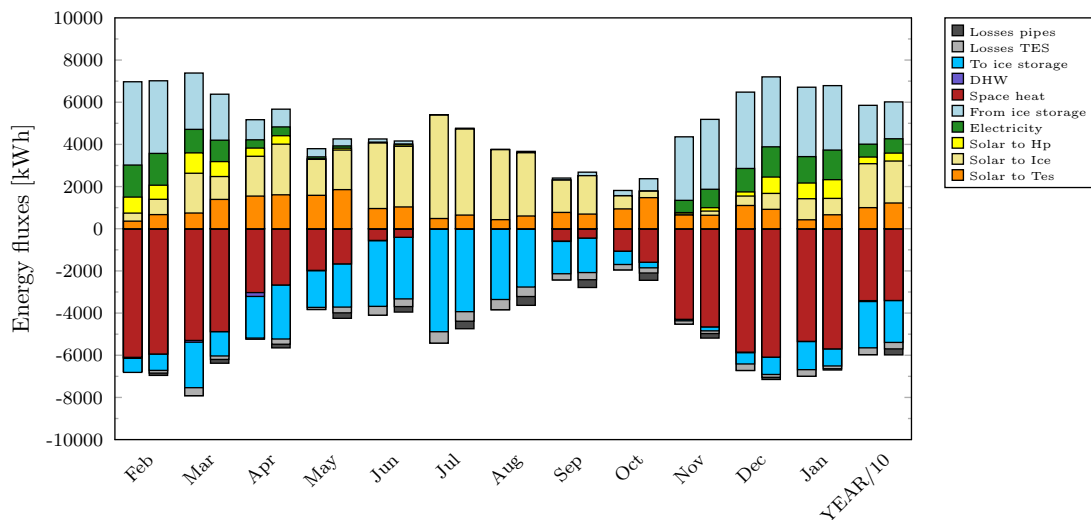
Figure 6.15: Comparison of system energy flows between monitored data (left column) and simulations (right column).

The electricity consumption and the system performance factor SPF_{SHP+} are presented in Fig. 6.16. The simulated yearly electricity consumption is in relatively good agreement with monitored data. Nevertheless, simulated results over-predict the electricity consumption of the heat pump in April, November and December due to the larger running times of the simulated heat pump. As a consequence, the yearly electricity consumption (last column of Fig. 6.16(a)) is also over-predicted.

The system performance SPF_{SHP+} is shown in Fig. 6.16(b) with a predicted yearly SPF_{SHP+} of 4.5. In general, results are in reasonable agreement with monitored data with larger differences in May and September. However, in those months the heating demand is low and therefore the effect of the monthly SPF_{SHP+} on the yearly system performance is not relevant. Because simulations over-predict the electricity consumption, the annual SPF_{SHP+} is slightly under-predicted.
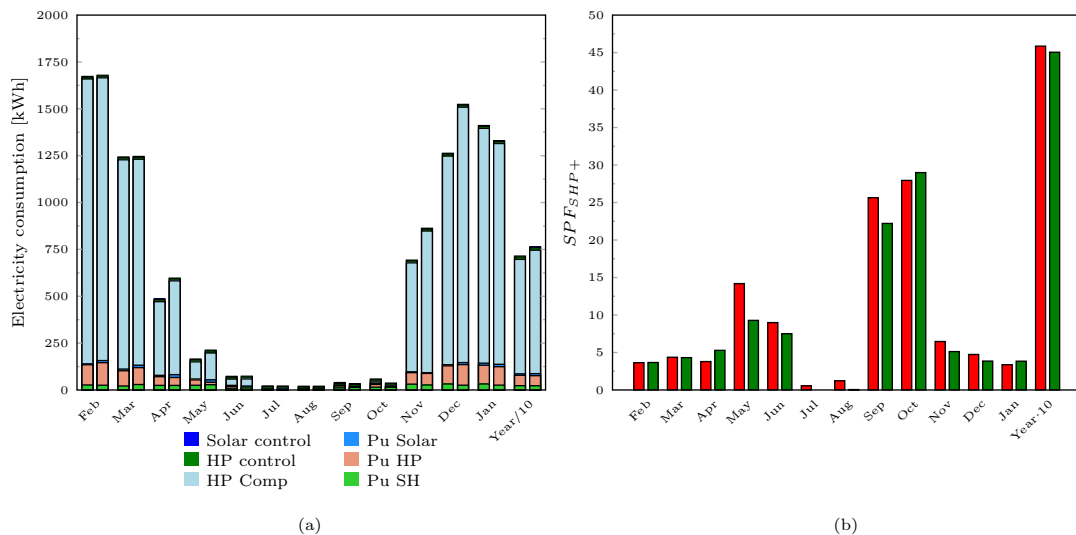
Figure 6.16: Comparison between monitored data (left column) and simulations (right column) for system (a) electricity consumption and (b) seasonal performance factor.

6.3. Conclusions

As first step, the validation of the model was provided by means of comparisons with experiments of a laboratory scale ice storage. Several operating modes were investigated in order to validate the model under all conditions of interest. The model describes successfully natural cooling, forced heating, natural melting and icing, and de-icing for the main variables of interest such as heat exchanger outlet temperature, energy exchanged, and production and melting of ice. The case when the ice storage is completely filled with ice plates has been shown to be a difficult case for the simulation and the model can not be very accurate under these conditions due to the large number of uncertainties, chaotic effects, and model simplifications.

As second step, an annual simulation has been compared with one year of monitored data from a pilot plant with a 75 m^3 buried ice storage. Averaged temperatures of the simulation are in very good agreement with experimental data. Nevertheless, stratification is not perfectly predicted and lower temperatures at the upper part of the storage, and higher temperatures at the bottom are observed in the simulation. The simulated energy transferred by the heat exchangers is in good agreement with experimental data. In particular, heat extraction is better predicted compared to heat loading, as temperatures in the storage are better predicted for the winter season. The loading in summer is not very well predicted and higher temperatures at the lower part of the storage are simulated.

Ground temperature predictions are in good agreement with experimental data. The simplification of modelling a cylindrical storage-interface in the ground have been found to be relevant for the prediction of temperatures close to the ice storage. However, the error was found to vanish rapidly and predictions of temperatures at higher distances were found to be in a reasonable agreement with monitored data. Given the number of uncertainties, such as ground properties, ground water flow and other non considered phenomena, and considering the simplifications made to ensure short simulation time, predictions of ground temperatures were found to be satisfactory.

A validation of the whole system has been carried out. Results for main values of interest such as energy flows in and out of key components, and the global system were found to be in good agreement with monitored data. However, some monthly data was not well predicted. Electricity consumption and system performance, probably the most relevant factors, were found to be in good agreement.

Concluding, the developed models for an ice storage and its surrounding ground have been successfully validated. Also the whole system simulation was found to predict the behaviour of a real heating system with success. All these validation tasks provide confidence in the simulation tools and the system analyses for the proposed solar-ice concept.

7. Annual simulations of solar-ice systems

With energy simulations in TRNSYS the dependence of the system performance factor SPF$_{SHP+}$ of the proposed solar-ice system on several parameters is analysed. In Section 7.1 effects of the heat exchanger size in the ice storage, of different control strategies, of components sizes like ice storage volume and collector field size, and of different types of collectors are investigated. Section 7.2 is about the effects when waste water heat recovery devices are included into the brine cycle of the system. In Section 7.3 deals with the performance of the solar-ice system under the different climatic conditions of Davos and Locarno.

7.1. System simulations for Zurich

7.1.1. Sizing of heat exchanger area in the ice storage

With the analysed de-icing concept the heat transfer capacity of the heat exchangers should be related to the highest accepted ice thickness on the heat exchanger and to the heat pump cooling power. Due to the de-icing concept the total area of the heat exchanger can be small and the heat exchangers does not have to be distributed all over the storage volume. In the simulations used here, the heat pump has a nominal capacity of 6 kW for building SFH45* with a COP of 4.8 (at B0/W35). This corresponds to an extraction power of the evaporator of 4.75 kW at the same conditions.

Results for building SFH45* with varying heat exchanger area and ice storage volume are presented in Fig. 7.1 using 20 m^2 of uncovered collectors. The results show that for A_{hx} between approximately 17 and 21 m^2, the SPF_{SHP+} is more or less constant for most of the simulated cases. This heat exchanger area corresponds to 8 and 10 heat exchangers with the specific area simulated (2.10 m^2 including both sides of the heat exchanger).

For theoretical calculations with a steel flat plate heat exchanger, an extraction power of 200 W/m^2 is obtained with an inlet temperature of -3 °C, a mass flow rate of 88 kg/(hm^2) and 1 cm of ice on the surface. The increase of temperature in the heat exchanger is assumed to be of 3 °C. Therefore, to use the full potential of the heat pump under this nominal conditions, around 23 m^2 of heat exchanger area would be needed for the 6 kW heat pump. This theoretical value corresponds quite well with the simulated results of SFH45* using 10 heat exchangers (maximum SPF_{SHP+} in Fig. 7.1a) and it will be used hereafter for SFH45* simulations. However, the choice of these nominal conditions, in particular the choice of 1 cm of ice thickness, depends on the system concept and on the size of components and cannot be extrapolated to other conditions and/or systems.

7.1.2. Control algorithm

In this section, the three main different controls strategies are investigated (see Chapter 3.2). Results using PriorWs and PriorCs are shown in Fig. 7.2 for covered (top) and uncovered collectors (bottom). With PriorWs the control tries to load the combi-storage with solar heat as often as possible also during winter, whereas PriorCs results in loading mainly the ice storage in winter. The control algorithm affects results significantly using covered collectors but it is not relevant when uncovered collectors are employed. The reason is that, when using uncovered collectors, even that PriorWs is activated in winter, the uncovered collectors can hardly load the combi-storage because of their low performance at high collector temperatures compared to the ambient temperature. Therefore, the conditions where the control stops the ice storage loading to switch to combi-storage loading are rather rare.

The system performance of all systems is strongly related to the backup electricity needed to deliver the heat demand, if the ice storage is full of ice and the heat pump evaporator temperature drops below the minimum value allowed [4]. The increase of SPF_{SHP+} per m^2 of additional collector area is higher when backup electrical auxiliary heat is still needed compared to the case when $P_{el,aux}$ is close to zero (see Fig. 7.2(a) and (b)).

For covered collectors the differences between PriorWs and PriorCs are higher. The transition region where the switch from PriorCs to PriorWs improves the SPF$_{SHP+}$ is shown in Fig. 7.2. This region with

---

[4] -10 °C has been used here as the minimum inlet brine temperature allowed
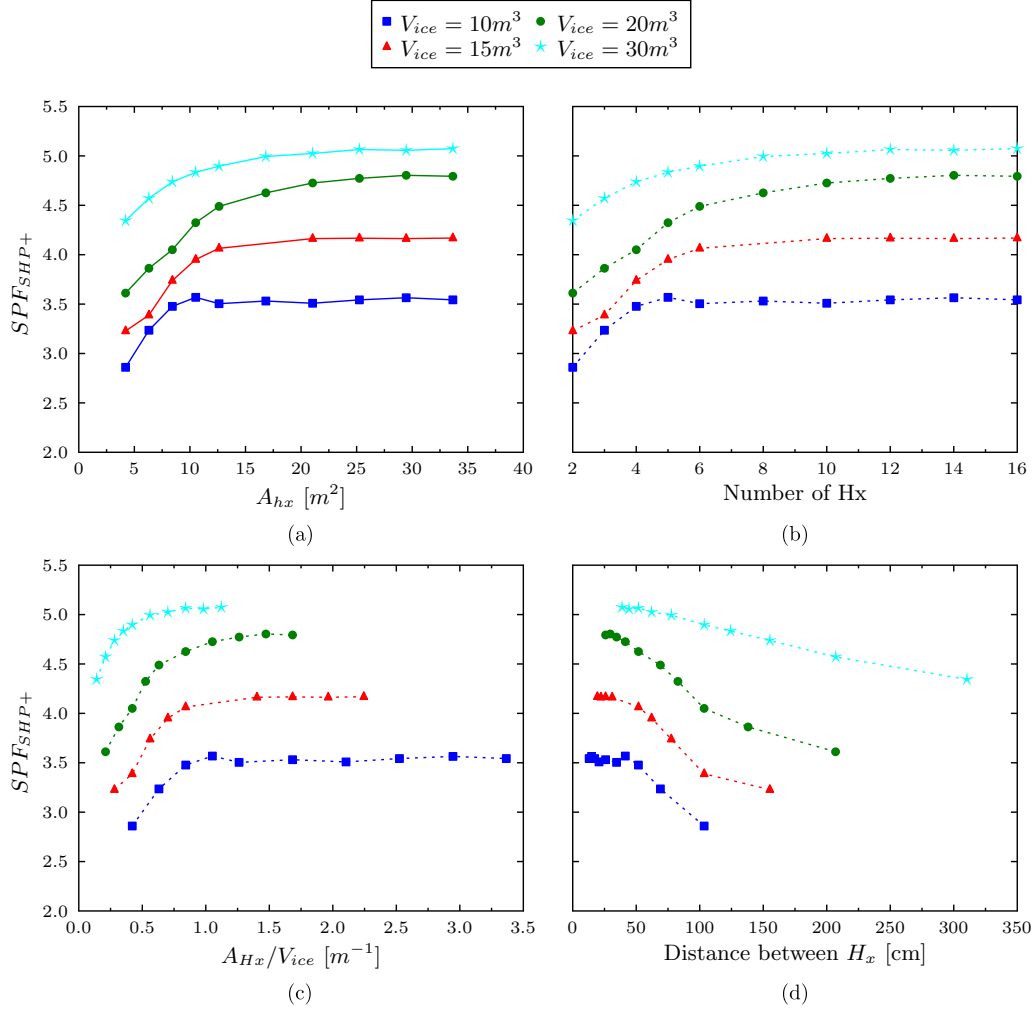
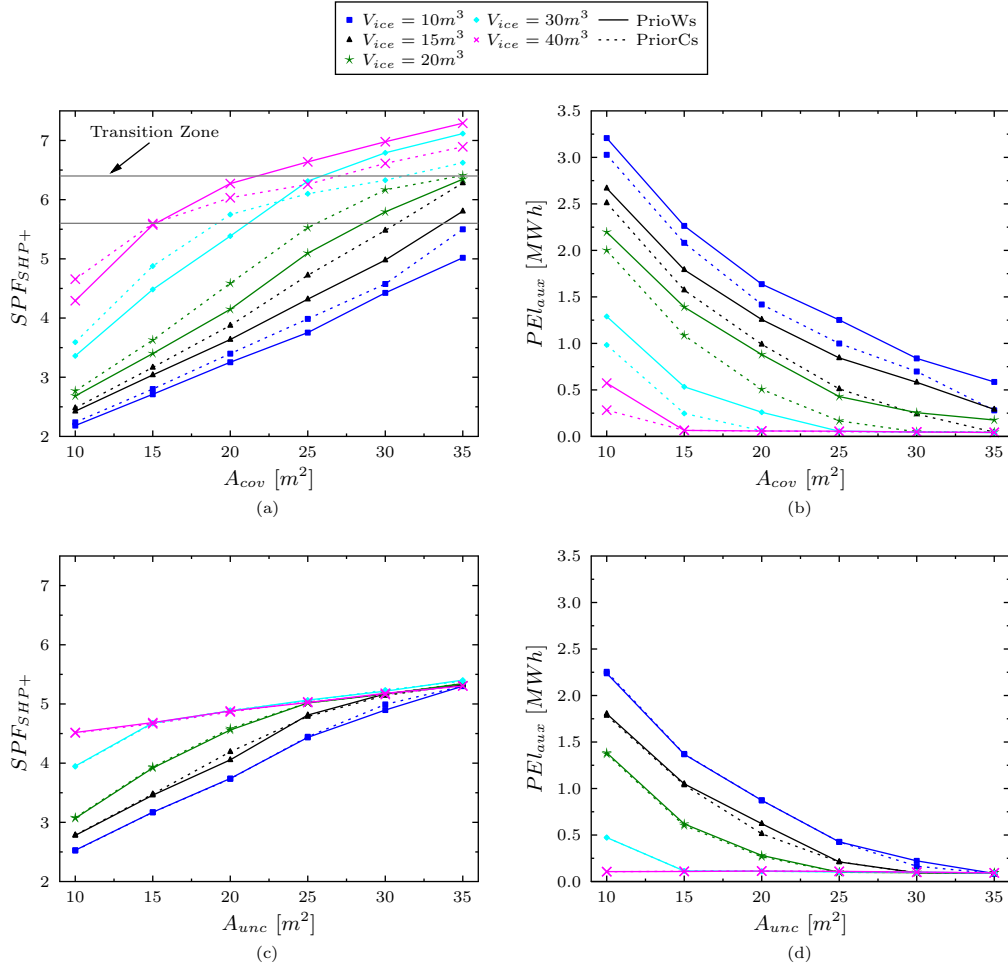**Figure 7.1:** Seasonal performance factor with varying ice storage volume for building SFH45* and $A_{unc} = 20$ m² as function of (a) heat exchanger area (b) number of heat exchangers (d) ratio between heat exchanger area and ice storage volume and (d) distance between heat exchangers.

values of SPF$_{SHP+}$ between 5.5 and 6.5 corresponds to the cases where the back-up electricity used for heating ($P_{el,aux}$) is almost zero. Here it should be stated that PrioWs is always used in warm periods, otherwise the SPF$_{SHP+}$ would be significantly lower.

Two situations are relevant in this case. When $P_{el,aux}$ is close to zero, then results for solar-ice systems are in accordance with the findings from Haller and Frank. (2011), i.e. the direct or parallel use of solar heat is usually a better option than the indirect or series use through the heat pump. This means that results using PriorWs would be better than using PriorCs. However, if the system is designed such that the electric backup is needed, it is better to avoid loading the combi-storage in winter because this implies that the ice storage will freeze earlier or for longer time, compared to the case with PriorCs, and thus increase the use of electric heating. Instead, for a system that needs backup, it is a better option to load the ice storage as often as possible during a specific time in winter to reduce or avoid the phase when the ice storage is completely frozen. This specific time is dependent on the system size. If it is chosen too short or too long the SPF$_{SHP+}$ drops significantly.

The accumulated heat as a function of the temperature for several energy flows in the system is shown in Fig. 7.3 for a large sized system with $V_{ice} = 30m^3$, $A_{cov} = 35m^2$ in SFH45*. Using PriorWs more energy is provided to the combi-storage and therefore the heat pump needs to deliver less energy. This corresponds to electricity savings. The SPF$_{SHP+}$ increases from 6.6 using PriorCs to 7.2 using PriorWs. By using PriorCs more energy is extracted from the collector field (17.4 compared to 16.7 MWh/year)

Figure 7.2: System seasonal performance (left) and electrical backup (right) with varying ice storage volume and collector area for building SFH45*. Upper figures (a, b) for covered and lower ones (c, d) for uncovered collectors.

but most is provided to the cold storage. With PriorCs 28% of the collector gains are given to the combi-storage in comparison to 35% when PriorWs is used.

Simulations shown in Fig. 7.4 have been performed using the control strategy ProgHt with wall heat exchangers. With ProgHt, heat from the ice storage can be used directly in the building at a high temperature level in the beginning of the heating season. In principle one might think that the consideration of ProgHt and wall-hx should always be of benefit or in the worst case have little effect on the system performance. However, simulations done within this project for the climate of Strasbourg (Carbonell et al., 2014b) showed a decrease of the performance when wall-hx were used for systems where the direct electric back-up was relatively often used. When the system is designed such that the ice storage is never completely filled and therefore no direct electric back-up is needed, then improvements with wall-hx could be observed.

Simulations have been carried out here only for large ice storages volumes of 30 and 40 m³ (Fig. 7.4). For ProgHt the benefit of using wall heat exchangers is rather low. However, the potential of this control is highly related the the maximum temperature achieved in summer in the ice storage. This temperature level depends on the size of the collector field and ice storage volume, and also on the control and the losses to the ground.

Figure 7.3: Acumulated heat as a function of temperature for different heat fluxes using control logics PriorCs (solid line, $\mathrm{SPF_{SHP+}}$ 6.6) and PriorWs (dashed line, $\mathrm{SPF_{SHP+}}$ 7.2) for $V_{ice} = 30m^3$ and $A_{cov} = 35m^2$.

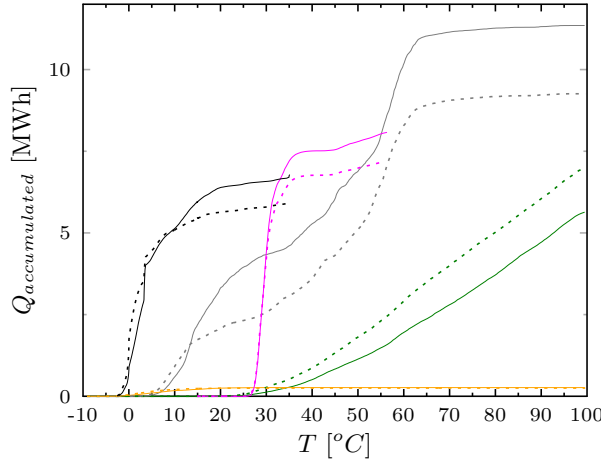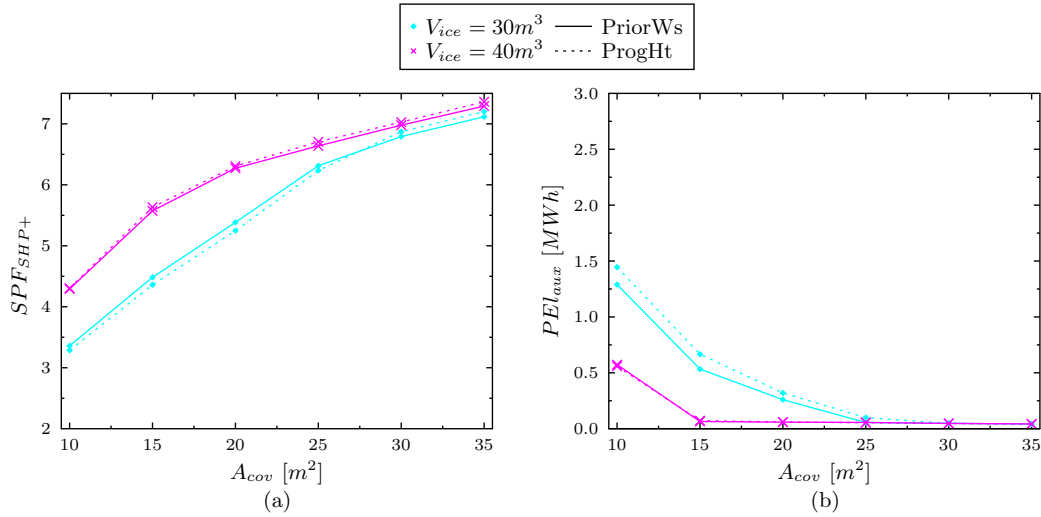**Figure 7.4:** Comparison between PriorWs and ProgHt for the system performance (left) and electrical backup (right) with varying ice storage volume and uncovered collector area for building SFH45*.

7.1.3. Hydraulic configurations

A hydraulic set-up without connection from the solar collectors to the combi-storage (called BlockWs) that is in contrast to the normally used hydraulics (see Fig. 3.1) has been investigated. The analyses of this hydraulic set-up are carried out by only simulating with uncovered collectors and PriorCs. Uncovered collectors perform better at the here studied low-temperature operation of the brine cycle. Results are shown in Fig. 7.5.

As one might expect, not allowing to load the combi-storage by the collector field even in summer leads to a worse performance compared the case where the loading is possible. However, for very low sized systems with collector areas in the order of 10 m^2, this seems not to be very relevant. Reasons why one would choose a system based on this hydraulic concept is because the system is expected to be cheaper and the control can be simplified if the collectors are not connected with the combi-storage. It should be considered that these results are only valid for uncovered selective collectors and for the ice storage concept used in this project.
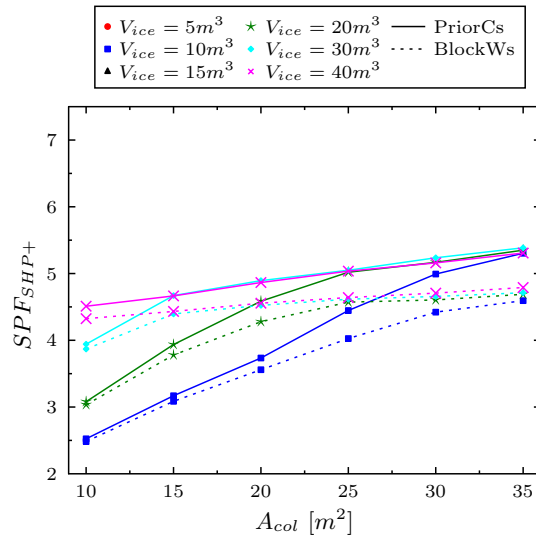
Figure 7.5: Influence of using solar gains of uncovered collectors exclusively direct in the combi-storage: system seasonal performance with varying ice storage volume and uncovered collector area for building SFH45*.

7.1.4. Collector type and area

The influence of the collector type is analysed for covered and uncovered collectors, both with selective coating, for several ice storage volumes. System performances are presented in Fig. 7.6 for building SFH45*. Results presented are combined ones based on the best control strategy (ProWs or ProCs) for each specific system size that was shown in Fig. 7.2.
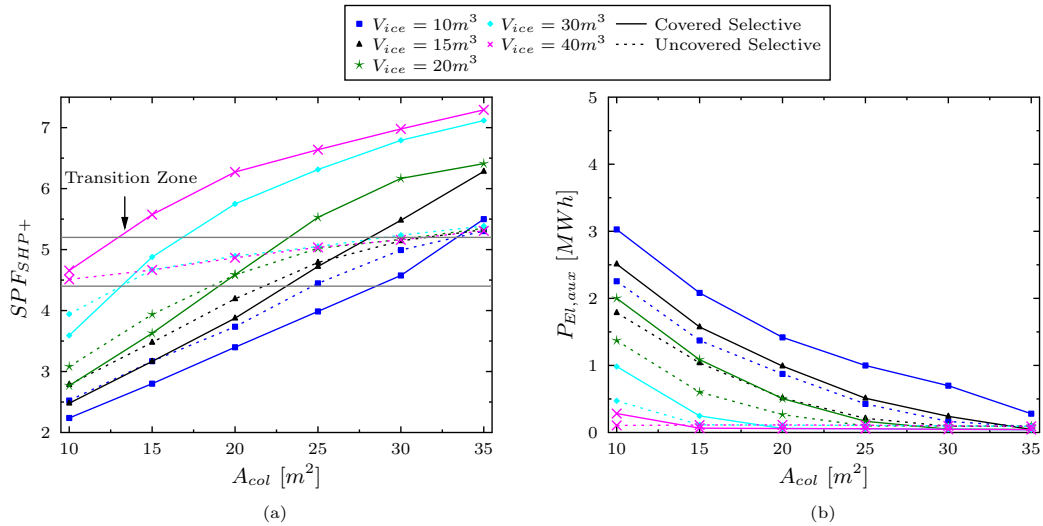
Figure 7.6: Comparison between covered (solid line) and uncovered (dashed line) collectors as function of collector area and ice storage volume for building SFH45* and (a) System performance factor and (b) electric back-up.

In Fig. 7.6 it can be observed that the SPF_{SHP+} range from 2 to approximately 7 using covered collectors and from 2.5 to 5.5 using uncovered collectors. The increase of SPF_{SHP+} per m² of collector area after $P_{el,aux} \sim 0$ is very small for uncovered collectors. This value corresponds to an SPF_{SHP+} in the order of 4.5. Once this system performance is achieved the increase of uncovered collector area or ice storage volume does not significantly increase the system efficiency. This upper SPF_{SHP+} limit using uncovered collectors can be explained by the low performance of those collectors when providing heat at a high temperature in warm periods. Winter performance during times the temperature of the collector is

above ambient is not the relevant factor because simulations using PriorWs and PriorCs – which stand for different control strategies during winter time – are very similar when uncovered collectors are used.

For covered collectors the potential to increase the SPF_{SHP+} is very high if the increase of sizes leads to reduced backup usage. When the electricity demand of the backup reaches values near Zero, the increase is smaller but still significant, specially compared to the results obtained with uncovered collectors.

Comparing covered and uncovered collectors one can see that for SPF_{SHP+} below approximately 5, uncovered collectors perform better. This threshold of SPF_{SHP+} correspond to the regions where $P_{el,aux} \sim 0$. Therefore, in systems where direct electric backup is needed, uncovered collectors tend to perform better. As soon as the back-up can be avoided, covered collectors perform considerably better.

In Fig. 7.7 the relationship between sizes of ice storage and collector field and the heating demand for space heating and domestic hot water in building SFH45* is shown for those systems, where the component sizes are just large enough to prevent the system from running with backup heating. Several combinations of component sizes per MWh of heat demand are possible for avoiding backup. The collector field area can range from 1 to 3.4 m² per MWh and the ice storage size from 1 to 3.9 m³ per MWh heating demand. Systems with covered collectors need a bit larger component sizes to avoid backup, but reach at the same time higher SPF_{SHP+} in the range of 5.5 to 6.1 compared to systems with uncovered collectors, that reach 4.5 - 5.2. For both curves in the figure the SPF increases with increasing collector field ratio.
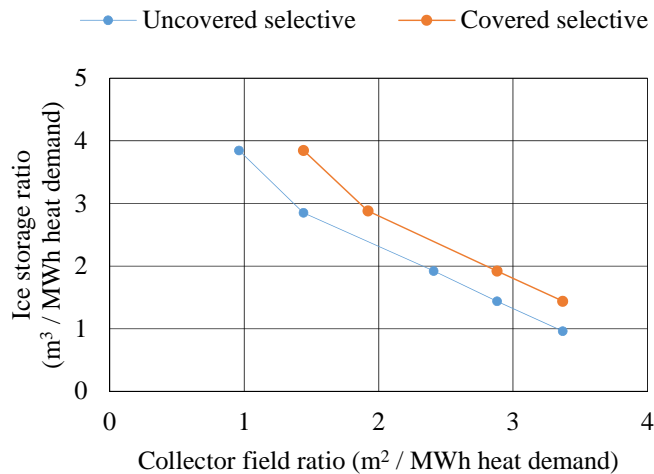
Figure 7.7: Ratio of component sizes per MWh heat demand (space heating and DHW) of building SFH45* for systems that are just large enough to not need electric backup. Range of SPF_{SHP+} for systems with uncovered and systems with covered collectors: 4.5 - 5.2 and 5.5 - 6.1 respectively. (Heat demand: 10.4 MWh/a in SFH45* for the climate of Zurich.)

7.1.5. Buildings with higher heat demand

In building SFH100*$_{LT}$ the SPF_{SHP+} of the solar-ice systems range from 1.8 to 4.5 (see Fig. 7.8). This is much lower than simulated for building SFH45*. A reason for this that building SFH100*$_{LT}$ has a much higher heating demand of around 18 MWh and therefore, using the same size of heating system as for SFH45*, the ice storage freezes completely for almost all analysed combinations of collector areas and ice storage volumes. This can be seen from the fact that the direct electric back up is always present. The potential of increasing performance by using covered collectors is rather low under these conditions, because the electric backup is always needed, and results are not shown.

For building SFH100*$_{HT}$ the SPF_{SHP+} range from 1.7 to 3.5 (see Fig. 7.9) which is lower than the results of building SFH100*$_{LT}$. The lower performances are due to the temperature setting of the heat distribution system, which, at nominal conditions, is 55/50 °C for flow and return respectively. Which such high temperature levels both the heat pump and the solar collectors have lower efficiencies which results in a higher electricity demand of the heat pump compressor and a lower contribution of the collectors with heat that is directly used in the building on high temperature levels.
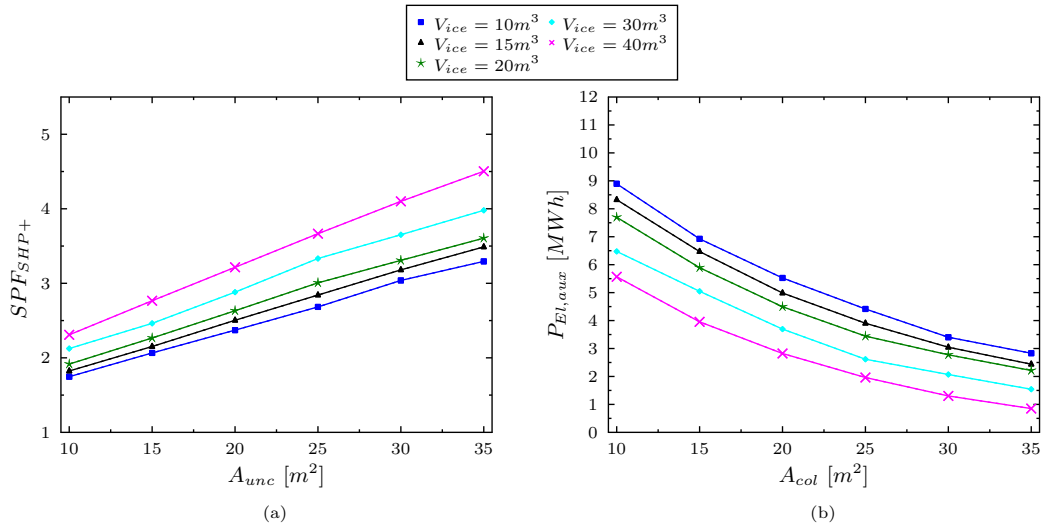
Figure 7.8: (a) System seasonal performance factor and (b) direct electric back-up as function of uncovered collector area and ice storage volume for building SFH100$^*_{LT}$.
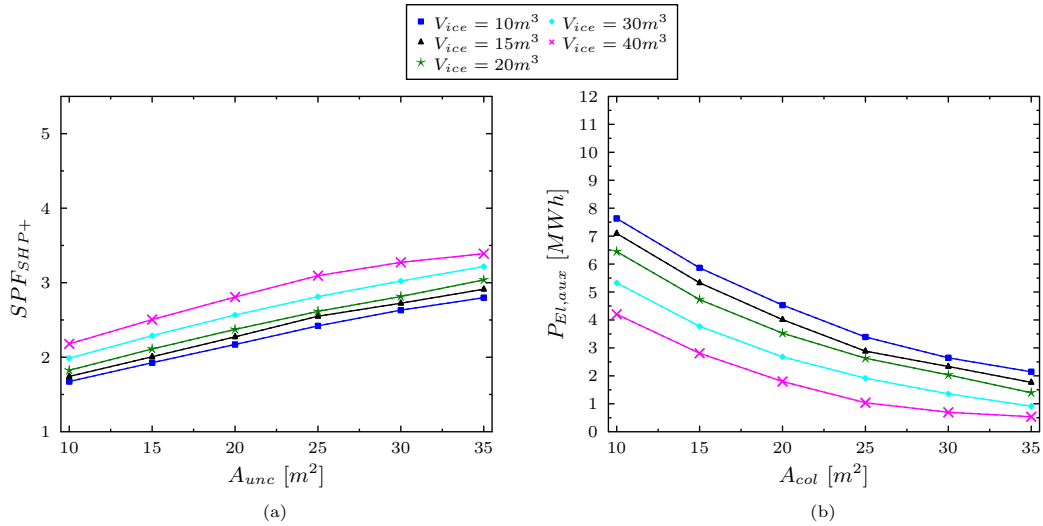
Figure 7.9: (a) System seasonal performance factor and (b) direct electric back-up as function of uncovered collector area and ice storage volume for building SFH100$^*_{HT}$.

7.1.6. Twelve year simulation for Zurich

System simulations were carried that use as input measured weather data that was obtained from Meteo Schweiz for the location of Zurich-Fluntern from 1999 to 2012. Two systems were selected for the simulations. One of them has an ice storage volume of 20 m^3 and a total area of 17 m^2 uncovered collectors with a reference SPF$_{SHP+}$ of 4, if the standard Meteonorm climatic data for Zurich is used. The second system was chosen such that the electrical backup is almost zero with the standard climatic data, resulting in a reference SPF$_{SHP+}$ of 5. The sizes for the latter system are 20 m^3 of ice storage volume and 25 m^2 of uncovered collectors.

Results for the twelve years are presented in Fig. 7.10 for the system with a reference SPF$_{SHP+}$ of 4. The year 1999 was used in the simulations to condition the system and is thereof not plotted. In the first column the reference calculation using Meteonorm data is shown. In the last column the values averaged over the twelve years is shown. All but one of the 12 years have higher SPF$_{SHP+}$ compared to the reference year (Fig. 7.10(a)). The differences are significantly large. Nine out of the twelve years have an SPF$_{SHP+}$ higher than 5, while the reference has an SPF$_{SHP+}$ of 4. The average SPF$_{SHP+}$ is in the order of 5, around 25% higher than the reference.
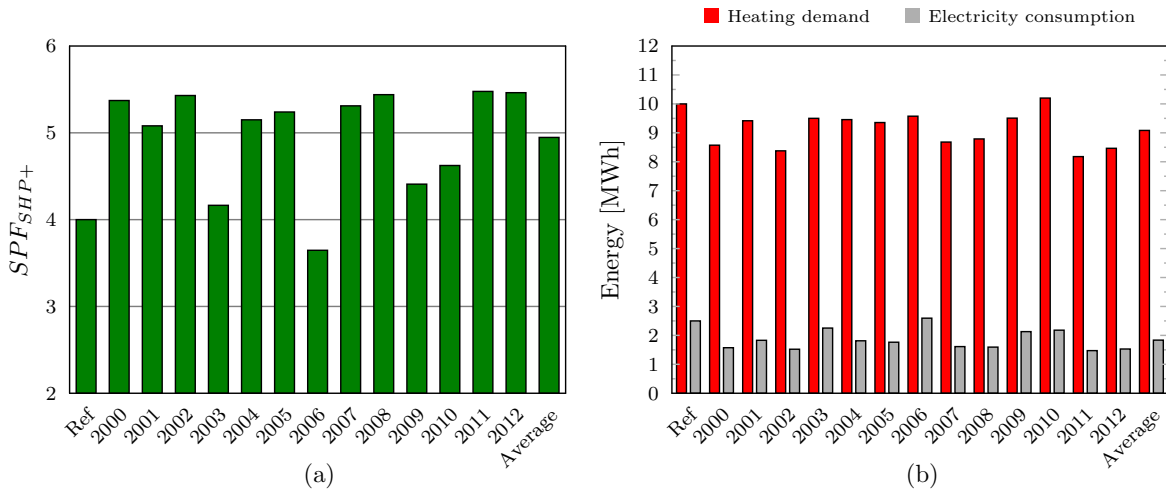
Figure 7.10: Simulations with 12 years with real weather data for Zurich-Fluntern from 2000 to 2012 for a reference system (Ref) with Meteornom data with $V_{ice} = 20m^3$ and $A_{unc} = 17m^2$ for (a) System performance and (b) heating demand and electricity consumption.

Results for the case where the reference does not need the backup are shown in Fig. 7.11. For this system size, the difference between the reference year and the averaged results of the 12 years with real climate is in the order of 17%. The reason of having lower differences in a relatively large system is because, as said in above sections, reducing the backup of a specific system either by increasing sizes or in this case by increasing solar irradiation, leads to highest increases of the performance.
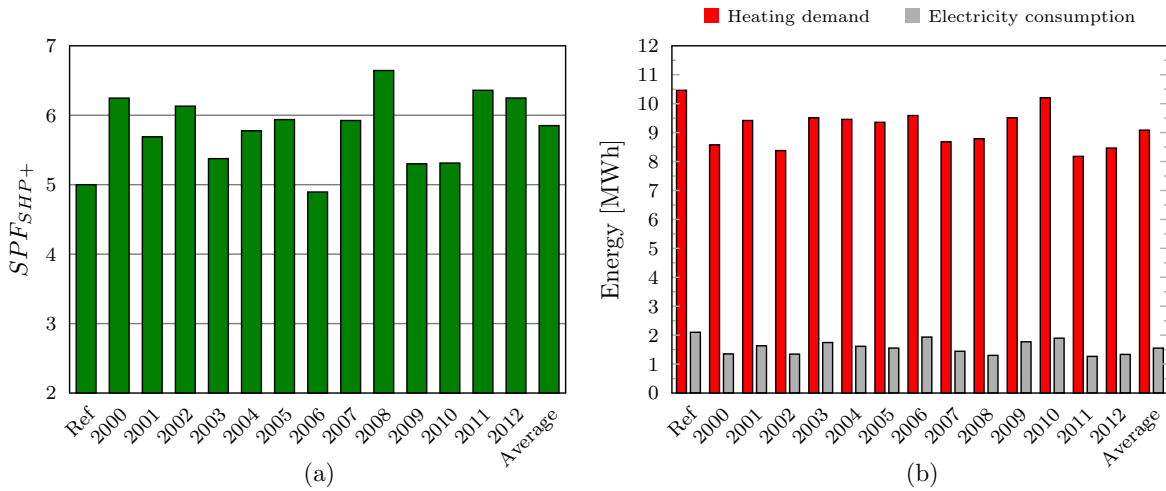
Figure 7.11: Simulations with 12 years with real weather data for Zurich-Fluntern from 2000 to 2012 for a reference system (Ref) with Meteornom data and Cr_{No-Aux}. (a) System performance and (b) heating demand and electricity consumption.

Simulations presented in above sections show that the same performance can be achieved using different combinations of ice storage volume and collector area. The decision whether one shall increase the collector area or the ice storage volume may depend on several factors, e.g. cost, roof available or cellar space. One question would be if the weather variations of a specific site could also be a factor to decide.

Two further simulations with the same SPF$_{SHP+}$ as well as the same heat generation cost as the one with $V_{ice} = 20m^3$ and $A_{unc} = 17m^2$ have bee performed. One system with a 25 m^3 ice storage and 14 m^2 of uncovered collectors and another with 15 m^3 ice storage and 20 m^2 of uncovered collectors. From results presented in Fig. 7.12 it can be observed that a system with larger collector field and smaller ice storage is more efficient as long as the SPF$_{SHP+}$ is above 5. In practice this means that larger collector areas are a better option as long as the ice storage hardly completely freezes in winter and no back-up is needed. For cases with SPF$_{SHP+}$ below 5, results with the highest ice storage volume are better. The twelve year average of all three systems is similar, but with the selected years one could say, from a system

performance point of view, that having a higher collector area is a slightly better option.
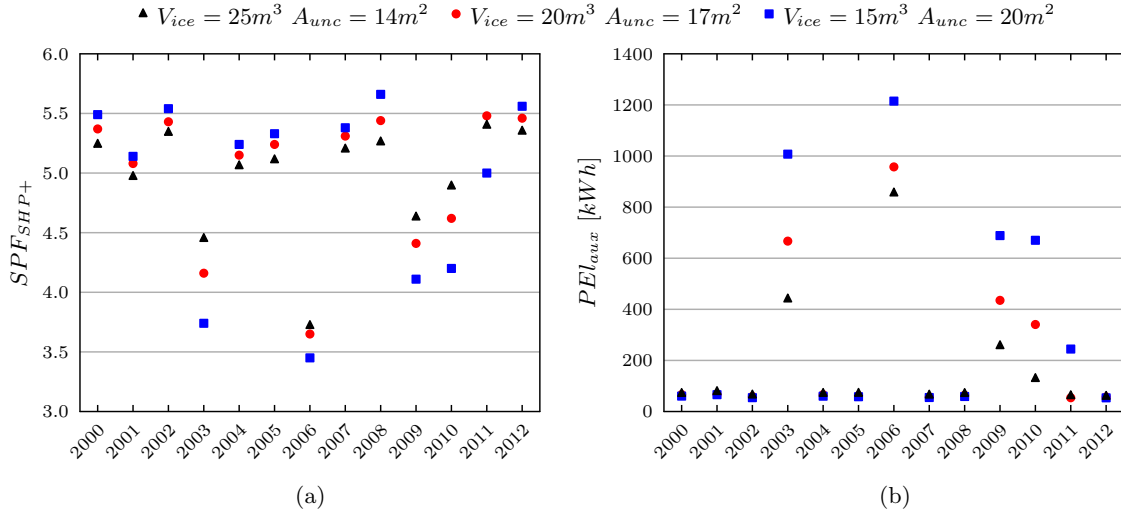
Figure 7.12: (a) System performance and (b) direct electric back-up for a 12 years simulation with three different system sizes with the same installation costs.

7.2. Waste water heat recovery (WWHR)

The dependence of the SPF_{SHP+} on devices for waste water heat recovery (WWHR), that are included in the brine cycle of the system, is analysed in this chapter. The investigated devices for heat recovery, a waste water storage ($WW_{storage}$) and a gravity film heat exchanger (WW_{GFX}), are explained in Section 3.7.

7.2.1. Fouling in the WWHR-system

If waste water circulates through a pipe, particles of the waste water fluid will stick to the surface of the heat exchanger and also a biofilm will grow. This layer formed is known as fouling layer. The heat transfer capacity of the heat exchanger is reduced by the fouling layer and dependent on its thickness and characteristics.

It is assumed that fouling will appear in each of the waste water heat recovery devices analysed. However, it is very difficult to estimate how much this layer will grow during several years. This depends very much on how often the WWHR system is cleaned and which type of waste water is used. Therefore assumptions need to be done in order to simulate WWHR systems. The approach here consists of defining an average fouling layer thickness. The assumption of this value can change radically the potential benefits of the WWHR systems.

Results for a system with $V_{ice} = 20m^3$ and $A_{unc} = 20m^2$ for SFH45* are shown in Fig. 7.13 for the two WWHR devices. The heat conductivity of the fouling layer is set to 0.7 $W/(mK)$ as recommended in VDI-Wärmeatlas (2006). The increase of the thickness of the fouling layer affects considerably the results for WW_{GFX} but not for $WW_{storage}$.

In a retentive system like the $WW_{storage}$ the waste water is stored, and there is enough time to extract almost all available heat form the waste water before the waste water flushes away. Directing brine through the storage is stopped when the minimum temperature allowed in the waste water storage of 4 °C is reached.

The influence of a fouling layer is relevant for the gravity film heat exchanger. The SPF_{SHP+} decreases from 4.9 to 4.75 when the thickness increases from 0 to 10 mm. After a fouling layer appears in the heat exchanger, the amount of usable waste heat decreases strongly. For example with a fouling layer of 2 mm the transferred heat from waste water to the heating system is only 40 % compared to the case without
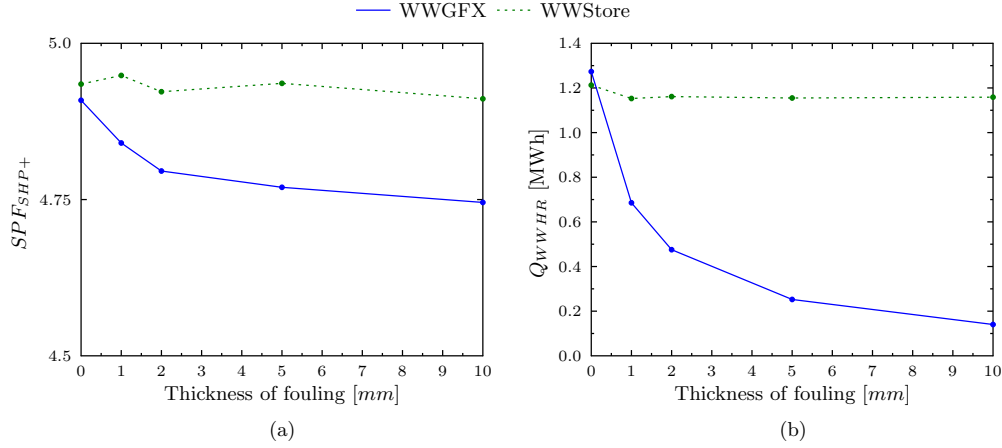
Figure 7.13: Influence of fouling thickness for different WWHR systems on (a) system performance and (b) energy provide by the WWHR device to the system.

any fouling. In order to be conservative a relatively high fouling layer thickness of 5 mm has been chosen for all WWHR simulations.

7.2.2. Influence of WWHR with varying collector area and ice storage volume

Two WWHR systems described in Section 3.7 are studied here for ice storage volumes of 10 and 20 m^3 with varying area of both covered and uncovered collectors. Results of the two WWHR systems are presented in Fig. 7.14 (a) and (b) for uncovered collectors and in (c) and (d) for covered collectors. Results from both uncovered and covered collectors clearly show that the WW$_{storage}$ is more efficient than the WW$_{GFX}$. In the WW$_{storage}$ the waste water remains in the storage for a longer period allowing a very good heat exchange, while in WW$_{GFX}$ the heat transfer occurs in a short period (while waste water is flushing) and the global efficiency of the heat exchanger is clearly lower.

When the WW$_{storage}$ system is added to a system configuration that needs electrical back-up, improvements due to the WWHR devices are high because they allow to reduce the period, where the ice storage is completely frozen. For example for $V_{ice} = 20m^3$ and $A_{cov} = 20m^2$ the SPF$_{SHP+}$ increases by 27% for WW$_{storage}$ and 6% for WW$_{GFX}$. As soon as the system without WWHR needs no back-up, the potentials of the WWHR are reduced. In the case of $V_{ice} = 20m^3$ and $A_{cov} = 30m^2$ the SPF$_{SHP+}$ increases by 5% using WW$_{storage}$ and by 2% for WW$_{GFX}$.

7.3. Simulation results for Davos and Locarno

The locations of Davos and Locarno were chosen in addition to Zurich to consider different Swiss climates. The heat demands for building SFH45* are 82 and 33 kWh/(m^{2}a) for Davos an Locarno respectively.

Results for Davos are shown in Fig. 7.15 for both covered and uncovered collectors. Like for the climate of Zurich, the same upper limit of 5.5 for the SPF$_{SHP+}$ when using uncovered collectors is observed. As Davos is a sunny and relatively cold location all over the year, the potential of using covered collectors is huge and results of SPF$_{SHP+}$ up to 9 can be achieved with $V_{ice} = 20m^3$ and $A_{cov} = 30m^2$.

Simulations for Locarno are shown in Fig. 7.16. For this location the upper limit SPF$_{SHP+}$ for uncovered collectors is around 6, a bit higher than the limit of 5.5 found in Zurich and Davos. As observed in the simulations for Davos, the system performance using covered collectors can reach very high SPF$_{SHP+}$ with relatively small system sizes. For example using $V_{ice} = 10m^3$ and $A_{cov} = 20m^2$ a SPF$_{SHP+}$ slightly higher than 7.5 can be reached. This performance is around 67% higher compared to the same system sizes in Zurich with uncovered collectors.
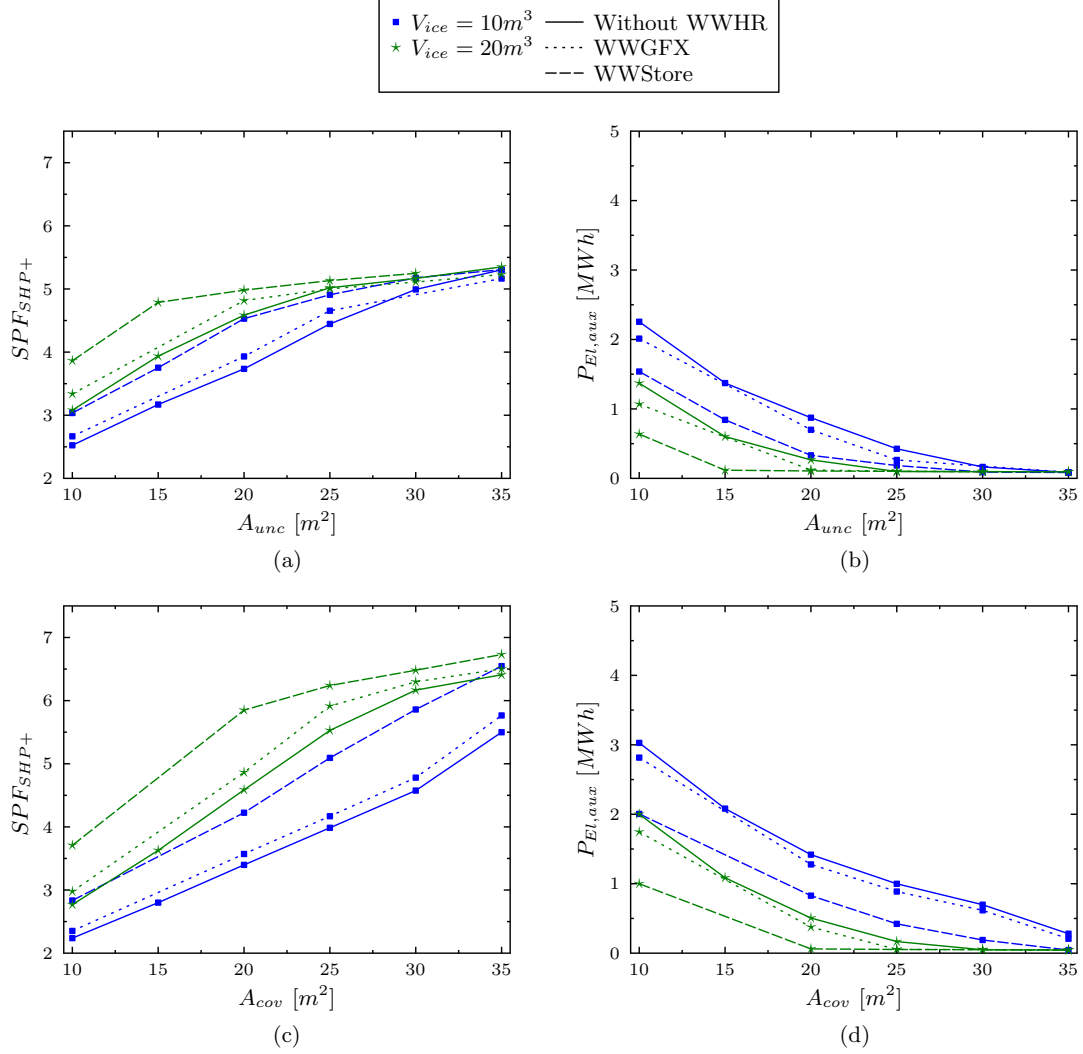
Figure 7.14: Comparison between WWStore (solid line) and GFX (dashed line) WWHR systems for covered (upper figures) and uncovered (lower figures) for building SFH45* in the city of Zurich.

7.4. Conclusions

The annual simulations show that the SPF_{SHP+} of the analysed solar-ice systems can range from 2 up to 7 in building SFH45* with ice storages volumes from 10 to 40 m³ and collector areas from 10 to 35 m² in the city of Zurich. Using the same range of sizes of ice storage and collector field, values of SPF_{SHP+} from 1.7 to 3.5 in $SFH100^*_{HT}$ and from 1.7 to 4.5 in $SFH100^*_{LT}$ can be achieved. An advantage of ice storage systems is that a high system performance can be reached with different combinations of collector area and ice storage volume.

In order to size the heat exchanger area in the proposed ice storage concept with de-icing, one needs to consider not only the heat pump extraction power but also the thickness of ice on the heat exchanger in order to define the design conditions. This ice thickness depends on the system design. In simulations for building SFH45* and a heat pump with nominal power of 6 kW, 21 m² of heat exchanger area have been found to be a good value for all simulations.

In order to select the size and type of collectors one should first think about the system performance that needs to be achieved and the available space for ice storage and collector field. From an efficiency point of view, covered collectors perform better at high SPF_{SHP+}, when the direct electric back-up is not needed. For building SFH45* in Zurich the threshold for covered collectors to perform better is relatively high, with SPF_{SHP+} in the range of 4.5 to 5.2. Therefore, for climates similar to Zurich, uncovered collectors are recommended unless a system design achieving a high system performance is desired.
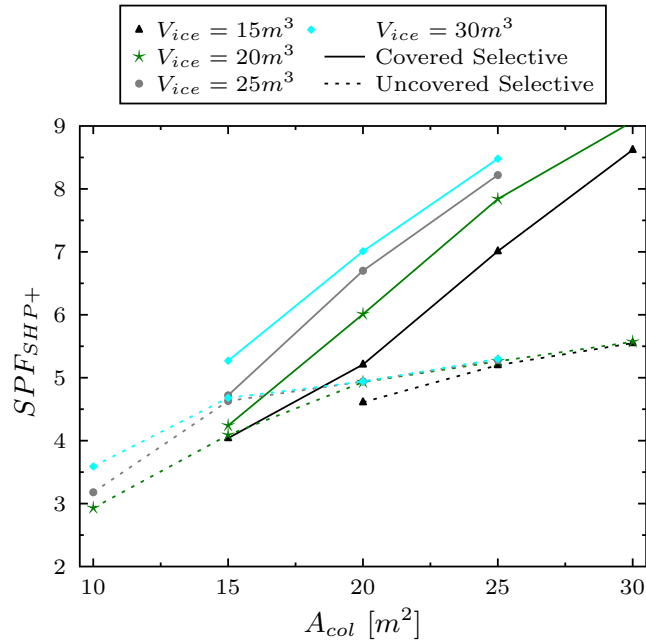
Figure 7.15: System performance factor comparison between covered (solid line) and uncovered (dashed line) collectors for building SFH82 in the city of Davos.
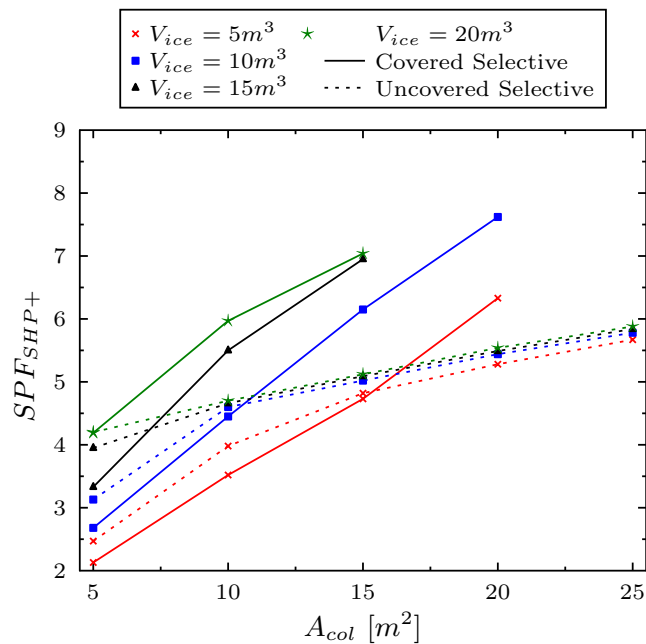
Figure 7.16: System performance factor comparison between covered (solid line) and uncovered (dashed line) collectors for building SFH33 in the city of Locarno.

The size of the system should be selected properly. For example the increase of collector area or ice storage may not significantly improve the system performance once a certain level of performance has been reached if uncovered collectors are used. Using uncovered collectors the performance is limited with SPF_{SHP+} values somewhere in the range between 4.5 and 5.5 and it's not possible to increase it considerably further. In order to achieve higher performances covered collectors are needed.

In general, using heat from the solar collectors directly to load the combi-storage should be always preferred as long as the ice storage does not tend to ice fully and the electric back up is not used. Not

using direct heat at all, i.e. eliminating the hydraulic connection between the solar field and the combi-storage, is not recommended with the selective uncovered collectors used here. Without any direct heat the system performance is limited to a value of around 4.5.

All conclusions provided above are based on a reference year with climate data from Meteonorm. Calculations using twelve years of real climate data for the city of Zurich show that the averaged SPF_{SHP+} over twelve years is 20% higher than the one for the reference year. The use of the reference year taken is a good option to size components under critical conditions, but it may not be the right choice to estimate an average efficiency of a solar-ice system.

The climate of Zurich has been extensively used in this project as it can be seen as a reference climate for the Swiss Mittelland, but its solar irradiation is quite low. Simulations in Swiss locations with higher solar irradiation such as Davos and Locarno show that the solar-ice system is very promising under high solar radiation conditions. For example an SPF_{SHP+} of 6 can be achieved in the alpine location of Davos using $V_{ice} = 20m^3$ and $A_{cov} = 20m^2$ for building SFH45*. For Locarno the same performance can be obtained using $V_{ice} = 10m^3$ and $A_{cov} = 15m^2$. For Davos an increase of the SPF_{SHP+} in the order of 33% compared to Zurich can be achieved, while for Locarno increases of SPF_{SHP+} in the order of 70% can be expected. In both locations, the potential of covered collectors are very large and with relatively small system sizes.

Waste water heat recovery systems can be of great help to increase system performance, especially if a waste water storage is used. An increase of SPF_{SHP+} in the range of 30% in respect to the case without WWHR can be expected using $WW_{storage}$, if the system without WWHR needs electrical backup. The improvement of SPF_{SHP+} decreases to around 5% if the system would need no backup without WWHR. Using a WW_{GFX} an increase of system performances in the range of 6% can be expected. However this improvement is dependent on the fouling layer of the waster water heat exchanger.

8. Cost analysis

A short analysis of costs for installation and operation of the heating systems is given in this chapter. For the derivation of the cost calculation see Section 4.5. Prices for the cost calculations are Swiss market prices of 2013/14. The prices for the ice storage components are based on a pilot installation and are rather high for the ice storage as they don't account for possible scaling effects from mass production.

The two methods net present value (NPV) and annuity (A) result in different costs. The costs calculated with annuity are always noticeably higher. For building SFH45* with $V_{ice} = 15m^3$, $A_{unc} = 25m^2$ for example the heat generation costs HGC_A are 20% higher (with 0.48 CHF/kWh compared to 0.40 CHF/kWh with HGC_{NPV}). The main reason for this difference is the dominant contribution of the investment cost in the total costs: with the net present value the nominal costs of the investment is taken into account whereas with the annuity the yearly maturity of the investment costs are affected by the interest rate. In the following considerations only the net present value is shown.

As an example Fig. 8.1 shows the share of investment costs of the components for a SFH45* building with $V_{ice} = 15m^3$ and $A_{unc} = 25m^2$. The investment costs here are 71'000 CHF in total. Highest share in the costs with 36% has the uncovered collector field (yellow segments) followed by the ice storage (28%) (blue) and the heat pump (19%) (green).

Looking more into the details for this system size it can be seen that the main contribution to the costs for the collector field comes from the collectors themselves. Piping and mounting contribute an almost similar amount. The share of the heat exchangers (stainless steel plates) in the total costs is as big as the one of the concrete storage casing for the presented ice storage size of $V_{ice} = 15m^3$.
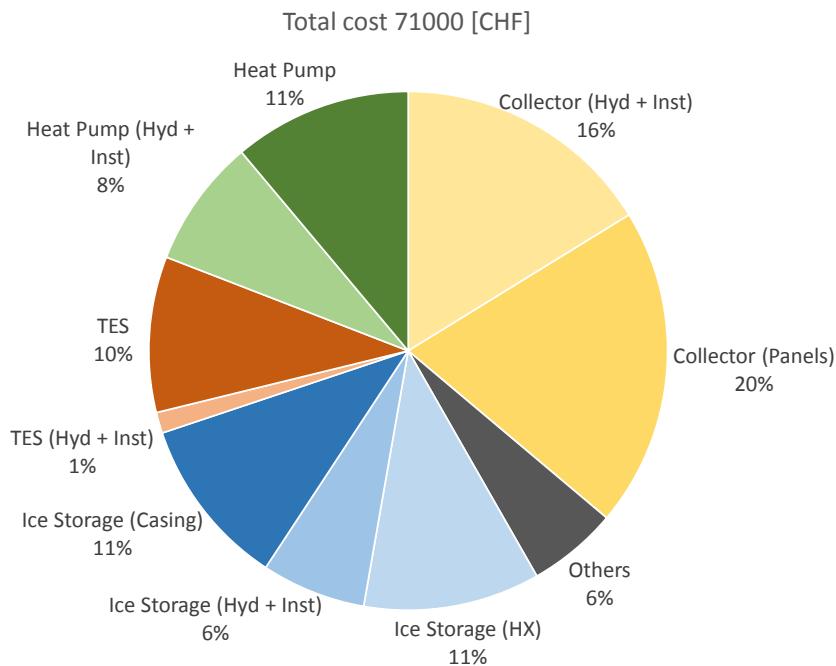
Figure 8.1: Shares of the investment costs for a system with $V_{ice} = 15m^3$, $A_{unc} = 25m^2$ and SFH45* with a total cost of 71'000 CHF.

The heat generation costs for a series of simulations with building SFH45* and an ice storage size of 15 m^3 are shown in Fig. 8.2. The total heat generation costs are high for the whole series with values between circa 33 and 42 CHF/kWh (HGC_{NPV}). The share of the investment costs is clearly dominant for all analysed collector field sizes. For small sizes its share is around 83% and for large systems 90%. The contribution of electricity to the costs is small compared to the investment. The contribution decreases from 15% (smallest system) to 9% (largest system). The figure shows that a slight decrease of electricity costs with increasing collector field size does not compensate the increase of costs due to the collectors.

In Fig. 8.3 SPF_{SHP+} and HGC_{NPV} are shown for building SFH45* with variations of both collector field and ice storage size. The heat generation costs with net present value (HGC_{NPV}) increase both with larger ice storage and with larger collector field – so, the smaller the system the lower the cost for the
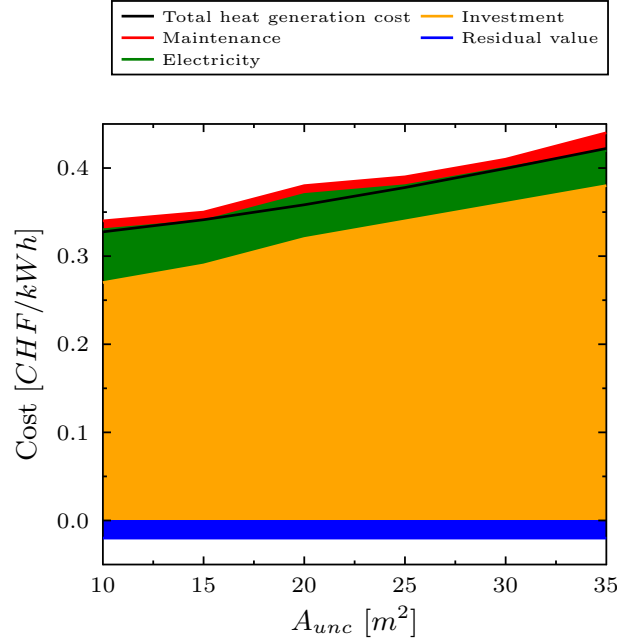
Figure 8.2: Shares of different system component costs in the total heat generation cost based on Net Present Value for SFH45* with $V_{ice} = 15m^3$.

heating demand. The HGC$_{NPV}$ range from 0.32 CHF/kWh for the smallest system to 0.49 CHF/kWh for the largest system (Fig. 8.3(b)). With decreasing slope of SPF$_{SHP+}$ the HGC$_{NPV}$ shows a rising increase. For same system sizes heat generations costs with uncovered collectors are slightly lower by 2 - 5% compared to the covered collectors, even though the systems with covered collector can have a much higher SPF$_{SHP+}$ at the same time. For systems with covered collectors with same SPF$_{SHP+}$ but different component sizes slightly lower HGC$_{NPV}$ result if a larger ice storage size is chosen instead of a large collector field.

The curves of heat generation costs are different for SFH100$^*_{LT}$ (see Fig. 8.4). The presented case with uncovered collectors shows that HGC$_{NPV}$ are lower by 30 - 45% compared to SFH45*. Systems with low SPF$_{SHP+}$ have also the lowest HGC$_{NPV}$ of 0.22 - 0.23 CHF/kWh. For this case of SFH100$^*_{LT}$ with uncovered collectors starting at small collector fields of 10 m^2 it is worth to increase the collector field to 15 m^2 for systems with 10 or 15 m^3 ice storage. However, these systems have also very low SPF$_{SHP+}$.

Also a ground source heat pump system without collectors and ice storage was analysed (SPF$_{SHP+}$ of 4.0). There the heat generation costs are 0.33 CHF/kWh for SFH45*. This is 18% less compared to 0.40 CHF/kWh of the above presented example of the solar-ice system with $V_{ice} = 15$ m^3 and $A_{unc} = 25$ m^2 which has a slightly higher SPF$_{SHP+}$ of 4.2. With building SFH45* similar HGC$_{NPV}$ of around 33 CHF/kWh are also reached – but with system sizes that have very small SPF$_{SHP+}$ of around 2.5. In building SFH100$^*_{LT}$ the ground source heat pump system has heat generation costs of 0.18 CHF/kWh.
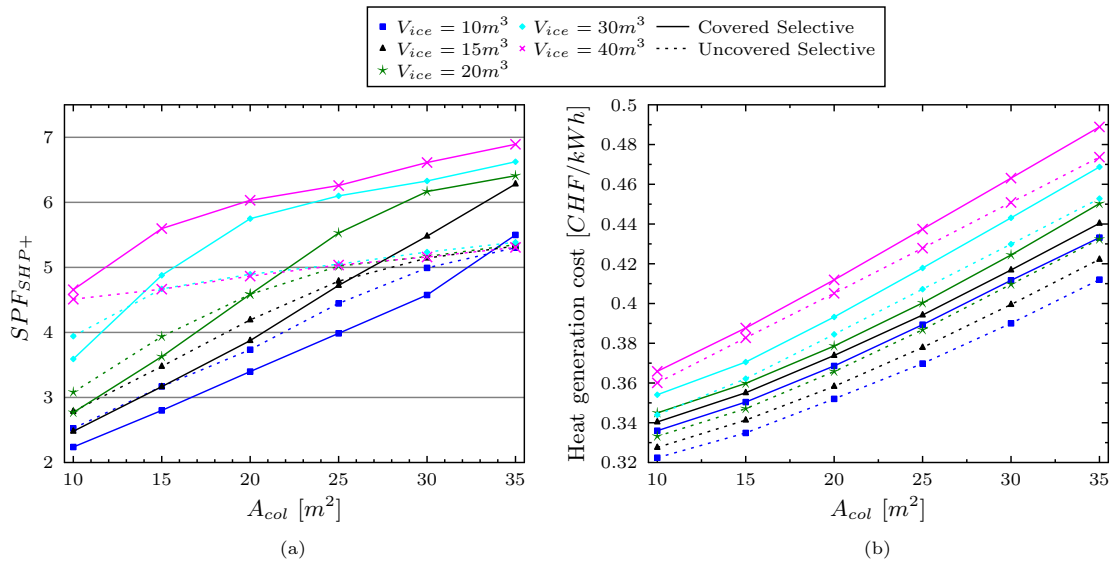
Figure 8.3: (a) System performance and (b) heat generation cost based on Net Present Value for SFH45*
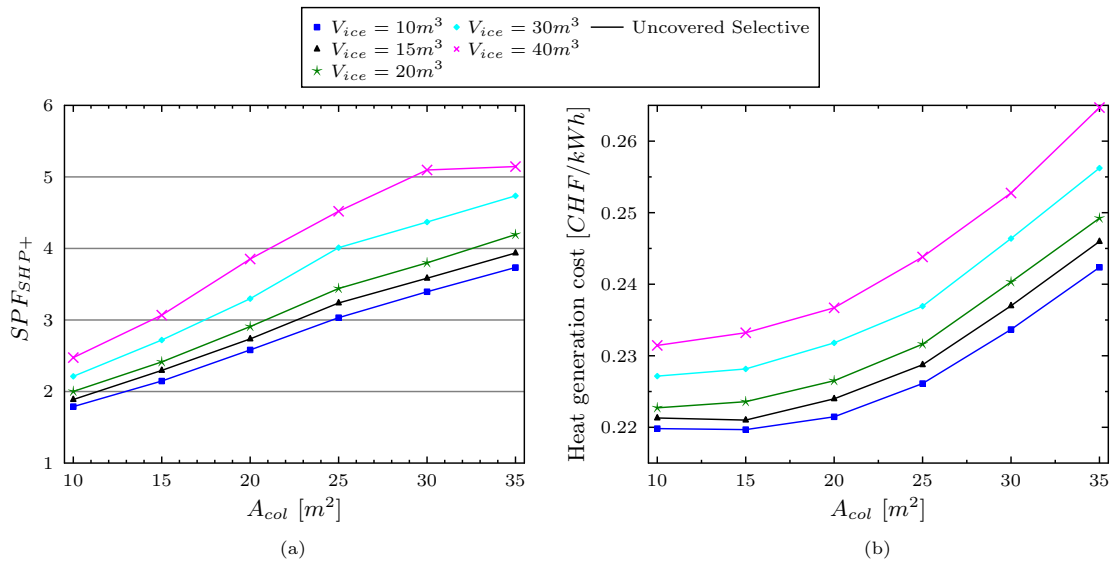

Figure 8.4: (a) System performance and (b) heat generation cost based on Net Present Value for SFH100$_{LT}^*$.

9. Life cycle assessment

The environmental impact of heat supply by a solar-ice system is analysed by means of a life cycle assessment (LCA). The applied methodology was presented in Section 4.6. In Sections 9.1 and 9.2 the life cycle inventories (LCI) of the infrastructure (including production and disposal) and of the use phase of the system are established. Section 9.4 contains the results of the impact assessment, while the key findings are summarized in Section 9.5.

9.1. LCI of the production and disposal of the infrastructure

The system components accounted for in the LCI are described in the following sections. The LCI was set up in a way that permitted to use parameters to scale the different components. Hence, the specifications given in the text are valid independently of scaling. Tables that summarize the different datasets can be found in Appendix B.

9.1.1. Ice Storage

Storage Casing (table B.1)

In the basic case, the storage casing is made of site-cast concrete. The concrete used contains 250 kg of cement of the type CEM II/B per cubic meter.[5] The concrete casing has the shape of a rectangular parallelepiped and lies 0.8 m under ground level. It has an average wall thickness of 0.17 m and is reinforced with 80 kg/m^3 reinforcing steel. The top of the casing is furnished with a manhole made of concrete, covered by a stainless steel grill and an aluminium lid. The upper half of the casing is insulated with a 0.16 m layer of extruded polystyrene (XPS). For the concrete and the excavated material an average road transport distance of 20 km is included. 95 % of the concrete and 100 % of the metal are assumed to be recycled, while XPS is disposed of by municipal incineration. As an alternative, casings where concrete is substituted with glass fibre reinforced plastic (FRP) or polypropylene (PP) are modelled. These casings have the shape of a cylinder and are furnished with a manhole. Like in the case of the concrete storage, half of the surface is insulated with 0.16 m of XPS. For the FRP storage casing, a wall thickness of 0.009 m and a material density of 2000 kg/m^3 are assumed. It is further assumed that the glass fibres, about 60 volume percent, are recycled, while the rest of the material is sent to municipal incineration. The PP casing has a wall thickness of 0.02 m and a material density of 900 kg/m^3. All the PP is disposed of by municipal incineration.

Heat Exchangers (table B.2)

The heat exchangers essentially consist of two rolled rectangular stainless steel sheets welded together. Each heat exchanger is furnished with two L-profiles made of stainless steel, allowing for the mounting on the ground slab of the casing. All metal parts are recycled.

Piping (table B.3)

Inside the ice storage the heat exchangers are connected by polypropylene collector pipes with a wall thickness of 3 mm. The pipe diameters are chosen such that for a flow rate of 1900 l/h (nominal flow of the 8 kW heat pump) the flow velocity is 0.6 m/s. Each heat exchanger is connected to the collector pipes with two DN16 corrugated chromium steel pipes of 0.29 m length. The ice storage is connected to the building via DN50 corrugated chromium steel pipes of 4.5 m length. These pipes are thermally insulated by a 5 cm layer of polyurethane foam, protected by a thin layer of low density polyethylene. All metal parts are recycled, while plastic parts are incinerated.

---

[5]Since the ice storage doesn't need to be fully water tight, this amount of cement is sufficient, according to an information of Fuchs AG.

9.1.2. Solar Thermal System

The components of the solar thermal system are described in the following paragraphs and summarized in table B.5.

Covered Collector

Based on a dataset of Stucki and Jungbluth (2010) a new dataset compatible with Ecoinvent 3 (EI3) was created. The original dataset describes a standard flat plate solar collector with a copper absorber and a black chrome selective coating. In the new dataset additional transports and packaging material are not included. In order to analyse the sensitivity of the impact on the material used, an additional dataset was created, in which the copper sheet of the absorber is replaced by a 0.5 mm aluminium sheet, while the copper tube is kept. The aluminium sheet has a selective coating of nickel pigmented aluminium oxide.

Uncovered Collector (table B.4)

The absorber of the uncovered collector is, like the ice storage heat exchangers, made of two rolled stainless steel sheets, of which one has a black chrome selective coating on one face. The absorber is mounted in an aluminium frame. Underneath the absorber, the collector contains two corrugated sheets made of fibre reinforced plastic (FRP). It is supposed that the glass fibres, i.e. about 60 volume percent of the FRP, are recycled, while the remaining material is incinerated. All metal parts are recycled.

Mounting system

The collectors are assumed to be mounted on a slanted roof and therefore, according to Stucki and Jungbluth (2010), an amount of 0.7 kg aluminium per m^2 collector area is needed.

Heat storage tank

The 1500 l heat storage tank is modelled by the Ecoinvent dataset describing a 2000 l tank scaled down in accordance with Stucki and Jungbluth (2010). The dataset takes into account the internal heat exchangers of the tank.

Hydraulics

The electric power consumption of the circulating pump is estimated to 1.5 W per m^2 collector area. The pump is taken into account by upscaling the Ecoinvent dataset for a 40 W pump with the ratio of the power consumptions. The volume of the expansion vessel is 4 l per m^2 collector area, corresponding to the value for a 20 m^2 system stated by Stucki and Jungbluth (2010). The Ecoinvent dataset for a 80 l expansion vessel is adopted and scaled with the ratio of the volumes. The collectors are connected to corrugated stainless steel pipes whose diameter is determined by the volume flow rate of 50 l/(h m^2 collector area) and the flow velocity of 0.6 m/s. In order to estimate the length of the collector pipes, a fit based on the values of Stucki and Jungbluth (2010) was established, resulting in a basic pipe length of 20 m plus 1.5 m per m^2 collector area. The pipes are insulated with a 2 cm layer of polyurethane foam protected by a thin layer of polyethylene. Metal parts are recycled, while plastic parts are incinerated.

9.1.3. Heat Pump

The heating power of the heat pump is 6 kW for the building SFH45* and 8 kW for the buildings SFH100$^*_{LT}$ and SFH100$^*_{HT}$. It is accounted for by scaling the existing Ecoinvent dataset for a 10 kW heat pump by the ratio of the heating powers. Further included are circulating pumps on the source and the sink side of the heat pump. The electrical power consumption of the pumps is assumed to be the same as in the Kindergarten pilot plant, i.e. 8 W per kW heating power of the heat pump. The pumps are modelled by the existing Ecoinvent dataset for a 40 W pump, scaled with the ratio of powers.

9.1.4. Waste Heat Recovery

In the LCA, only waste heat recovery by means of a waste water storage device is considered (cf. table B.6). Only very approximate information regarding the material content of such a device could be obtained from a manufacturer. A waste water storage device with a volume of 130 l has a total weight of 120 kg. Half the weight is attributed to stainless steel (heat exchanger and additional pipes) and the other half to polyethylene (storage tank). The inner volume of the heat exchanger and the pipes, necessary to determine the amount of heat carrier liquid needed, is estimated to 10 % of the storage volume. For the connection of the device to the brine loop, 2 DN12 chromium steel pipes of 2 m length each are included. It is assumed that metal parts are fully recycled and plastic parts are incinerated.

9.1.5. Heat Carrier Liquid

The heat carrier liquid consists of 33 volume percent of propylene glycol and 67 volume percent of softened water. The necessary treatment of the liquid after its disposal is accounted for by the corresponding Ecoinvent dataset. The respective amounts of heat carrier liquid are included in the datasets of the individual system components.

9.2. LCI of the use phase

Component lifetimes

In order to determine the "amount of infrastructure" necessary to provide a unit of useful heat, one needs to estimate the lifetimes of the various system components. The lifetime of the ice storage and all its components is assumed to be 50 years. This would correspond to the lifetime of a borehole heat exchanger as estimated in Jungbluth (2007). For the solar thermal system, except for the circulating pump, a lifetime of 25 years is assumed, corresponding to the estimate of Stucki and Jungbluth (2010). According to estimates of Lovvorn (2001) and Heck (2010), the lifetime of the heat pump is taken to be 20 years. All circulating pumps are exchanged every 15 years, according to the estimate of Jungbluth (2007). The heat carrier liquid is replaced every 10 years, as suggested by Stucki and Jungbluth (2010). The lifetime of the waste heat recovery system is estimated to be 25 years.

System operation

The amount of electricity needed for the system to provide a unit of useful heat corresponds to a unit of heat divided by the average system performance factor (SPF_{SHP+}). The values for the SPFs of the different system configurations are taken from the TRNSYS simulation results. Only results for the climate of Zurich are considered. The electricity input is modelled via Ecoinvent datasets of the Swiss consumer electricity mix and, alternatively, of the European (ENTSO-E) consumer electricity mix. During its use, for the providing of one MJ of useful heat, the heat pump emits about 2.5E-6 kg of refrigerant to the air (Jungbluth (2007))[6]. The same amount of refrigerant needs to be replenished. As is assumed for solar thermal systems by Stucki and Jungbluth (2010), the assumption is included that a maintenance team travels 50 km every 5 years by van.

9.3. LCI for a unit of heat

Finally, the information on infrastructure, lifetimes and system operation can be compiled to an LCI for the functional unit, i.e. for the providing of a 1 MJ of useful heat (cf. table B.7). The useful heat provided by the system over a year amounts, for the climate of Zurich, to 10.45 MWh (37'620 MJ) for the SFH45* building, to 20.05 MWH (72'180 MJ) for SFH100$^*_{LT}$ and to 19.4 MWh (69'840 MJ) for SFH100$^*_{HT}$. The "amounts of infrastructure" needed to provide a unit of useful heat correspond to one divided by the amount of useful heat the system delivers during the lifetime of the considered component.

---

[6]The refrigerant assumed in the dataset is R-134-a (CH_2FCF_3).

9.4. LCIA

In this section the results obtained with the different impact assessment methods (cf. section 4.6) are presented. All impact values, unless otherwise stated, refer to the impact of 1 MJ of useful heat. First, the dependence of the ecological impact on the system dimensioning, the used collector type and the optional inclusion of a waste heat recovery system is analysed. Further, the results for the different buildings types are compared, followed by a discussion of the dependence of the ecological impact on the assumed electricity mix. The sensitivity of the impact on some of the important assumptions is shown next. Finally, the ecological impact of heat provision by the solar-ice system is compared to the impact of heat provision via more conventional systems.

9.4.1. Ecological impact for different system sizings

Varying the volume of the ice storage, the area of the collector field and the type of collectors used, the ecological impact was computed according to the different impact assessment methods (Fig. 9.1). The building corresponds to SFH45* and the system is operated with the Swiss consumer electricity mix.

For increasing system sizes (ice storage and/or collector field) the SPF increases. Hence, the impact of the use phase, which predominantly corresponds to the impact of the electricity consumption, decreases. The rate of this decrease, however, decreases with growing component sizes. The ecological impact of the infrastructure, on the other hand, gradually increases with increasing system size. Therefore, independently of the indicator, there is a system size beyond which an increase of the component sizes doesn't further reduce the ecological impact, but at some point starts increasing it. This critical system size, however, depends on the indicator.

In terms of CED_{nre} the impact of the infrastructure is very similar for systems with covered and uncovered collectors. For the simulated system sizes it represents a relatively small share of the total impact (5-29 %), which therefore mainly depends on the SPF of the system. For small collector field areas and small ice storage volumes, systems with uncovered collectors have a slightly higher SPF and consequently a lower impact. At large system sizings, covered collectors perform better and allow to reach smaller impact values. The lowest CED_{nre} value reached with covered collectors is 0.47 MJ. For systems with uncovered collectors the minimum value is 0.58 MJ. With a large storage volume of 30-40 m^3, these minimal impacts are practically reached at collector field areas of 20 m^2 (covered collectors) and 15 m^2 (uncovered collectors) respectively. For a small storage size of 10 m^3 the minima are reached somewhat above 35 m^2 (covered) and at 30 m^2 (uncovered).

Judging by the global warming potential GWP, like for CED_{nre}, the impact of the infrastructure is similar for covered and uncovered collectors. Again, uncovered collectors are slightly better at small system sizes and covered collectors at large system sizes. The lowest values, both for systems with covered and uncovered collectors, lie around 0.02 kg CO2-eq. In the case of covered collectors they can be reached with a storage of 40 m^3 and 15 m^2 collector field area on one extreme or with a 10 m^3 storage and 35 m^2 on the other extreme. For systems with uncovered collectors the lowest values are obtained with storage volumes in the range of 10-20 m^3 and collector areas of 20-30 m^2. Overall, in terms of GWP, the differences between the simulated systems are relatively small. The relative contribution of the infrastructure to the GWP (25-62 %) is higher than its contribution to the CED_{nre}. Therefore, the critical system sizes are reached at smaller component sizes.

In terms of UBP, covered collectors have a higher impact than uncovered collectors. This is mainly due to the impact of the copper, which the absorbers are made of. The relative contribution of the infrastructure is again substantial (27-72 %). Like in the case of GWP, the larger ones of the simulated systems are disadvantageous. The minimum UBP values, independently of the collector type chosen, lie around 40 Pts. For systems with covered collectors they can only be reached with large storage volumes (30-40 m^3) and 15 m^2 collector area. For systems with uncovered collectors, the low impact values can be reached with all simulated ice storage sizes, if the collector field area is chosen accordingly.

In summary, the lowest values for CED_{nre} are reached with covered collectors, while judging by GWP and UBP, the minimum values can be reached with both types of collectors. Concerning the size of the components, the results for CED_{nre} suggest to consider somewhat larger systems than the results in terms of GWP and UBP. Nevertheless it is possible to choose a system dimensioning, that corresponds to low values for all indicators. A comparison of the results for the ecological impact with the simulation results (cf. figure 7.6) shows that the component sizes at which the ecological impact becomes minimal
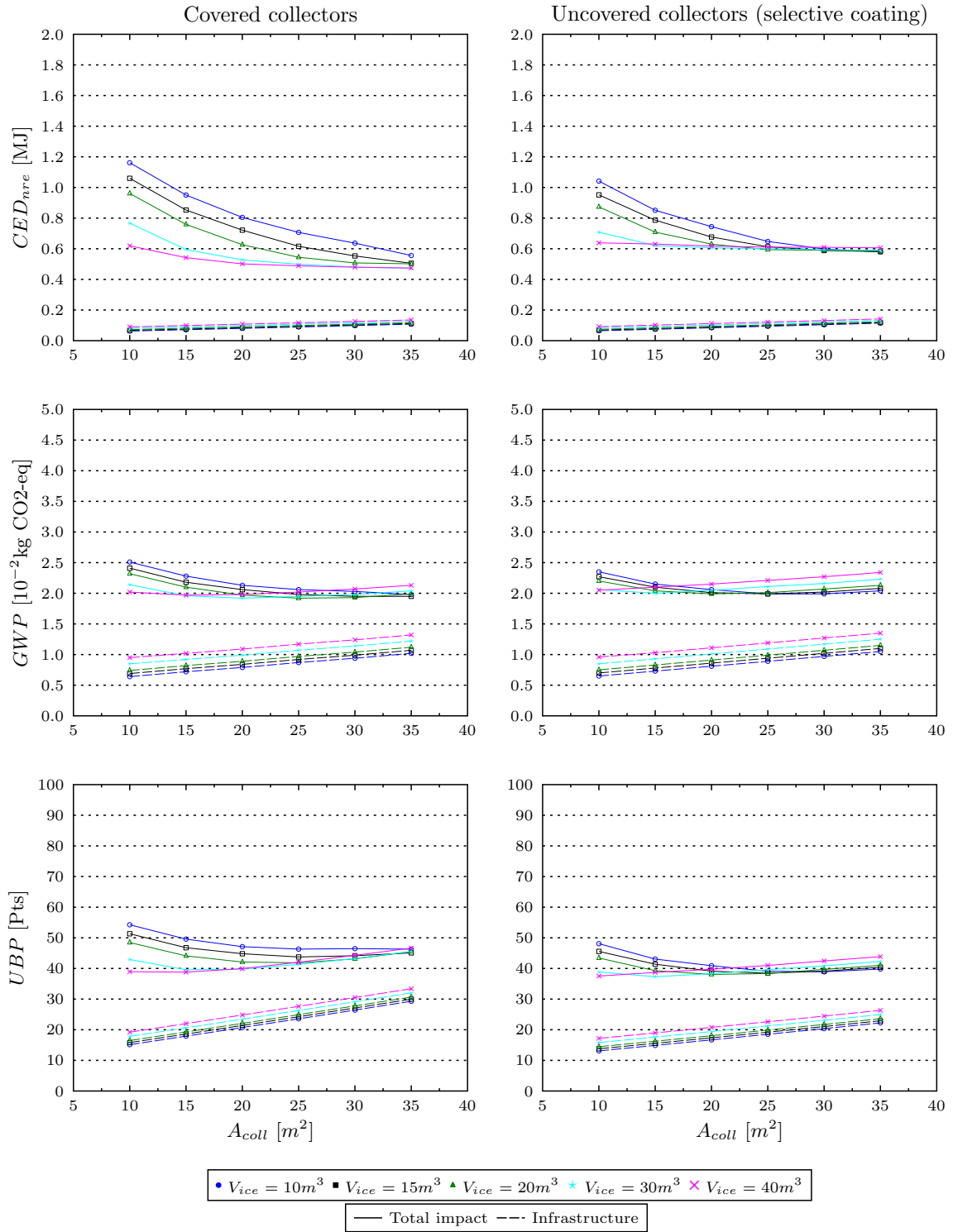
Figure 9.1: Ecological impact for different system sizings without waste heat recovery, for building SFH45* and assuming the Swiss consumer electricity mix.

practically correspond to the component sizes beyond which no more auxiliary heating is needed.[7] The small decrease of electricity consumption, that can be obtained by further increasing the component sizes, is not justified from the LCIA point of view.

---

[7]Only in the case of uncovered collectors in combination with a small ice storage, the ecological minimal impact is reached with a slightly smaller collector field than the $P_{El,aux} = 0$ criterion.

In order to look in some more details at the different contributions to the ecological impact, we select the system with an ice storage volume of 20 m^3 and 20 m^2 of covered collectors, whose impact scores lie in a good range for all three indicators. The partition of the total impact into the contributions of the main infrastructure components and the contribution of the use phase is shown in figure 9.2 (left).
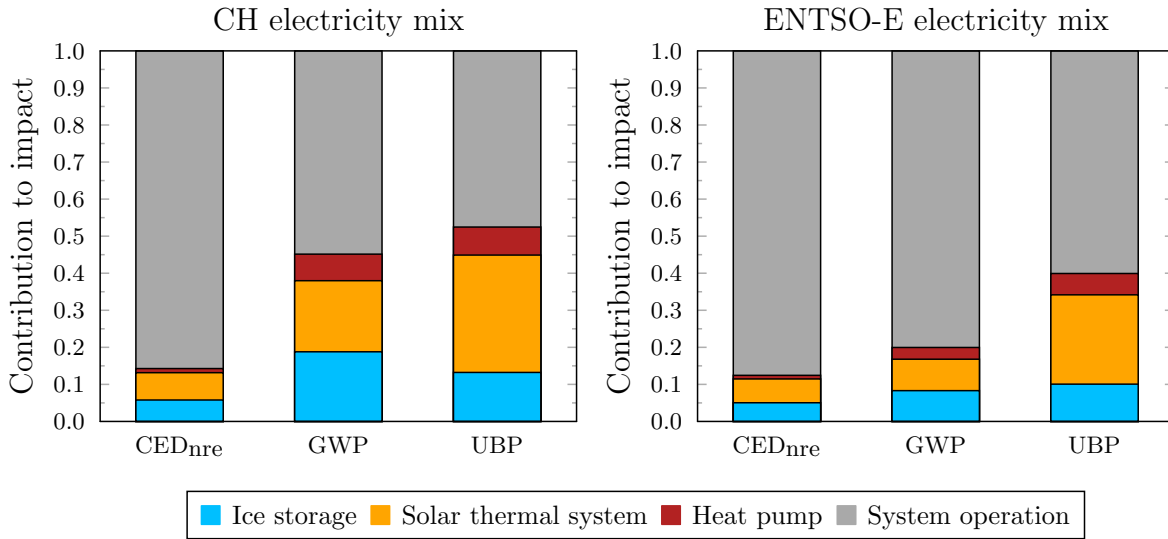
Figure 9.2: Relative contributions of the different system parts (infrastructure) and the system operation to the ecological impact for a system with a 20 m^3 ice storage and 20 m^2 of covered solar collectors, assuming the CH electricity mix (left) and the ENTSO-E electricity mix (right).

As already mentioned above, the use phase makes for a big part of the total ecological impact. This contribution will be discussed in more detail in Section 9.4.4.

The impact values of the infrastructure per MJ of delivered heat, for the particular dimensioning chosen here, are 0.089 MJ (14 %) for the CED$_{nre}$, 0.0089 kg CO2-eq (45 %) for the GWP and 22.1 Pts (52 %) for UBP, where the values in parentheses correspond to the relative contributions of the infrastructure to the total impact. Knowing the specific energy demand of building SFH45* (212 MJ/(m^{2}a) for space heating and 55 MJ/a for DHW), one can compute the impact values per m^2 of living space and per year: 23.9 MJ/(m^2 a), 2.38 kg CO2-eq/(m^2 a) and 5902 Pts/(m^2 a). These values can be compared to the impact of a complete building, in order to get an idea of their order of magnitude. Impact values for the infrastructure of residential buildings (including heating system and other expenditures) are for instance provided by the Swiss Society of Engineers and Architects (SIA) (cf. Table 9.1). The reported figures correspond to the present values (for new buildings and building conversions) and guiding values for new buildings motivated by the 2000-Watt-Society (see references Pfäffli and Preisig (2011a) and EnergieSchweiz).

Table 9.1: Present values and guiding values (2000-Watt-Society) for the yearly ecological impact of the infrastructure of residential buildings per m^2 of living space, as provided in the SIA-Effizienzpfad Energie (Pfäffli and Preisig, 2011a,b). The values include the infrastructure for space heating and DHW.

	CED$_{nre}$ MJ/(m^2 a)	GWP kg CO2-eq/(m^2 a)
Present value	139	11.2
Guiding value	110	8.5

The two big contributions to the impact of the infrastructure are due to the ice storage on one hand and the solar thermal system on the other hand. Their respective contributions to the CED$_{nre}$ and to the GWP are of similar magnitude. In terms of UBP, the solar thermal system has a bigger impact. The impact of the heat pump is also non-negligible, when looking at the GWP and UBP. Figures 9.3 and 9.4 show a further splitting of the contributions of the ice storage and the solar thermal system. The impact of the ice storage is clearly dominated by the concrete casing. The other two relevant contributions come

from the heat exchangers and the heat carrier liquid. The impact of the solar thermal system is dominated by the contribution of the collectors. The second major contribution is associated to the buffer storage tank. The remaining contributions are rather small in comparison.
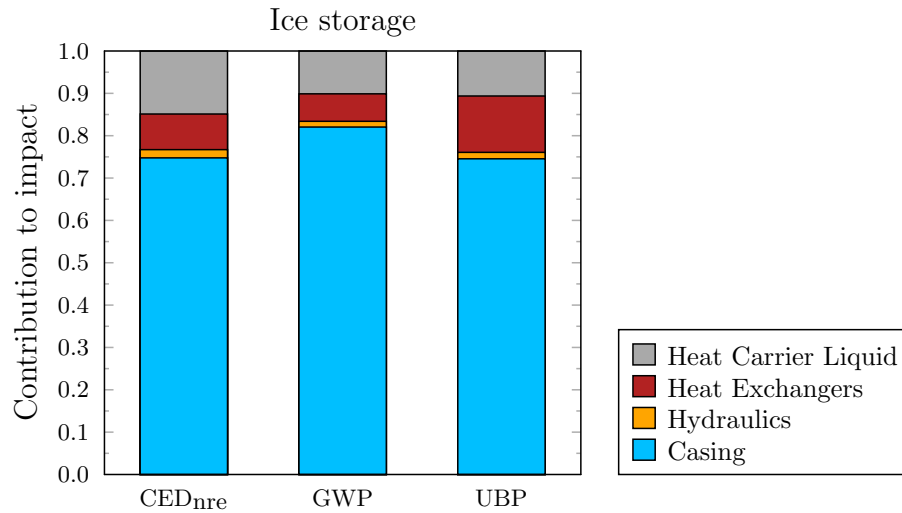
Figure 9.3: Relative contributions to the infrastructure impact of an ice storage with a volume of $20\,m^3$.
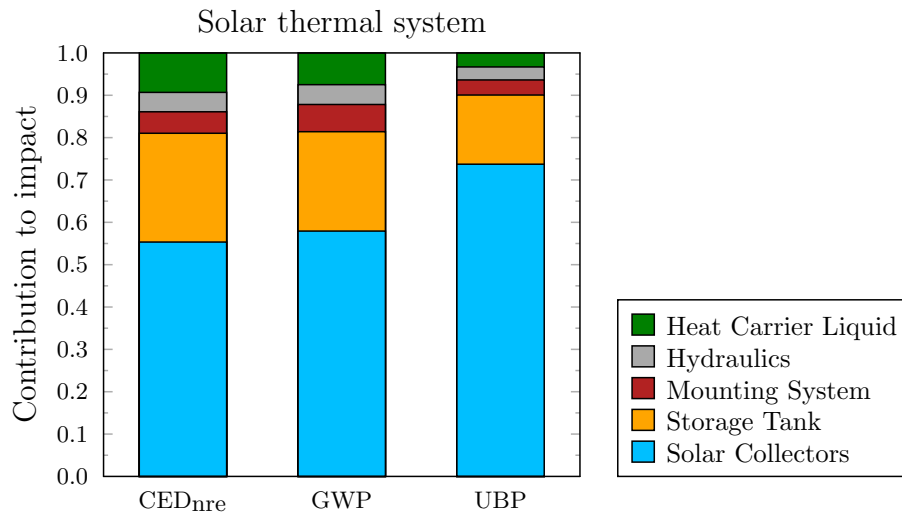
Figure 9.4: Relative contributions to the infrastructure impact of a solar thermal system with 20 m^2 of covered collectors.

9.4.2. Dependence on building type

For systems with uncovered collectors, the ecological impact was determined, in addition to SFH45*, for the building types SFH100$^*_{LT}$ and SFH100$^*_{HT}$. The results are shown in Figure 9.5. As could be expected, the component sizes at which the minimal impacts are reached are larger for the SFH100$^*_{LT}$ and SFH100$^*_{HT}$ compared to SFH45*. For SFH100$^*_{LT}$ and SFH100$^*_{HT}$ the lowest impact values can only be obtained with large collector fields (beyond 25 m^2). Presumably the same values could also be reached with smaller collector fields together with very large storage volumes (> 40 m^3). These cases, however, were not simulated, since such storage volumes don't seem to be a realistic option for single family houses.

The building SFH100$^*_{LT}$ reaches a minimal CED$_{\mathrm{nre}}$ value of 0.55 MJ, which is close to the value of SFH45*. The value for SFH100$^*_{HT}$ is almost 40 % higher. In terms of GWP, the minimal values for SFH45* and SFH100$^*_{HT}$ are very similar ($\sim$ 0.02 kg CO2-eq), while SFH100$^*_{LT}$ reaches a value that is 15 % lower. Also in terms of UBP, SFH45* and SFH100$^*_{HT}$ are similar, while the minimal value for SFH100$^*_{LT}$ is about 20 % lower.

In the case of the buildings SFH100$^*_{LT}$ and SFH100$^*_{HT}$ the system delivers a larger amount of useful heat during its lifetime. Hence, a bigger infrastructure can be built in order to reach the same infrastructure impact per unit of useful heat. This explains why, even though the SPF$_{\mathrm{SHP+}}$ values of these buildings are somewhat lower than the ones of SFH45*, the systems can reach similar and in the case of SFH100$^*_{LT}$ even lower impact values for the total impact per unit of useful heat.
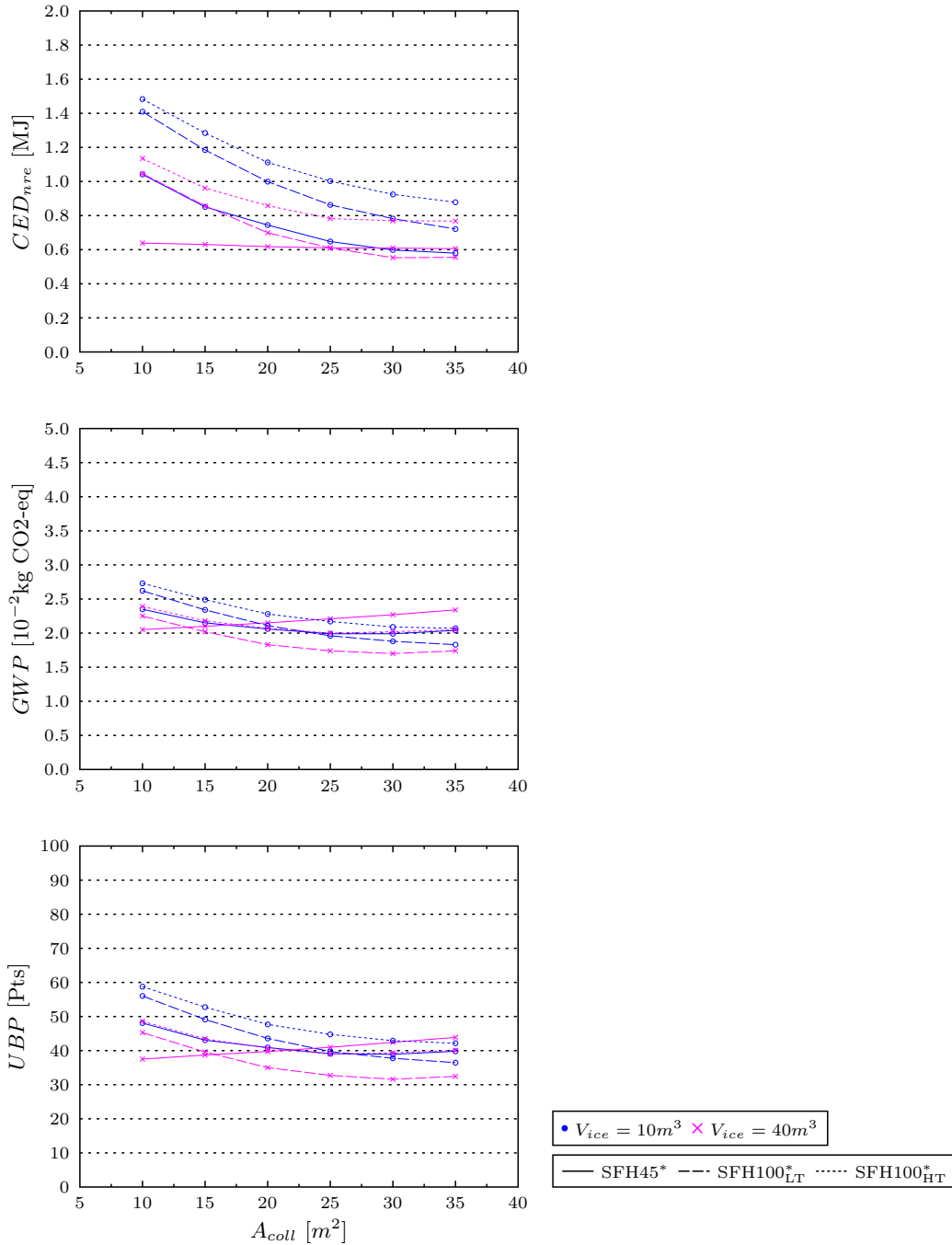
Figure 9.5: Comparison of the ecological impact for the different buildings SFH45*, SFH100$^*_{LT}$ and SFH100$^*_{HT}$ and varying component sizes, assuming the CH electricity mix.

9.4.3. Inclusion of waste heat recovery

For the systems with smaller storage sizes (10 m³ and 20 m³) the effect of including a waste water heat recovery storage was analysed (cf. figure 9.6).
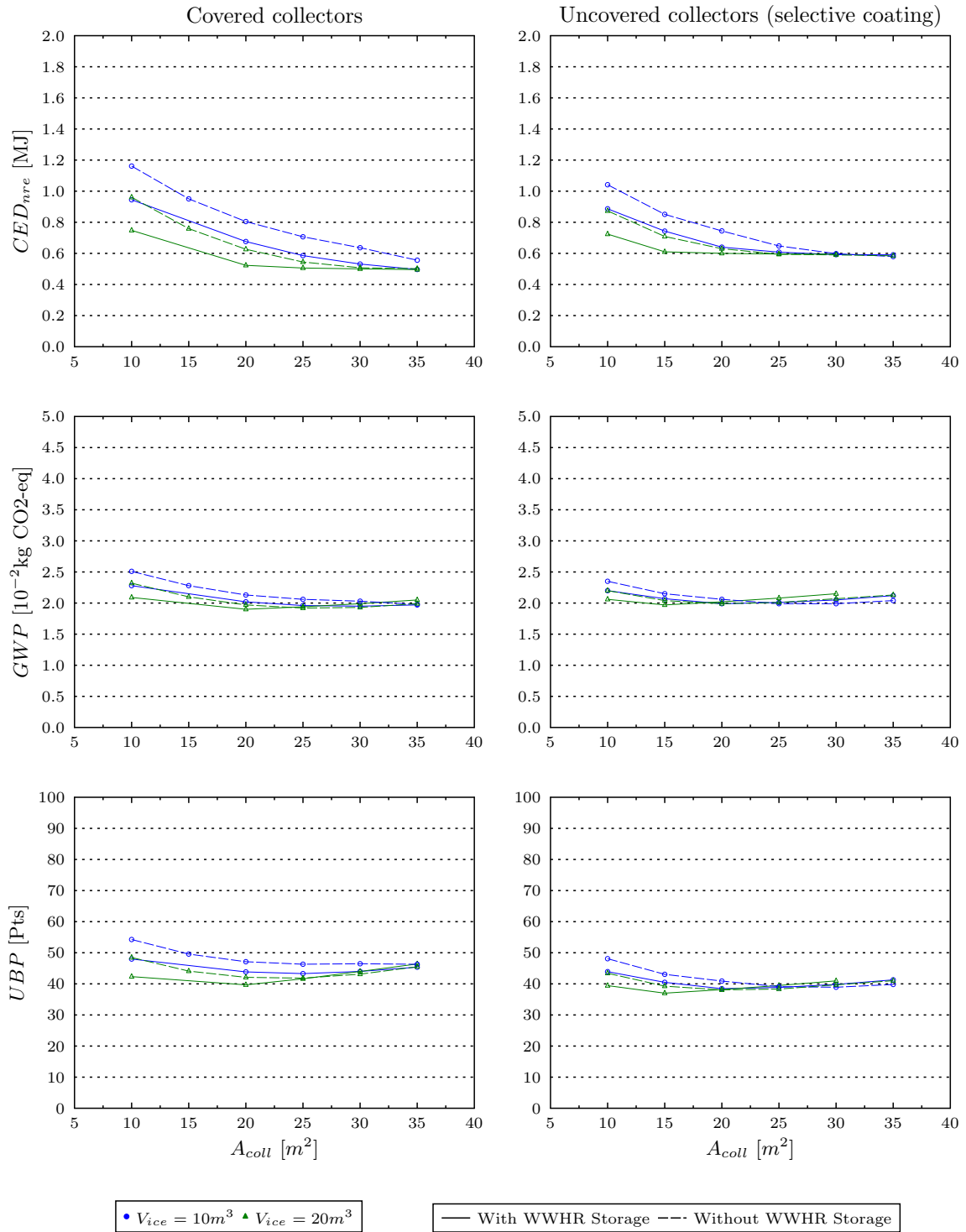
Figure 9.6: Ecological impact for different system sizings with and without waste heat recovery, for SFH45* and assuming the CH electricity mix.

Such a device plays a role similar to the one of the collectors. Therefore, adding a WWHR storage brings a stronger reduction of the SPF_{SHP+} and hence of the ecological impact in the case of systems with small collector fields. And, just like the increase of the collector field area becomes disadvantageous at some point, the addition of a WWHR device to systems with big collector fields increases their total impact. This effect can be seen in the results for the GWP and UBP and could also be observed in the CED_{nre}, if one went to collector field sizes > 35 m^2.

Except for the UBP of systems with covered collectors, the addition of a WWHR device doesn't lower the minimal impact scores. Using WWHR, however, allows to reach the same impact values at smaller collector fields (area reduced by 5-10 m^2) or smaller ice storage sizes.

9.4.4. Dependence on electricity mix

As already mentioned above, the impact of the use phase is a substantial contribution to the total ecological impact. As a consequence, the results strongly depend on the assumed electricity mix. In order to study this dependence, both the Swiss (CH) consumer electricity mix and the European (ENTSO-E) consumer electricity mix are considered. The composition of these two electricity products is shown in figure 9.7.

The CH mix mainly consists of nuclear power (46 %) and hydro power (39 %). It contains a rather small share (11 %) of fossil based electricity. The ENTSO-E mix, on the other hand, has a fossil share of about 51 %, mainly based on coal and natural gas. The other major contributions are nuclear power (27 %) and hydro power (16 %). The data is taken from the EI3 database and the related publication by Treyer and Bauer (2014) and is based on electricity statistics of the year 2008 for the ENTSO-E mix and 2009 for the CH mix.
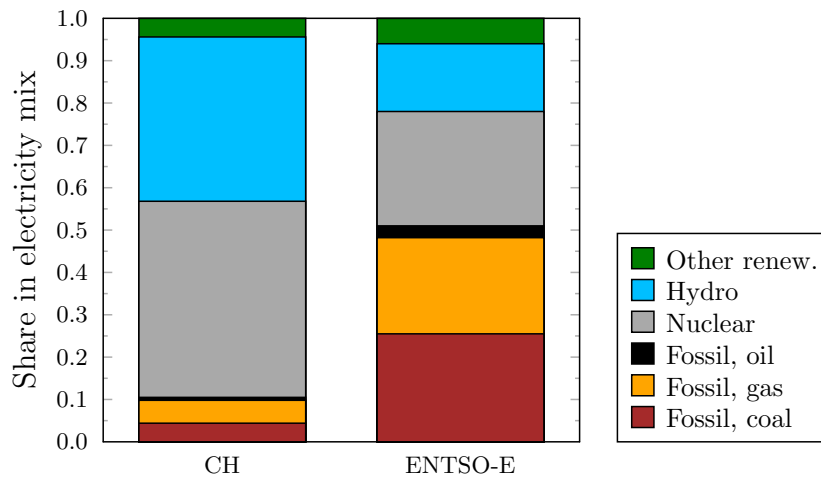
Figure 9.7: Composition of the Swiss and the ENTSO-E consumer electricity mix.

Figure 9.8 shows the comparison of the ecological impacts of the two electricity mixes. The bars show the relative magnitudes for the different impact indicators. The figures on the bars are the impact scores for the supply of 1 MJ of electricity to the consumer. It can be seen, that the ENTSO-E mix has higher values in all three indicators. The biggest difference appears for the GWP, where the score of the ENTSO-E mix, due to its higher content of fossil energy, is bigger by a factor of 4.3. Smaller, but still significant, is the difference in UBP, where the value of the ENTSO-E mix is about 70 % higher. In terms of CED_{nre} the impact is 17 % higher.

Like for the CH electricity mix, the total impact of a 1 MJ of useful heat was computed for systems with different component sizes (ice storage volume and area of covered collectors) operated by the ENTSO-E mix. The results are shown in figure 9.9, where the solid lines correspond to the systems with ENTSO-E mix and the dashed lines to the systems with the CH mix. In order to make the plots easier to read,
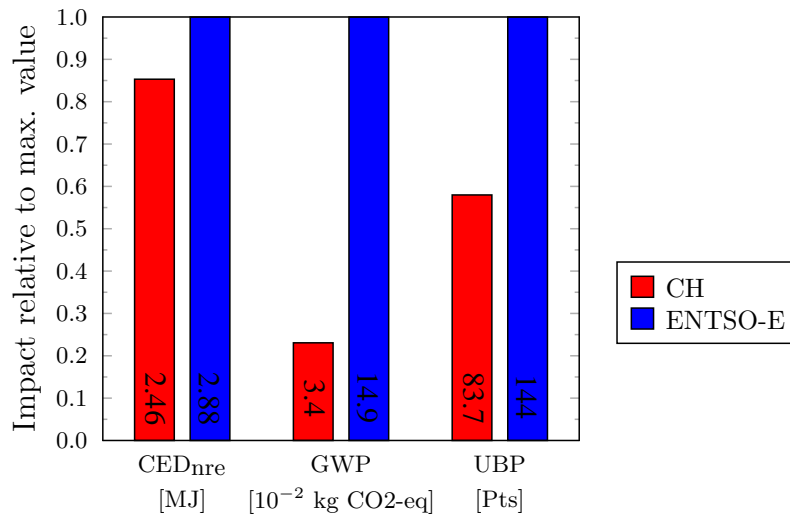
Figure 9.8: Comparison of the ecological impact of the Swiss and the ENTSO-E consumer electricity mix. Figures correspond to the impact of 1 MJ of electricity supplied to the consumer.

results are only shown for two ice storage sizes. With the ENTSO-E electricity mix the best systems reach CED_{nre} values of 0.53 MJ, i.e. 13 % higher than with the CH mix. The minimal GWP value is 0.036 kg CO2-eq, i.e. 90 % higher than for the CH mix. The minimal value for UBP is 50 Pts, i.e. 28 % higher. The component sizes at which the lowest values for the CED_{nre} are obtained, are very similar for both electricity mixes, since they have similar primary energy factors. The lowest values for the GWP and UBP, however, are reached at larger component sizes for systems operated with the ENTSO-E mix. This is due to the fact, that in these systems the contribution of the use phase (especially in terms of GWP and UBP) is yet more important (figure 9.2) than for systems operated with CH electricity mix.

9.4.5. Further sensitivity tests

Besides the assumed electricity mix, the LCA depends on a number of other assumptions. A few of the main assumptions were varied in order to study the sensitivity of the results. The main assumptions are related to the ice storage (buried into the ground). For this type of ice storage, little empirical data exists. Therefore, the lifetime and the casing material of the ice storage are varied. Further, the sensitivity of the ecological impact on the absorber material of the covered collectors is tested. The results for a system with 20 m^3 storage volume and 20 m^2 of covered collectors, supplying heat to a building of the type SFH45* and operated by the CH electricity mix, are shown in figure 9.10. For the purpose of comparison, also the sensitivity on the electricity mix is shown.

Reducing the lifetime of the ice storage by a factor of 2 significantly increases the total impact, especially the GWP (15 %) and the UBP (10 %). The reduction of the impact obtained by an extension of the lifetime by 25 yrs ranges from 1 to 5 %, depending on the indicator, and hence is hardly significant. Changing the casing material from stainless steel reinforced concrete to polypropylene or to glass fibre reinforced plastic has no significant influence on the impact ($\leq$ 4 %), independently of the indicator. The effect of substituting the copper/copper solar absorbers with aluminium/copper absorbers is a reduction of the UBP value by 10 %, while the values of other indicators remain virtually unaffected.

For the system dimensioning chosen here, changing from the CH to the ENTSO-E electricity mix significantly increases all impact values: + 15 % (CED_{nre}), + 126 % (GWP) and + 31 % (UBP). This illustrates once more the crucial role of the electricity mix.
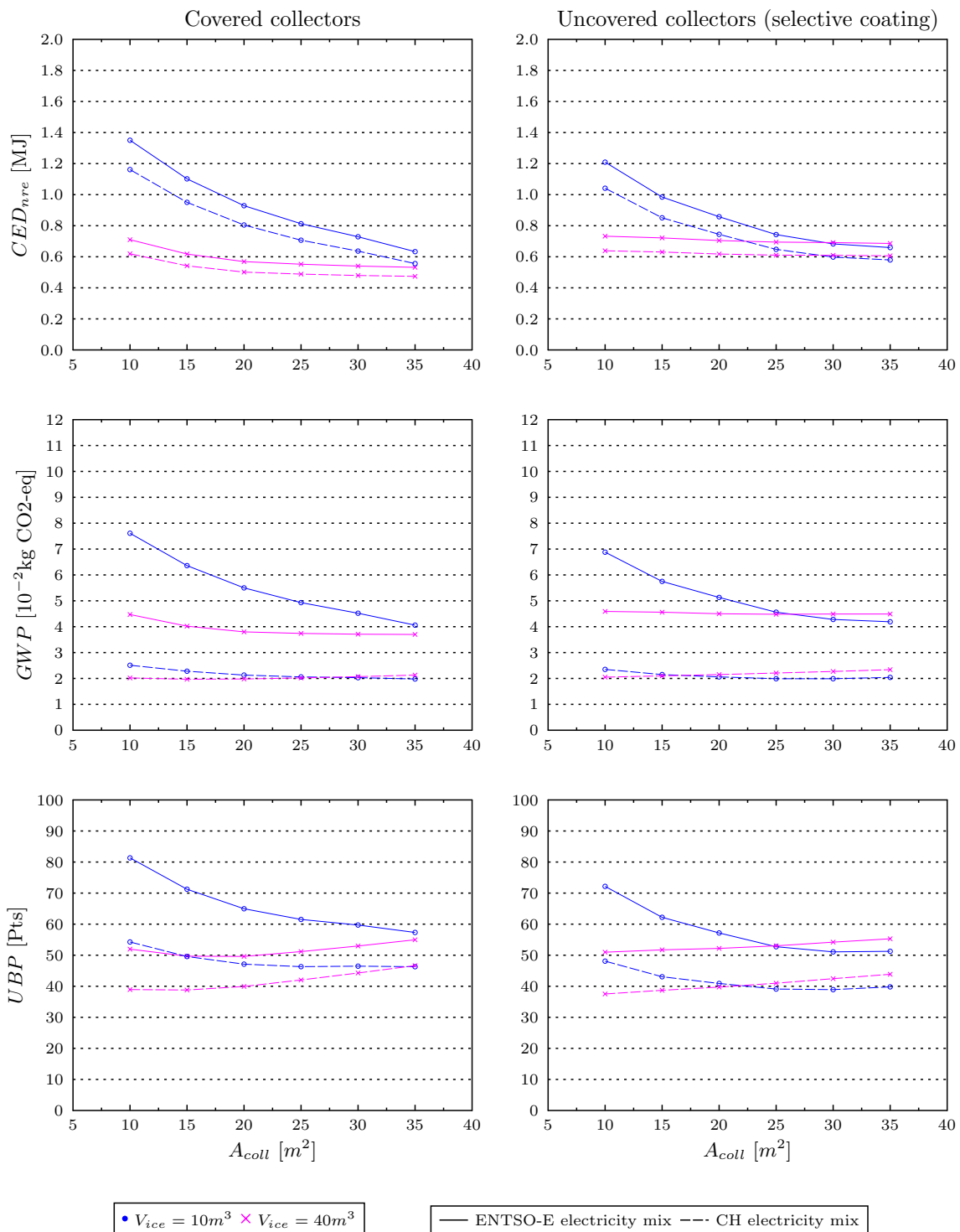
Figure 9.9: Comparison of the ecological impact for different system sizings without waste heat recovery for the CH and the ENTSO-E electricity mix. The assumed building is SFH45*.
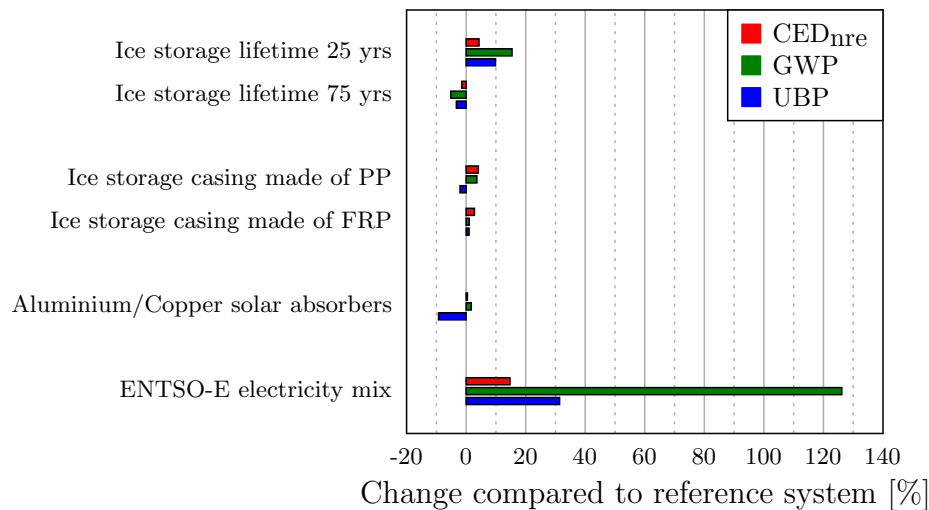
Figure 9.10: Sensitivity of the ecological impact to different assumptions. The reference is taken to be a system with a 20 m^3 ice storage (with a concrete casing and a lifetime of 50 yrs) and 20 m^2 of covered solar collectors (with absorbers made of copper only), for the building SFH45* and operated with the Swiss electricity mix.

9.4.6.   Comparison with other heating systems and with a complete building

Apart from using LCIA in order to optimize the design of the solar-ice system, it is also interesting to compare the obtained results with values for other heating systems. To this aim, a solar-ice system with an ice storage volume of 30 m^3 and 20 m^2 of covered collectors without waste heat recovery is considered. The chosen dimensioning yields values very close to the minima for all impact indicators (cf. figure 9.1), i.e. 0.53 MJ (CED$_{nre}$), 0.019 kg CO2-eq (GWP) and 43 Pts (UBP). Datasets for common heating systems were taken from the Ecoinvent database. The following heating technologies are considered:

- Light fuel oil boiler, 10 kW, condensing, non-modulating

- Natural gas boiler, < 100 kW, condensing, modulating

- Wood pellet furnace, 9 kW, state-of-the-art 2014

- Air/Water heat pump, 10 kW, SPF = 2.8

- Brine/Water heat pump with borehole heat exchanger, 10 kW, SPF = 3.9

The heat pump systems are, like the solar-ice system, operated with the Swiss consumer electricity mix. The functional unit is the supply of a unit of useful heat.

The comparison of the different impact scores is shown in figure 9.11. One has to bare in mind that the quality and level of detailedness of the different datasets can vary significantly. Therefore, the comparison presented here can only serve to show the respective orders of magnitude.

The biggest differences appear in the GWP, where the two fossil-based systems expectedly reach much higher scores than all other systems. The wood pellet system has the lowest GWP, while the GWP value of the solar-ice system is comparable to the values of the conventional heat pump systems. In terms of CED$_{nre}$, again, the fossil-based systems have the highest scores, while the pellet system clearly has the lowest impact, due to the renewable nature of the wood. The solar-ice system, having a comparably high SPF$_{SHP+}$ of 5.75, has a CED$_{nre}$ value that is $\sim$ 25 % below the value of the brine/water heat pump and $\sim$ 70 % below the one of the air/water heat pump. In terms of UBP, the oil boiler has the highest score. The brine/water heat pump reaches the lowest score, about 35 % below the one of the solar-ice system. All other systems have values comparable to the solar-ice system.
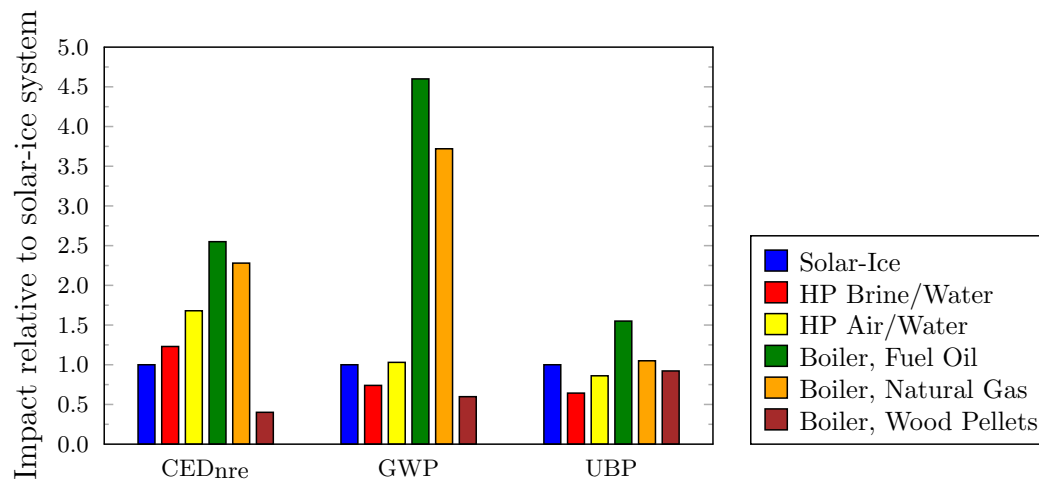
Figure 9.11: Comparison of the ecological impact of different heating systems. The reference is taken to be the solar-ice system with a 30 m^3 ice storage and 20 m^2 of covered solar collectors (i.e. a system dimensioning with very low impact scores), operated with the Swiss electricity mix.

9.5. Conclusions

When designing a new heat supply system, it is desirable to aim at a minimal ecological impact. The methodology of life cycle assessment (LCA) was used to analyse the solar-ice system from this perspective. The ecological impact was quantified with the help of three impact assessment methods: CED$_{nre}$, GWP and UBP.

In a first step, the different variants and sizings of the solar-ice system were compared in order to find the configurations with the lowest impact scores. Varying ice storage volume and collector field area, it was found that the minimal values for GWP and UBP are very similar for systems with covered and systems with uncovered collectors, while covered collectors allow to reach values 10 % lower for the CED$_{nre}$. Such minimal values necessarily exist, because above some critical component size, the decrease of the impact of the use phase is smaller than the impact of the added infrastructure. An important finding of the LCA is, that this happens very close to the point beyond which no more auxiliary heating, i.e. direct electric heating, is needed.

With both types of collectors, it is possible to choose a combination of ice storage volume and collector field area in such a way as to obtain values close to the minima for all three indicators simultaneously. In the case of covered collectors, these combinations need to have a large storage volume of $\sim$ 40 m^3, while for uncovered collectors, both large and small storage volumes can give low impact scores, if the collector field is sized appropriately.

Besides the reference case of a solar-ice system in a SFH45* building, impact scores were computed for the more poorly insulated buildings SFH100$^*_{LT}$ and SFH100$^*_{HT}$ (for systems with uncovered collectors). As could be expected, the lowest impact scores for these buildings are obtained at higher component sizes. The impact per unit of useful heat is of the same order of magnitude as for the SFH45*. Compared to the SFH45*, the SFH100$^*_{HT}$ reaches similar values in GWP and UBP and a value about 30 % higher in CED$_{nre}$. For the SFH100$^*_{LT}$, the GWP value is 15 % lower than for the SFH45*, the UBP value 20 % lower and the CED$_{nre}$ value roughly equal.

It was found that the inclusion of a waste heat recovery device in the system doesn't allow to lower the minimal values of the impact scores. However, as one could expect, it permits to reach the same values with smaller collector fields (reduced by 5-10 m^2) or/and smaller storage volumes.

Independently of the impact indicator, the most important contribution is due to the use phase, i.e. the electricity consumption of the system. As a consequence, the impact strongly depends on the assumed electricity mix. Changing from the Swiss (CH) to the European (ENTSO-E) electricity mix results

in higher (minimal) impact values for all three indicators: $+13\%$ in CED_{nre}, $+90\%$ in GWP and $+28\%$ UBP. The strong increase of the GWP is due to the big proportion of fossil based electricity contained in the ENTSO-E mix. Moreover, somewhat larger components are needed in order to reach the minimal values. It should be mentioned at this point, that the CH electricity mix contains a large share of nuclear energy. And, even though the ecological consequences of nuclear power production are contained in the UBP method, other impact assessment methods, that would for instance give more weight to radioactive waste, would yield less favourable scores to the CH electricity mix.

Regarding the infrastructure, the main contributions are due to the ice storage tank and the solar thermal system, the impacts of which, in turn, are dominated by the concrete ice storage casing and the solar collectors respectively. A sensitivity analysis showed that if the lifetime of the ice storage is only 25 years instead of the assumed 50 years, the impact of a unit of useful heat is higher by 10% (UBP) and $\sim 15\%$ (GWP). Changing the material of the ice storage casing from stainless steel reinforced concrete to polypropylene or fibre reinforced plastic brings no significant change. Using covered solar collectors with aluminium/copper instead of full copper absorbers reduces the UBP value by 10%.

Finally, the impact of heat supply by the solar-ice system was compared to database values for other heating systems. The comparison with the more conventional heat pump systems revealed that in terms of GWP and UBP the solar-ice system lies in the range of air/water heat pump systems, while brine/water heat pump systems have slightly lower values. Regarding the CED_{nre}, a well-dimensioned solar-ice system is better than the other heat pump systems. Fossil-based systems have the highest impact values, especially in terms of GWP. Wood pellet boilers clearly have the lowest CED_{nre} values.

10. Development of an ice storage with de-icing concept

As a practical part of the project an ice storage with heat exchangers that can be de-iced was developed with the aim of using materials that can be produced at low costs. For both, the ice storage casing and the heat exchanger products and semi-manufactured products were chosen. The concept of heat exchangers that can be de-iced, meaning that the forming ice on the heat exchanger surface is removed periodically, is developed further in this work. For advantages and disadvantages of using heat exchangers in the ice storage that can be de-iced and principle ways of how to de-ice see Chapter 2.

Different types of heat exchanger-shapes, -materials and -distribution in the ice storage were investigated in the laboratory. The experiments with the heat exchanger were performed in an ice storage with a volume of 1 m^3. A closed brine cycle was used that can be pressurised to increase the inner pressure inside the heat exchanger compared to the ambient pressure of the storage water. The cycle has an adjustable basic pressure and can periodically be pressurized with compressed air that is let into and removed from a vessel. The vessel is filled with brine and connected to the brine cycle.

10.1. Development of heat exchangers that can be de-iced

10.1.1. Coil type heat exchangers made of elastic tubes

Flexible tubes made of plastics were used to construct heat exchanger coils for de-icing experiments (Fig. 10.1). The sizes of the tubes were in the range of 10 mm outer diameter and 1.5 mm wall thickness to 30 mm outer diameter and 3 mm wall thickness with a length of around 2 m. During ice formation with inlet temperatures around -10°C the pressure in the tubes was increased until the ice around the coil was breaking. Depending on the ice thickness the basic pressure of around 0.7 bar had to be doubled to 1.4 bar to break the ice of several millimetres thickness. For the 30 mm tube the increase of diameter after breaking the ice was approximately +33 % (10 mm).

(a)   (b)
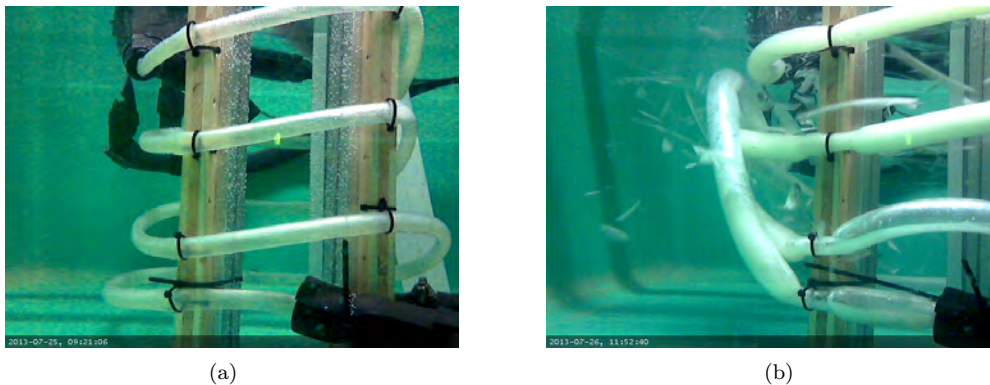
Figure 10.1: (a)Tube coil before de-icing (b) Tube coil during de-icing.

After inflating the tube and breaking the ice, the ice fragments often did not separate well from the coil. Many longer fragments were only lifted up some millimetres during the expansion. After finishing the expansion these fragments moved back at the surface of the coil. Some of the smaller fragments were sticking at the surface of the coil. However, in some de-icing experiments with small tubes a reproducible de-icing was shown.

Inflating tests were done with tubes made of Silicone, ethylene propylene diene monomer (EPDM), nitrile butadiene rubber (NBR), and polychloroprene (Neoprene) (Fig. 10.5). A principle disadvantage of all analysed tubes is that the thickness of the tube walls is not perfectly homogeneous which leads to an uneven expansion when the tubes are inflated. The sections with the widest expansion tend to get weak and may eventually burst if the pressure gets to high. This negative effect is enhanced if the surface is covered with ice: sections where ice brakes first absorb most of the volume increase of the heat exchanger. If the stability of the ice is in the range or even higher than the one of the tube, there is a risk that the tube will burst at the section where the ice brakes first before the coil is de-iced. The tube with 30 mm diameter was destroyed by bursting of a "bubble" of 15 cm diameter that was formed at 2 bar pressure.

Based on these results – a frequent adherence of ice at heat exchanger surface and a high risk of destroying the tube – it was decided to use flat plate heat exchangers.

10.1.2. Inelastic flat plate heat exchangers

Flat plate heat exchangers made of stainless steel and of Polypropylene were used to test whether a mechanical de-icing is possible. The heat exchangers were inelastic in the sense that they cannot expand if the pressure of the brine is increased. Bending of the heat exchangers on the other hand is possible.

Ice is sticking on the analysed heat exchanger surfaces very strongly during ice-formation and also as long as the surface of the heat exchanger is below 0°C during phases the heat pump is off and ice is not formed. In de-icing experiments with flat plate heat exchangers made of polished stainless steel the ice could not be separated from the heat exchangers. Even strong bending and scraping the ice manually with metal tools did not lead to de-icing. Apparently, even on a clean steel surface where the ice can not stick mechanically at uneven parts of the surface the adhesion forces between the heat exchanger surface and the ice are too large to separate the ice. The same results were obtained with a flat plate heat exchanger made of Polypropylene.

To test a highly hydrophobic surface with presumably low interaction also with ice, water was frozen on a 10 to 10 cm aluminium plate covered with PTFE (Teflon) in a freezer. The edges of the plate were kept free from water to prevent the water from mechanically sticking to them. The ice could not be taken off the PTFE surface with pushing or hitting against it as also here the adhesion forces were too strong. The experiments have shown that de-icing a flat plate heat exchanger mechanically by separating the ice from the surface by moving scrapers or bending the heat exchanger is not possible with moderate forces (no rigid de-icing-tools were mounted at the heat exchanger). In addition, it probably would be difficult to develop long lasting devices for this kind of mechanical de-icing that could operate in water and that could be produced at low cost.

10.1.3. Pre-tests with elastic flat plate heat exchangers

All analysed flat plate heat exchangers are constructed in a way that the main ice layers can be separated. The separation is reached by preventing the ice on both sides of the flat plate from growing together and by a partitioning of the ice that grows around the hydraulic connections from the main ice layers.

Using elastic flat plate heat exchangers, the expansion for de-icing increases the area of the plate. This increase leads to a widespread splitting up of the connection between the stiff ice and the surface and thus to a de-icing provided that the buoyancy forces are high enough to separate the ice layer totally. It is assumed that the inflation can be smaller compared to coil-type heat exchangers especially if the inflation increases primarily the surface area and not the plate's thickness.

Using elastic flat plate heat exchangers in the ice storage instead of a coil-type the flat ice plates that are formed will accumulate in the upper part of the storage with only few water in between which leads to a possibly higher maximum of usable latent heat.

Figure 10.2: Flat heat exchanger plate made of silicone tubes that are cast in silicone

Heat exchanger made of silicone

A flat plate heat exchanger made of silicone was built by casting small silicone tubes (Di: 7 mm, Da: 10 mm, length: 1 m, 30 pieces) in parallel into liquid two-compound silicone that hardened afterwards (Fig. 10.2). The silicone tubes were connected to rigid header pipes excluding the outermost two tubes. These were closed at the ends and used as barriers to avoid the ice on the two sides growing together what would make de-icing impossible.

The experiments showed that it is possible to de-ice thin ice layers until 10 mm with an overpressure inside the heat exchanger of 2 bar (overpressure inside the heat exchanger at start: 0.8 bar) as shown in Fig. 10.3 and 10.4. During the expansion the heat exchanger changed its shape longitudinal and also in crosswise direction. Thicker ice plates could not be de-iced as the barriers that prevent the ice layers from connecting with the ice that grows around the header pipes were designed too small. The 2-compound silicone was damaged after carrying out about ten de-icing cycles. Because of this and also because of the high price for semi finished silicone products it was decided to develop a heat exchanger made of EPDM.
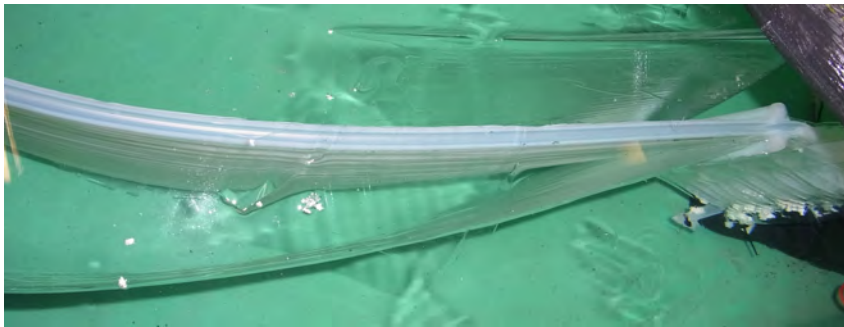
Figure 10.3: Detaching ice plates from the silicone heat exchanger realized with inflating the heat exchanger (here ice sticks at the rough glue of the barriers).
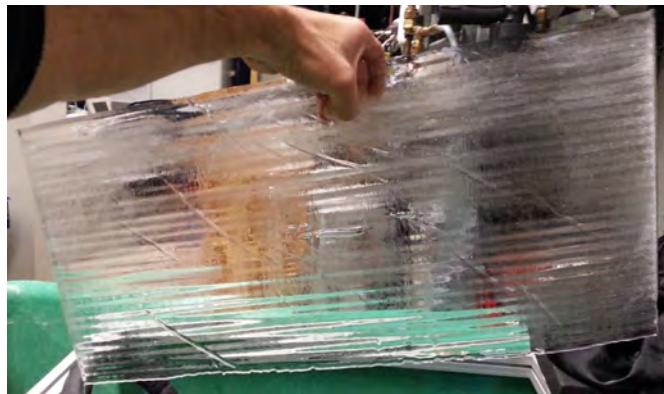
Figure 10.4: Detached ice plates from silicone heat exchanger.

Measurements of elongation

To select appropriate tubes for the construction a prototype of an elastic plate made that is designed similar to the silicone plate of the above section, elongation test of tubes were carried out.

The elongation of different plastic tubes were measured in ice water to find suitable materials that can be inflated. The analysed tubes were made of ethylene propylene diene monomer (EPDM), nitrile butadiene rubber (NBR), and polychloroprene (Neoprene). For the tests the tubes were inflated with pressurized air ranging from 0 to a maximum of 10 bar relative to the ambient. Then the diameter of the inflated tube was measured and the pressure converted to actual tension σ in the material and relative elongation ε with:

$$\sigma_{tangential} = p * \frac{d_{i0}}{d_{o0} - d_{i0}} \tag{48}$$

$$\varepsilon = (\frac{d_{o1}}{d_{o0}} - 1) * 100\% \tag{49}$$

Where d_{i0} is the inner and d_{o0} the outside diameter without and d_{o1} the outside diameter with pressure. P the applied pressure. For EPDM the elongation rises very rapidly in Fig. 10.5 from 3 to 3.5 bar. This seems to be an interesting working point were a large deformation of EPDM can be achieved with a small pressure increase.
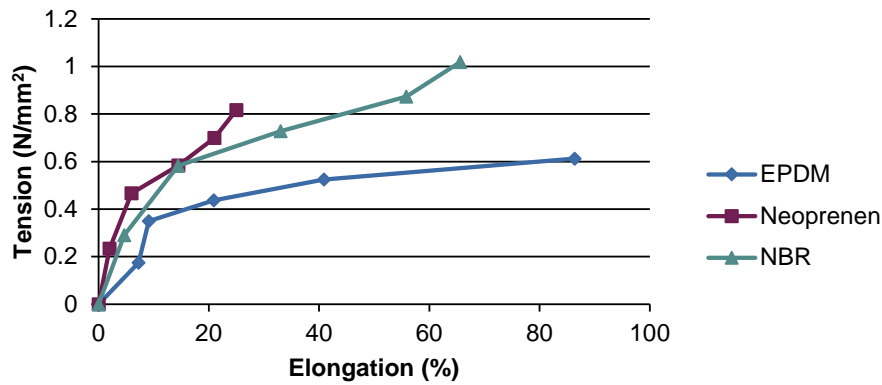
Figure 10.5: Elongation curve of 3 tubes made of EPDM, Neoprene, and NBR measured in ice water.

Flat plate heat exchanger made of EPDM

With the aim of using cheap products already existing on the market it was tried to find solar thermal pool absorbers made of EPDM that have both an appropriate shape and an elastic wall. Several collectors were tested but non of them could be inflated with a suitable pressure of below 6 bar.

Therefore an elastic heat exchanger made of EPDM was built to find materials with an appropriate strength and to optimize the shape of the heat exchanger (Fig. 10.6). A heat exchanger with semi-finished products made of EPDM rubber tubes, foil and glue was built with almost the same shape like the silicone heat exchanger (Di: 7 mm, Da: 11 mm, L: 1 m, Pipes: 60 Shore-A, Foil: 25 Shore-A). To get a smooth surface an EPDM foil was used to cover the pipes. However, only partial de-icing was possible at a high overpressure of 5.5 bar. At low brine temperatures of ca. -5°C the EPDM lost softness, which led to an insufficient inflation. The glue that was cast around the EPDM tube during the production led to a strong surface of the heat exchanger while the partition walls between the channels remained soft. Therefore the increase of area during inflation was smaller compared to the increase of heat exchanger thickness.

Functional model of an elastic heat exchanger printed in a 3D-printer

The previous tests had shown that depending on the ratio of thickness of walls between the channels of the heat exchanger and the wall of its surfaces the expansion leads mainly to an increase of its thickness and not to an increase of its area. As only the increase of the surface area makes a de-icing possible, the cross section had to be improved in a way that the inflation affects mainly the surface. For this purpose a new heat exchanger geometry was designed and sketched in a CAD drawing (Fig. 10.7). The plate contains channels for the brine and is meant to be extruded. The header pipes were meant to be glued or cast at the open ends of each plate. To test the new design a functional model was printed in a 3D-printer (Fig. 10.8).

(a)   (b)
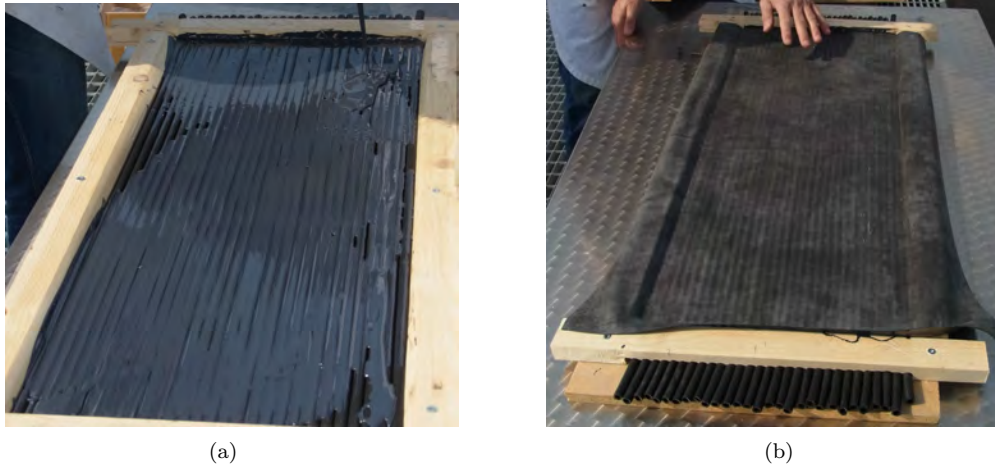
Figure 10.6: (a) Casting of the heat exchanger plate with EPDM tubes and glue (b) EPDM foil as cover of the plate.
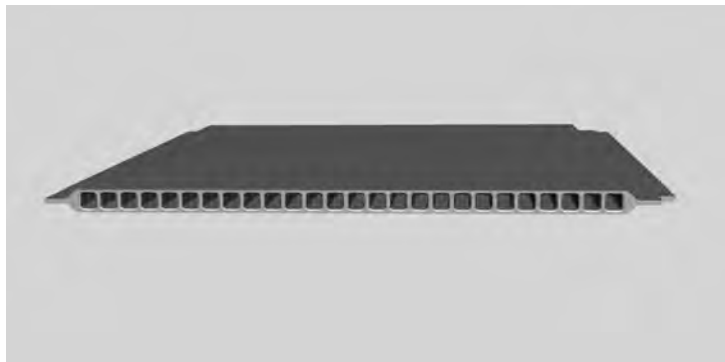
Figure 10.7: CAD-sketch of the heat exchanger plate with open channels in direction of the header pipes.

Figure 10.8: Functional model of the elastic heat exchanger printed in a 3D-printer.

Unfortunately, and in contrary to the producers statement the printed elastic prototype could not be sealed in way that it was tight. Nevertheless, this functional model could be used to test the expansion when it was set under pressure with air. Due to the inflation the area of the plate was increasing in both directions right-angled and parallel to the header pipes which is promising for de-icing. Because of the lacking tightness no de-icing experiments could be done.

10.1.4. Extruded flat plate heat exchanger made of EPDM

Based on the experience with the 3D-printed functional model, 30 m of an extruded EPDM-plate were ordered for building heat exchangers. The plate was extruded by a manufacturer with 63 Shore-A EPDM and the same cross-section that was tested with the functional model. Pieces of the extruded strip were glued into slotted header pipes for assembling the heat exchangers (Fig. 10.9).

In first de-icing tests the ice plates were breaking but they could not detach as the surface of the extruded EPDM apparently is too rough. Pictures with the microscope showed that the surface of the EPDM is to some extent porous. In the cavities the ice stays attached. By applying a thin layer of liquid coatings like silicone or EPDM-glue to get a smooth surface this problem was solved (see Fig. 10.10). The coating used in the experiments was the two-compound glue "REMA SC2000 Cement".

Figure 10.9: Heat exchanger with extruded EPDM plate for tests in the small ice storage.
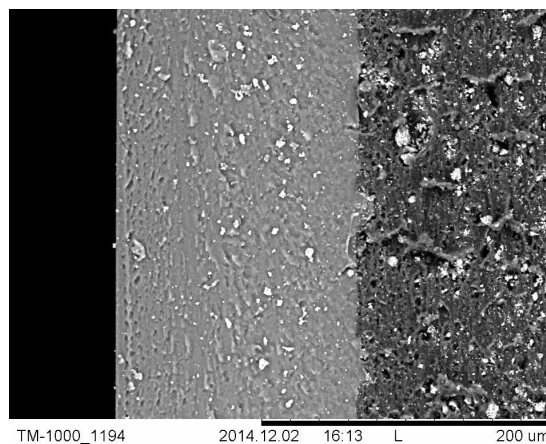
Figure 10.10: Cross-section of the extruded EPDM surface heat exchanger covered with a silicone layer that fills up uneven parts of the EPDM surface (microscope picture). Right side (dark grey): EPDM heat exchanger; middle (light grey): silicone layer which fills up the rough EPDM-surface; left side (black): air.

Tests with numerous de-icing cycles were carried out. The EPDM heat exchanger reaches U-Values of around 60 W/m^2K when ice starts to grow (conditions: mass-flow of 290 L/h and inlet/outlet-temperatures of -7.8 °C resp. -7 °C). A typical de-icing cycle defined for the experiments consisted of an icing phase of 1.5 hour and a inflation of 30 seconds with a pressure difference to water side of 3.2 bar. This pressure difference corresponds to an elongation of about 8 % in each heat exchanger dimension, which is necessary to de-ice successfully. Experiments at different temperatures of the storage water around the heat exchangers showed that a purely mechanical de-icing is only possible if the surrounding water has a higher temperature than approximately 1°C. After cooling down the ice storage over a long time the temperature of the water around the heat exchangers at the bottom of the storage was below 1°C. When during de-icing the ice layer is pushed away from the surface, cold surrounding water fills the gap between the ice and the heat exchanger. As the heat exchanger surface is very cold at this time [8]

---

[8]depending on the chosen brine temperature in tests between -2°C and -7°C

the water between the heat exchanger and the ice layer freezes immediately thereby re-attaching the ice plate to the heat exchanger. If the brine cycle is heated up to around 0.5 °C before expanding, de-icing is also possible at lower water temperature. The temperature rise in the brine cycle then serves not for ice melting but for preventing new ice-building in the water-filled gap.

A further finding is that the EPDM looses strength when the heat exchanger is pressurized and heated above circa 20°C. The following behaviour of the heat exchanger during de-icing is then different as the tension of the EPDM is decreased and a higher pressure has to be used for de-icing. However, the tension of the EPDM can be "set back" to the original status if inner pressure is reduced while the heat exchanger is at higher temperatures (above 20°C). This behaviour has to be taken into account for real systems where during the summer semester the temperatures in the ice storage can be high.

For one of the heat exchangers the glue that was used to evening out the surface was not stable and peeled off partly. This had a negative effect and stopped the de-icing capability of the affected surfaces.

10.2. Cylindrical ice storage

A cylindrical storage in a lying position was built as shown in Fig. 10.11 in collaboration with the Swiss storage manufacturer Rotaver. The storage has an inner diameter of 1.4 m and contains 3.4 m^3 water. Whether the round cross-section can be filled successfully with ice layers that detach from the heat exchangers after de-icing was tested in experiments.

Figure 10.11: Test set-up for a cylindrical ice storage in laboratory.

Table 10.1: Characteristic data, length L_{hx} height H_{hx} and area A_{hx} for the EPDM flat plate heat exchangers with a hx thickness of 9.5 mm, wall thickness δ_p of 1.7 mm and conductivity λ_p of 0.3 W/mK. The z_{in} and z_{out} are the absolute input/output height of the pipes connections (in parentheses values are relative to tank height).

Heat Exchanger	L_{hx}	H_{hx}	A_{hx}	z_{in}	z_{out}
	m	m	m^2	m	m
middle-hx (hx$_1$ and hx$_4$)	1.6	0.22	0.352	0.18 (12.8%)	0.4 (28.5%)
centre-hx (hx$_2$ and hx$_3$)	1.6	0.22	0.352	0.09 (6.4%)	0.31 (22.1%)

To investigate the de-icing behaviour of the heat exchanger with extruded EPDM plates more closely, 4 heat exchangers as described in Chapter 10.1 were installed upright at the bottom of the cylindrical ice storage with a distance between the heat exchangers of 30 cm, and connected in parallel. All of them are used to build ice (see Fig. 10.12). According to the cylindrical shape of the ice storage both heat exchangers in the middle (referred to as middle-hx) are located further down than the outer heat exchangers (referred to as outside-hx). Details of the heat exchangers are provided in Table 10.1. The storage temperature was measured at four different heights: 10%, 21%, 33% and 58% relative to the storage diameter. Experiments showed that detached ice layers will float well distributed and dense on

the water surface. At the beginning of the experiment de-icing was always successful. The temperature of the surrounding water was > 1 °C and thus the re-attachment of separated ice-plates did not happen (see Section 10.1.4).

Figure 10.12: Four elastic heat exchangers with 1.6 m length each in the cylindrical ice storage before (left) and after (right) mechanical de-icing by inflating the heat exchangers.

Figure 10.13: With de-icing detached and accumulated ice layers (white) that float in the cylindrical storage.

10.3. Conclusions

The experiments with heat exchanger plates made of different materials showed that heat exchangers plates that can be bent but not inflated could not be de-iced. Neither bending nor efforts to break off the ice from the surface of the plates were successful. The attaching forces between ice and surfaces are evidently very strong – even on a plate covered with PTFE (Teflon), ice was attaching too strong below 0°C.

It was shown that elastic plates can be de-iced successfully if it is possible to inflate them sufficiently and if they expand in an appropriate way. An important result of the experimental work was the design of an optimized shape of an extruded elastic plate made of EPDM. However, the surface of the EPDM was too rough after production and had to be coated with a smooth material. An aim should be to find a material other than the used EPDM or a better extrusion process that results in a extruded plate that does not have to be coated.

De-icing with the coated plate was always possible as long as the temperature of the storage water around the immersed heat exchangers was above approximately 1 °C. Below that the ice plates could not be separated if the heat pump was still extracting heat with brine temperatures below -5 °C. Most probably water that pours into the gap between heat exchanger and ice plate during de-icing immediately freezes and connects the ice plate with the heat exchanger again. It thus prevents the ice plate from detaching.

However, when the extraction of the heat pump was stopped and the de-icing was carried out after waiting until the heat exchanger temperature was close to 0 °C[9], de-icing by inflation was possible again. For the developed heat exchanger an elongation of at least 8 % in one direction of the heat exchangers surface was necessary to detach the ice. This corresponds to a pressure increase inside the heat exchanger of about 3.2 bar.

In a heating system with solar collectors it can be assumed that also during winter the ice storage will be loaded frequently and thus the water around the heat exchangers is cooled down less than in the experiments. For example the temperature at the bottom of the ice storage of the pilot plant (see Section 4.3) has dropped below 2 °C only during a few days in winter. In principle, in ice storages heat gains through the walls will accumulate at the bottom of the storage due to the convection regime after change of the density gradient of water below 4 °C. Thus, depending on the extraction power of the heat pump and its running time, the brine temperatures, and heat gains (from solar and walls) the conditions in a real heating system can be less harsh than in the performed experiments. Therefore the developed mechanical de-icing might be applicable in a real system. The experiments have shown that an active strategy for ensuring mechanical de-icing could also be to stop the heat pump and to wait until the surface temperature of the heat exchangers rises near 0 °C before inflating the plates. The temperature rise could be accelerated by circulating fluid in the brine cycle and thus bringing heat gains from the piping or from other sources into the ice storage. However, this would be to some extent a combination of mechanical and thermal de-icing.

The experiments with a cylindrical storage in a horizontal position with a volume of 3.4 m^3 have proved that also with an ice storage with round cross-section it is possible to accumulate the detached ice well distributed and dense in the upper part of the ice storage. The shape is promising for large ice storages that are buried in ground as the shape is statically very stable also with small wall thickness and several manufactures are selling standard casings of this type.

---

[9]what could be accelerated with holding the mass flow of the brine cycle and using heat gains of the pipes to the heat up the heat exchangers slightly

11. General conclusions

The annual simulations of the proposed solar-ice systems for the climate of Zurich have shown that a high system performance can be reached with different combinations of collector area and ice storage volume. This makes it possible to adapt the system size to local requirements regarding storage volume or collector area. Particularly high system performance factors (SPF_{SHP+}) are reached by systems with covered collectors. The largest system considered had an ice storage volume of 40 m^3 and 35 m^2 of covered collectors and reached an SPF_{SHP+} of 7.2 for building SFH45*. The simulations results for systems with uncovered selective collectors show that using this kind of collectors allows to reach high SPF_{SHP+} already with moderate system sizes.

The direct electric backup, used for heating the building when the ice storage is fully iced and when using the heat pump is no longer possible, has a crucial influence on the system performance. The increase of component sizes results in a strong increase of the SPF_{SHP+}, as long it helps to reduce the need for electric backup heating. For system sizes where no backup is needed, a further increase of the component sizes brings a smaller advantage in the performance.

In systems that do need electric backup, it is advantageous to use uncovered collectors, since they have a higher efficiency at low temperatures and a better heat exchange with the ambient air when no solar irradiation is available. For reaching very high SPF_{SHP+} above about 5, covered collectors should be used. The simulations have shown that it is of high importance to minimize the use of electric backup heating. For smaller systems, the control thus has to be defined in such a way that it stops the direct use of solar heat for the building early enough and instead uses the heat for the melting of ice in the storage.

Different combinations of component sizes (collector field area and ice storage volume) can be found, that are just big enough to cancel the need for electric backup. For a better comparability of the results, the sizes can be related to the heat demand (space heating and DHW) of the building. For building SFH45* and covered collectors these combinations range from 1.4 m^2 collector area together with 3.9 m^3 ice storage volume per MWh to 3.4 m^2 and 1.4 m^3 per MWh. Combinations in between are also possible. For systems with uncovered collectors with similar collector field sizing, the ice storage volume can be smaller by roughly 0.5 m^3 per MWh. The area of the de-icable heat exchanger can be related to the thermal power of the heat pump. With the assumption that a maximum ice thickness of 1 cm is accepted the heat exchanger area should be in the range of 3 m^2 per kW nominal power of the heat pump.

When the system was simulated using 12 years of real meteorological data from the city of Zurich, it was found that the standard-file with meteorological data for Zurich that was normally used in this project (METEOTEST, 2012) represents a poor year in terms of solar gains. When using the 12 years of real weather data, all but one of the simulated years reached significantly higher SPF_{SHP+} compared to the value obtained with the standard-file. In average, the resulting SPF_{SHP+} were 22% higher for a system that needed electrical back-up and 16% for a system that had no need for it. This comparison suggests that the general results of this project, which were all calculated with the standard-file, might be at the lower limit. However, further analysis of the mentioned differences in the weather data could not be carried out in this project.

The high sensitivity of the system performance on the available solar radiation could also be seen in simulations carried out for Davos, an alpine and thus cold but sunny climate, and Locarno, a sunnier location with mild winters in the southern part of the Alps. Results for these two locations show that a very good performance with an SPF_{SHP+} in the range of 6 for building SFH45* can be achieved with moderate system sizes, i.e. $V_{ice} =$20m^3 and $A_{cov} = $20m^2 for Davos and $V_{ice} =$10m^3 and $A_{cov} =$15m^2 for Locarno.

Waste water heat recovery (WWHR) devices can be of great help to increase the system performance, specially if a waste water storage (WW$_{storage}$) is used. Performance improvements in the range of 20% can be expected for systems that, without WWHR, would need electric backup heating. Despite the potential of a WW$_{storage}$ to improve the system performance, its high cost and maintenance needs may prevent it from being the favourable choice for a single family house. Nevertheless, the obtained results can be extrapolated to buildings with higher demands, such as multi family houses, where a WW$_{storage}$ could be affordable and even reduce the total system costs if the sizes of the ice storage or the collector area could be reduced. Moreover, the results show the general potential of using waste heat, which might also be obtained from other sources, for the ice storage regeneration.

The cost analysis has shown that, except for very small systems in building SFH100$^*_{LT}$, reducing the component sizes will lead to reduced heat generation costs. However, as the system concept is still under research and development, the economic results should not be overvalued. Moreover, as mentioned before, the weather data used in the analysis represents a year that is poor in solar irradiation compared to the 12 years of real weather data. Assuming higher solar gains, the system components could be sized smaller, which would lead to a reduction of the heat generation costs. Still, it will be a challenge to significantly reduce the costs of the studied systems, without reducing their energetic efficiency.

The Life cycle assessment (LCA) shows that there exists a critical system size, beyond which an increase of component sizes has no further benefit and even becomes disadvantageous from the ecological perspective. The results reveal that the advantage of the reduced electricity consumption is always larger than the additional impact of the infrastructure, as long as it helps to reduce the need for backup heating. This conclusion holds both for the Swiss consumer electricity mix and the European ENTSO-E electricity mix, the latter even allowing for larger system dimensioning.

The environmental impact of heat supply by the solar-ice system strongly depends on the assumed electricity mix. The biggest difference appears in the Global Warming Potential, where the impact roughly doubles when changing from the CH to the ENTSO-E mix. On one hand this shows a way to reduce the ecological impact, namely by using more ecologically produced electricity – which is out of the scope of this project. On the other hand, it shows that future changes in the Swiss consumer electricity mix can strongly affect the ecological impact of heat pump based heating systems.

The importance of the electricity demand of the systems and thus the SPF$_{SHP+}$ is very different in the LCA and the cost assessment. In the LCA, electricity consumption strongly matters. In order to reach a low ecological impact relatively large systems should be realized that ensure a low electricity consumption. In the cost analysis, on the other hand, electricity plays a minor role. With the objective to minimize costs, an investor would choose a small system that guarantees low heat generation costs, as long as the electricity prices remain moderate. This constitutes a principle problem for the considered system concept, as the choice to reduce the ecological impact is not economical for the investor. This conflict of goals, however, applies to a number of other heating concepts that have an energy input with a high share of renewable energy.

In practical work, a prototype of an elastic heat exchanger plate made of EPDM was developed, which is mounted at the bottom of the ice storage and can be de-iced by inflation. The experiments have shown that as long as the storage water is warm (in the experiments above circa 1.5 °C) the mechanical de-icing is possible. However, if the temperature of the storage water drops below this value, the ice can only be detached via a combination of mechanical and thermal de-icing, which shows a limitation of the proposed concept. Ice storages in real heating systems might be loaded regularly, even during winter. Therefore, in real operating conditions, the temperatures of the storage water are likely to be high enough to allow for reliable de-icing by the mechanism proposed here. The experiments with a cylindrical ice storage of 3.4 m^3 volume in a horizontal position, with 4 heat exchangers, have shown that the detached plates can accumulate well and densely. Especially for ice storages buried in ground the cylindrical shape is interesting, as standard products of that kind are available.

The High-Ice project focused on a system concept optimized for large system performances based on heat exchangers with de-icing capabilities. For small systems sizes, that are the most attractive from an economical point of view, the proposed ice storage concept with de-icable heat exchangers might not be the concept of choice. For systems with relatively small ice storages, filling the storage with evenly distributed heat exchangers may be a better option. For this reason, the follow up project IceEx aims at characterizing heat exchanger concepts for ice storages without de-icing capabilities, that are available on the market or were developed recently. The heat exchanger concepts will be analysed with experiments and simulations in order to find an optimum for the design of heating systems. Costs, system efficiency, and primary energy demand over the whole lifetime will be used to assess the different systems.

Nomenclature

Abbreviations

A	Annuity
B0\W45	brine temperature 0 °C, water temperature 45 °C
CED_{NRE}	Cumulative non-renewable energy demand
CH	Switzerland / Swiss
CI	Continuous icing
$Cr_{SPF\sim 4}$	Design criterion corresponding to an SPF close to 4
Cr_{No-Aux}	Design criterion corresponding to no need for electric back-up heating
DHW	Domestic hot water
COP	Coefficient of performance of the heat pump
DN	Nominal diameter
ENTSO-E	European network of transmission system operators for electricity
EPDM	Ethylene propylene diene monomer rubber
FH	Forced heating
FRP	Fibre reinforced plastic
GSHP	Ground source heat pump
GFX	Gravity film heat exchanger
GWP	Global warming potential
H	Height (m)
HGC	Heat generation costs
HPP	Heat Pump Program
hx	Heat exchanger
IDI	Icing and de-icing
IDI-F	Icing and de-icing until fully iced storage
IEA	International Energy Agency
ISO	International Standard Organisation
L	Length (m)
LCA	Life cycle assessment
LCI	Life cycle inventory
LCIA	Life cycle impact assessment
LMTD	logarithmic mean temperature difference
lt	Lifetime
NBR	Nitrile butadiene rubber
NC	Natural cooling
NM	Natural melting
NPV	Net present value
PIR	Polyisocyanurate
PTFE	Polytetrafluoroethylene
PU	Polyurethane
PVC	Polyvinyl chloride
SFH	Single family house
SH	Space heating
SHP	Solar and heat pump system
SPF	Seasonal (annual) system performance factor
T44/A38	Task 44 Annex 38
TDMA	Tridiagonal matrix algorithm
TES	Thermal energy storage
UBP	Umweltbelastungspunkte
W	Width
WS	Warm storage
WW	Waste water
HR	Heat recovery
XPS	Extruded polystyrene

Variable and parameter names

A	Area (m^2)
A_c	Collector area (m²)
A_{cov}	Covered collector area (m²)
A_{hx}	Heat exchanger area inside the ice storage (m²)
A_{unc}	Uncovered collector area (m²)
C	Fitting coefficient in Eq.33
c_p	Specific heat at constant pressure (J/kgK)
D	Total energy demand (kWh)
F_{FR}	Removal factor
f_l	Liquid fraction
F_P	Efficiency of the heat exchanger
F_{PP}	Flow factor
h	Specific enthalpy (J/kg)
h_f	Specific enthalpy of fusion (J/kg)
U	Global heat transfer coefficient (W/m^2K)
UA	Area dependent heat transfer coefficient (W/K)
M	Total mass (kg)
M_{ice}	Mass of ice (kg)
$\dot{m}$	Mass flow rate (kg/s)
n	Fitting coefficient in Eq.33
Nu	Nusselt number
$\dot{q}$	Heat per unit volume (W/m^3)
$\dot{q}_v$	Source heat per unit volume (W/m^3)
$\dot{Q}$	Heat (W)
P	Annual electric energy consumption (kWh)
Q	Annual energy heat load (kWh)
Ra	Rayleigh number
t	Time (s)
T	Temperature (^oC) (without subscript refers to water)
V_{ice}	Ice storage volume (m³)
$\vec{v}$	Velocity vector (m/s)
V	Volume (m³)
V_r	Ratio of total ice volume (%)
$V_{r,float}$	Ratio of floating ice volume (%)
y	Vertical coordinate (m)
Δt	Time increment (s)
$\Delta \delta$	Distance increment (m)
α	Heat transfer coefficient (W/m^2K)
λ	Thermal conductivity (W/mK)
ρ	Density (kg/m^3)

Subscripts

a	accumulated
av	averaged
c	Conduction
col	Collector
ext	external or surrounding
f	Fluid (brine)
$float$	Floating
fr	Freeze
hcl	Heat carrier liquid
in	Inlet or internal conditions
$loss$	Referred to heat loss
o	Outlet conditions
p	Plate

r	Ratio
ref	Reference
s	Surface
sk	Sink
hx	Heat exchanger
GFX	Gravity film heat exchanger

Superscripts

o	Value at previous time step
m	Melting
$*$	The asterisk indicates that the heat demands of the buildings are different from the ones defined in Task44/Annex38 (see Section 3.5)

References

Abrahamsson, T., Jonson, S., and Lagerkvist, K.-O. (1981). *Heat from solar energy and air with storage in water and ice, The Bramhult project in Boras: design, building, and performance evaluation of a Swedish solar energy and heat pump system for six detached houses.* Swedish Council for Building Research in Stockholm, Sweden.

Afjei, T. and Wittwer, D. (1995). Yearly utilization model yum wp, holzbenutzerhandbuch mit beispielen. Technical Report INFEL/KRE, Zürich.

Ahbe, S., Braunschweig, A., and Müller-Wenk, R. (1990). *Methodik für Ökobilanzen auf der Basis ökologischer Optimierung.* Schriftenreihe Umwelt. Bundesamt für Umwelt, Wald und Landschaft.

Baehr, H. D. and Stephan, K. (2010). *Heat and mass transfer.* Springer, 7th edition.

Bangerter, H. (1985). *Baukostendaten 1985, Rentenbarwert- und wahre Mittelwertfaktoren.* Band 1.

Cadafalch, J., Carbonell, D., Cónsul, R., and Ruiz, R. (2015). Modelling of storage tanks with immersed heat exchangers. *Solar Energy*, 112:154–162.

Carbonell, D., Cadafalch, J., and Consul, R. (2013). Dynamic modelling of flat plate solar collectors. analysis and validation under thermosyphon conditions. *Solar Energy*, 89:100– 112.

Carbonell, D., Cadafalch, J., Paerish, P., and Consul, R. (2012). Numerical analysis of heat pump models. comparative study between equation-fit and refrigerant cycle based models. In *Proceedings of EuroSun*, Rijeka and Opatija, Croatia. International Solar Energy Society (ISES).

Carbonell, D., Haller, M. Y., Philippen, D., and Frank, E. (2014a). Simulations of combined solar thermal and heat pump systems for domestic hot water and space heating. *Energy Procedia*, 48(0):524 – 534. Proceedings of the 2nd International Conference on Solar Heating and Cooling for Buildings and Industry (SHC 2013).

Carbonell, D., Philippen, D., Granzotto, M., Haller, M. Y., and Frank, E. (2014b). Simulation of combined solar thermal, heat pump, ice storage and waste water heat recovery systems. Design criteria and parametric studies. In *Proceedings of EuroSun*, Aix les Bains, France. International Solar Energy Society (ISES).

Carbonell, D., Philippen, D., Haller, M. Y., and Frank, E. (2015). Mathematical model of an ice storage tank for heating applications based on a de-icing concept. *Solar Energy*, (accepted).

Causi, A. (2014). Simulation und Vergleich von Wärmepumpen-Heizungen welche Erdsonden respektive Eisspeicher und Solarkollektoren als Wärmequellenutzen, Bachelor Thesis, Hochschule für Technik Rapperswil.

Churchill, S. W. (2002). *Free convection around immersed bodies*, pages 2.5.7–1–2.5.7–31. Heat Exchanger Design Handbook, Hewitt G.F., Washington: Hemisphere Publishing Corporation.

Cooper, A. and Usher, J. D. (2002). *Plate heat exchangers*, pages 3.7.5–1. Heat Exchanger Design Handbook, Hewitt G.F., Washington: Hemisphere Publishing Corporation.

Dott, R., Haller, M. Y., Ruschenburg, J., Ochs, F., and Bony, J. (2012). The reference framework for system simulation of the IEA SHC Task44/HPP Annex 38: Part B : Building and space heat load. Technical Report IEA-SHC Task44 Subtask C.

Drees, K. H. and Braun, J. E. (1995). Modeling of area-constrained ice storage tanks. *HVAC&R Research*, 1(2):143–158.

Drück, H. (2007). *Mathematische Modellierung und experimentelle Prüfung von Warmwasserspeichern für Solaranlagen.* PhD Thesis, Aachen, Germany.

Duffie, J. A. and Beckman, W. A. (2006). *Solar Engineering of Thermal Processes.* John Wiley & Sons, 3rd edition.

Egli, M. (1944). *Verfahren zum Betrieb einer Wärmepumpenanlage, Patent Nr. 231449*. Schweizer Patentamt.

EnergieSchweiz. Technical report.

Frischknecht, R. (2005). Methoden der Umweltbewertung technischer Systeme: Ökobilanzen. Technical report, ETH Zürich, Studiengang Umweltnaturwissenschaften.

Frischknecht, R., Steiner, R., and Jungbluth, N. (2009). The Ecological Scarcity Method – Eco-Factors 2006 - A method for impact assessment in LCA. Technical report, Bundesamt für Umwelt BAFU, Bern, Switzerland.

Gfxtechnology (2015). [online] http://gfxtechnology.com/contents.html.

Hadorn, J. C. (2015). *Solar and Heat Pump Systems*. Wiley (in press), 1st edition.

Haller, M. Y. (2012). Intercomparison of system simulation results for the IEA SHC Task44/HPP Annex 38. Technical Report IEA-SHC Task44 Subtask C.

Haller, M. Y., Dott, R., Ruschenburg, J., Ochs, F., and Bony, J. (2012). The reference framework for system simulation of the IEA SHC Task44/HPP Annex 38: Part A : General simulation boundary conditions. Technical Report IEA-SHC Task44 Subtask C.

Haller, M. Y. and Frank., E. (2011). On the potential of using heat from solar thermal collectors for heat pump evaporators. In *Proceedings of Solar World Congress*, Kassel, Germany. International Solar Energy Society (ISES).

Haller, M. Y., Haberl, R., Carbonell, D., Philippen, D., and Frank., E. (2014a). *SOL-HEAP - Solar and Heat Pump Combisystems*. Institut für Solartechnik SPF for Swiss Federal Office of Energy SFOE Research Programme Solar Heat and Heat Storage CH-3003 Bern.

Haller, M. Y., Perers, B., Bales, D., Paavilainen, J., Dalibard, A., Fischer, S., and Bertram, E. (2014b). TRNSYS TYPE 832 - dynamic collector model. unpublished.

Heck, T. (2010). Wärmepumpen. ecoinvent report No. 6-X. Technical report, Paul Scherrer Institut, Swiss Centre for Life Cycle Inventories, Dübendorf (CH).

Hegele, F. (2002). *Verfahren zur Eiserzeugung mit einer Wärmepumpe, insbesondere zur Gebäudeklimatisierung und Kühlung von Lebensmitteln, DE 198 39 867 C2*. Deutsches Patent- und Markenamt.

Heilemann, S., Haupt, M., and Oehr, C. (2013). *Eisspeicher mit verbessertem Wärmetauscher, Offenlegungsschrift DE 10 2012 208 941 A1 2013.12.19*. Deutsches Patent- und Markenamt.

Heinz, A., Lerch, W., Breidler, J., Fink, C., and Wagner, W. (2013). *Wärmerückgewinnung aus Abwasser im Niedrigenergie- und Passivhaus: Potenzial und Konzepte in Kombination mit Solarthermie und Wärmepumpe, WRGpot*. im Auftrag des Bundesministeriums für Verkehr, Innovation und Technologie, Österreich.

Hirsch, H. (2010). *Latentwärmespeicher auf Wasser/Eis-Basis mit horizontaler Wärmeübertragungsfläche*. Bachelor, FH Nordhausen, Germany and Institut für Solartechnik SPF, Switzerland.

Hischier et al. (2010). Implementation of Life Cycle Impact Assessment Methods. ecoinvent report No. 3, v2.2. Technical report, Swiss Centre for Life Cycle Inventories, Dübendorf (CH).

Incropera, F. P., Dewitt, D. P., Bergman, T. L., and Lavine, A. S. (2006). *Fundamentals of Heat and Mass Transfer*. John Wiley & Sons, 6th edition.

IPCC (2007). Climate change 2007 - the physical science basis: Working group 1 contribution to the fifth assessment report of the ipcc. Technical report, Intergovernmental Panel on Climate Change.

ISO 13790:2008 (D). Energy performance of buildings – calculations of energy use for space heating. Standard, European Committee for Standardization, Brüssel, BE.

Jekel, T. B., Mitchell, J. W., and Klein, S. A. (1993). Modeling of ice storage tanks. *ASHRAE Transactions*, 99(1):1016–1024.

Jones, E., Oliphant, T., Peterson, P., et al. (2001). SciPy: Open source scientific tools for Python.

Jungbluth, N. (2007). Sonnenkollektor-Anlagen. ecoinvent report No. 6-XI. Technical report, Swiss Centre for Life Cycle Inventories, Dübendorf (CH).

Klein et al. (2010). Trnsys 17: A transient system simulation program, solar energy laboratory. Technical report, University of Wisconsin, Madison, USA, http://sel.me.wisc.edu/trnsys.

Kleinbach, E. M., Beckman, W. A., and Klein, S. A. (1993). Performance study of one-dimensional models for stratified thermal storage tanks. *Solar Energy*, 50(2):155 – 166.

Leconte, A., Chèze, D., and Jobard, X. (2014). TYPE 5897 - ISO building model, model description. unpublished.

Lee, A. H. W. and Jones, J. W. (1996). Modeling of an ice-on-coil thermal energy storage system. *Energy Conversion and Management*, 37(10):1493–1507.

Logie, W. R. and Frank, E. (2013). A transient immersed coil heat exchanger model. *Journal of Solar Energy Engineering*, 135:041006.

Lovvorn, N. C. (2001). Reliability and lifetime of residential heat pumps. In *Proceedings of Joint HPC and IPUHPC Workshop "Hands-On Experience with Heat Pumps for Buildings"*.

Malenkovic, I., Eicher, S., and Bony, J. (2012). *Definition of main system boundaries and performance figures for reporting on SHP systems*. IEA-SHC Task44 Subtask B.

Mehling, H. and Cabeza, L. (2008). *Heat and cold storage with PCM: an up to date introduction into basics and applications*. Berlin Heidelberg: Springer-Verlag.

MeteoSchweiz (2015). Bundesamt für Meteorologie und Klimatologie, Klima-Normwerte, [online] http://www.meteoschweiz.admin.ch/home/klima/vergangenheit/klimanormwerte/normwert-karten.html#temp;8110;yy.

METEOTEST (2012). Meteonorm - global meteorological database for engineers, planners and education.

Minder, S., Wagner, R., Mühlebach, M., and Weisskopf, T. (2014). *Eisspeicher-Wärmepumpen-Anlagen mit Sonnenkollektoren, Technologiestudie*, volume Schlussbericht 15. September 2014.

Morgan, V. T. (1975). The overall convective heat transfer from smooth circular cylinders. In *Advances in Heat Transfer*, volume 11, pages 199–264, New York. Academic Press Inc.

Newton, B. J., Schmid, M., Michell, J. W., and Beckman, W. A. (1995). Storage tank models. In *Proceedings of ASME/JSME International Solar Energy Conference*, volume 2, pages 1111–1116, Maui, Hawai. American Society of Mechanical Engineers.

Paerisch, P., Mercker, O., Warmuth, J., Tepe, R., Bertram, E., and Rockendorf, G. (2014). Investigations and model validation of a ground-coupled heat pump for the combination with solar collectors. *Applied Thermal Engineering*, 62:375–381.

Patankar, S. V. (1980). *Numerical heat transfer and fluid flow*. Hemisphere publishing corporation.

Perers, B. and Bales, C. (2002). A Solar Collector Model for TRNSYS Simulation and System Testing. Technical Report IEA-SHC Task26 Subtask B, www.iea-shc.org/task26.

Pfäffli, K. and Preisig, H. (2011a). SIA-Effizienzpfad Energie. Technical Report Schweizerischer Ingenieur- und Architektenverein, Merkblatt 2040.

Pfäffli, K. and Preisig, H. (2011b). SIA-Effizienzpfad Energie, Ergänzungen und Fallbeispiele zum Merkblatt SIA 2040. Technical Report Schweizerischer Ingenieur- und Architektenverein, Dokumentation 0236.

Philippen, D., Carbonell, D., Haller, M. Y., Frank, E., and Brunold, S. (2014). Auslegung und Betrieb einer hocheffizienten Solarthermie-Wärmepumpen-Heizung mit Eisspeicher. In *24. OTTI Symposium Thermische Solarenergie*, Kloster Banz, Germany.

Philippen, D., Haller, M. Y., Logie, W., Thalmann, M., Brunold, S., and Frank, E. (2012). Development of a heat exchanger that can be de-iced for the use in ice stores in solar thermal heat pump systems. In *Proceedings of EuroSun*, Rijeka and Opatija, Croatia. International Solar Energy Society (ISES).

Pré Consultants (2014). SimaPro Database Manual Methods Library, version 2.7. Technical report, Pré Consultants, Amersfoort (NL).

Pré Consultants (2014). Simapro lca software version 8. Technical report, Pré Consultants, Amersfoort (NL).

Ruschenburg, J., Herkel, S., and Henning, H.-M. (2013). A statistical analysis on market-available solar thermal heat pump systems. *Solar Energy*, 95:79–89.

Schrammel, D. (1986). *Vefahren zm Ablösen des Eisansatzes beim Abtauen eines Wärmetauschers einer Wärmepumpenanlage, DE 2637784 C2*. Deutsches Patent- und Markenamt.

Senghas, W. (2015). *Energiespeichersystem mit einem Eisspeicher, DE 10 2013 213 823 A1*. Deutsches Patent- und Markenamt.

Stucki, M. and Jungbluth, N. (2010). Update of the Life Cycle Inventories of Solar Collectors. Technical report, ESU-services Ltd., Uster (CH).

Treyer, K. and Bauer, C. (2014). Life cycle inventories of electricity generation and power supply in version 3 of the ecoinvent database—part ii: electricity markets. *The International Journal of Life Cycle Assessment*, pages 1–14.

Trinkl, C., Zörner, W., and Hanby, V. (2009). Simulation study on a domestic Solar/Heat pump heating system incorporating latent and stratified thermal storage. *Journal of Solar Energy Engineering*, 131:041008.

van Velsen, S. and Benz, M. (2013). Waermerueckgewinnung aus Schmutzwasser, Vorabklaerung bezueglich des Potentials der Waermerueckgewinnung aus Schmutzwasser im Gebaeude respektive auf dem Grundstueck. Technical report.

VDI (2012). *VDI-Richtlinie, Economic efficiency of building installations, Fundamentals and economic calculation, Part 1*.

VDI-Wärmeatlas (2006). *VDI - Wärmeatlas, 10. Auflage 2006*, chapter Od2.

Weidema, B. P., Bauer, C., Hischier, R., Mutel, C., Nemecek, T., Reinhard, J., Vadenbo, C. O., and Wernet, G. (2013). Overview and Methodology, Data quality guidline for the ecoinvent database version 3. Technical report, Swiss Centre for Life Cycle Inventories, St. Gallen (CH).

Winteler, C., Dott, R., Afjei, T., and Hafner, B. (2014). Seasonal performance of a combined solar, heat pump and latent heat storage system. *Energy Procedia*, 48(0):689–700. Proceedings of the 2nd International Conference on Solar Heating and Cooling for Buildings and Industry (SHC 2013).

Publications

Conference proceedings

- Carbonell, D., Philippen, D., Haller, M., and Frank, E. (2014d). Development and validation of a mathematical model for ice storages with heat exchangers that can be de-iced. *Energy Procedia*, 57(0):2342 – 2351. 2013 ISES Solar World Congress.

- Carbonell, D., Haller, M. Y., Philippen, D., and Frank, E. (2014b). Simulations of combined solar thermal and heat pump systems for domestic hot water and space heating. *Energy Procedia*, 48(0):524 – 534. Proceedings of the 2nd International Conference on Solar Heating and Cooling for Buildings and Industry (SHC 2013).

- Carbonell, D., Philippen, D., Granzotto, M., Haller, M. Y., and Frank, E. (2014c). Simulation of combined solar thermal, heat pump, ice storage and waste water heat recovery systems. Design criteria and parametric studies. In *Proceedings of EuroSun*, Aix les Bains, France. International Solar Energy Society (ISES).

- Granzotto, M., Philippen, D., Carbonell, D., Haller, M. Y., and Brunold, S. (2015). Entwicklung eines mechanisch enteisbaren Wärmetauschers für den Einsatz in Eisspeichern. In *Proceedings of OTTI-Anwenderforum Thermische Energiespeicher*, Neumarkt i.d.O., Germany.

- Philippen, D., Zenhäusern, D., Carbonell, D., Granzotto, M., Haller, M. Y., and Brunold, S. (2015). Systemauslegung und Ökobilanzierung von Solarthermie-Wärmepumpen-Heizungen mit Eisspeichern und Abwasser-Wärmerückgewinnung. In *25. OTTI Symposium Thermische Solarenergie*, Bad Staffelstein, Germany.

Journal paper with contributions from this project

- Carbonell, D., Philippen, D., Haller, M. Y., and Frank, E. (2015). Mathematical model of an ice storage tank for heating applications based on a de-icing concept. *Solar Energy*, (accepted).

Student works

- Sebastian Sommer (2013). Development of an elastic heat exchanger for ice storages. Scientific project. SPF, Rapperswil

- Arian Causi (2014). Simulation und Vergleich von Wärmepumpen-Heizungen welche Erdsonden respektive Eisspeicher und Solarkollektoren als Wärmequelle nutzen. Bachelor thesis. SPF, Rapperswil

- Harini Murali (2014). Influence of Weather Data on a Combined Solar Thermal System with Heat Pump and Ice Storage. Scientific project. SPF, Rapperswil

A. Cost functions for solar-ice systems

Ice storage	Variation A: Prefabricated-concrete casing		
	Excavation	4.53	$m^3_{Ground}/m^3_{StorageWater}$
	Casing (prefabricated concrete)	275	$Fr./m^3_{StorageWater}$
	Variation B: Cast-in-place casing		
	Excavation	7.56	$m^3_{Ground}/m^3_{StorageWater}$
	Casing (cast in place)	610	$Fr./m^3_{StorageWater}$
	Variation C: glassfibre-reinforced plastic		
	Excavation	4.57	$m^3_{Ground}/m^3_{StorageWater}$
	Casing (prefabricated concrete)	340	$Fr./m^3_{StorageWater}$
	Excavation costs	50	$Fr./m^3_{Ground}$
	Manhole	2000	$Fr.$
	Insulation ice storage	29	$Fr./m^2_{TotalSurfaceArea}$
	Wall heat exchanger (optional)	233	$Fr./m^2$
	De-iceable heat exchanger (fix)	173	$Fr./Hx$
	De-iceable heat exchanger (variabel)	187	$Fr./m^2$
	Mounting hx in ice storage	80	$Fr./hx$
	Core holes etc.	2000	$Fr./Storage$
	Piping:	3	$m_{Pipe}/m_{StorageLength}$
		2	$m_{Pipe}/m_{StorageHeight}$
		1	$m_{Pipe}/m_{StorageWidth}$
		10	$m_{Pipe}/ConnectionCellar$
		86	$Fr./m_{pipe}$
Collectors	Uncovered collector	566	$Fr./m^2_{Absorber}$
	Covered collector	691	$Fr./m^2_{Absorber}$
	Mounting (piping, fluid, work)	240	$Fr./m^2_{Absorber}$
	Insulation pipes	60	$Fr./m^2_{Absorber}$
	Hydraulic in Cellar for Solar	80	$Fr./m^2_{Absorber}$
	Scaffold	2000	$Fr.$
Heatpump	HP fixed costs	6500	Fr./Heatpump
	HP variable costs	234	$Fr./kW_{NominalPowerHP}$
	Hydraulics fixed costs	3122	$Fr./Heatpump$
	Hydraulics variabel costs	173	$Fr./kW_{NominalPowerHP}$
	Insulation pipes	1500	Fr./Heatpump
Combi Storage	Fixed costs	5760	Fr./Storage
	Variable costs	770	$Fr./m^3_{Storagevolume}$
	Mounting	300	$Fr./m^3_{Storagevolume}$
	Insulation pipes	500	Fr./Storage
Electrician	Electrical installations	4000	Fr./System
Waste water heat recovery	Waste water tank (fix)	3982	Fr./Storage
	Waste water tank (variable)	39	Fr./Liter
	Waste water tank (mounting)	1000	Fr./Storage
	GFX (fix)	400	Fr./GFX
	GFX (variable)	3000	Fr./m
	GFX (mounting)	1000	Fr./GFX
	Coil-in-PCM		

B. LCI data tables for different system components

This section contains tables summarizing the inventory data related to the production and disposal of different components of the solar-ice system. For the scalable components, the numbers are valid for the component sizes indicated in the first line of the table. The last row of the tables indicated the unit, "p" standing for "piece" and "tkm" for "ton*km". We use the abbreviation "lt" for "lifetime". "hcl" for "heat carrier liquid" and "wwhr" for "waste water heat recovery".

Table B.1: Infrastructure - ice storage - casing

Ice storage 20 m^3 - Casing		p
INPUT		
Basic materials:		
Concrete site-cast (with CEM II/B, 250 kg/m3)	8.8	m3
Reinforcing steel	684	kg
Stainless steel	8.2	kg
Aluminium	7.6	kg
Extruded Polystyrene (XPS)	135	kg
Processes:		
Excavation	265.9	m3
Transport:		
Lorry 16-32t	1293	tkm
OUTPUT		
Final disposal:		
Concrete to final disposal	5	%
XPS to municipal incineration	100	%
Recycling:		
Concrete	95	%
Reinforcing steel	100	%
Stainless steel	100	%
Aluminium	100	%

Table B.2: Infrastructure - ice storage - heat exchanger

Ice storage - Heat exchanger (surface 2.1 m^2)		p
INPUT		
Basic materials:		
Stainless steel	10.9	kg
Propylene glycol	$1 \cdot \dfrac{\text{lt}_{\text{ice stor.}}}{\text{lt}_{\text{hcl}}}$	kg
Water, completely softened	$1.9 \cdot \dfrac{\text{lt}_{\text{ice stor.}}}{\text{lt}_{\text{hcl}}}$	kg
Processes:		
Sheet rolling, stainless steel	10.3	kg
Welding, stainless steel	5.4	m
Section bar rolling, stainless steel	0.6	kg
OUTPUT		
Final disposal:		
Heat carrier liquid to waste water treatment	100	%
Recycling:		
Stainless steel	100	%

Table B.3: Infrastructure - ice storage - piping

Ice storage - Piping (storage size 20 m^3, hx surface 8 · 2.1 m^2)		p
INPUT		
Basic materials:		
Stainless steel pipes	6.8	kg
Polypropylene	5	kg
PU/PIR	4.5	kg
PVC sheet	0.4	kg
Propylene glycol	$12.9 \cdot \frac{\text{lt}_{\text{ice stor.}}}{\text{lt}_{\text{hcl}}}$	kg
Water, completely softened	$25.2 \cdot \frac{\text{lt}_{\text{ice stor.}}}{\text{lt}_{\text{hcl}}}$	kg
Processes:		
Extrusion, plastic pipes	5	kg
OUTPUT		
Final disposal:		
Polypropylene to municipal incineration	100	%
PU/PIR to municipal incineration	100	%
PVC sheet to municipal incineration	100	%
Heat carrier liquid to waste water treatment	100	%
Recycling:		
Stainless steel	100	%

Table B.4: Infrastructure - uncovered collector 2.03 m^2

Uncovered collector		p
INPUT		
Basic materials:		
Stainless steel	19.9	kg
Aluminium	4.5	kg
Glass fibre reinforced plastic (FRP)	5.8	kg
Selective coating, black chrome	2	m2
Propylene glycol	$1.9 \cdot \frac{\text{lt}_{\text{collector}}}{\text{lt}_{\text{hcl}}}$	kg
Water, completely softened	$3.7 \cdot \frac{\text{lt}_{\text{collector}}}{\text{lt}_{\text{hcl}}}$	kg
Processes:		
Sheet rolling, stainless steel	19.9	kg
Welding, stainless steel	6.4	m
Section bar extrusion, aluminium	4.5	kg
OUTPUT		
Final disposal:		
Plastic part of FRP to municipal incineration	100	%
Heat carrier liquid to waste water treatment	100	%
Recycling:		
Stainless steel	100	%
Aluminium	100	%
Fibre part of FRP	100	%

Table B.5: Infrastructure - solar thermal system 20 m2 covered collectors

Solar thermal system 20 m^2 covered collectors		p
INPUT		
Components:		
Covered collector	20	m2
Uncovered collector	0	p
Heat storage tank 1500 l	1	p
Circulating pump 20 · 1.5 W	$1 \cdot \frac{\mathrm{lt_{solar\,th.\,system}}}{\mathrm{lt_{pump}}}$	p
Expansion vessel 20 · 4 l	1	p
Basic materials:		
Stainless steel pipes	13.2	kg
Aluminium	14	kg
PU/PIR	4.3	kg
PVC sheet	1	kg
Propylene glycol	$7.9 \cdot \frac{\mathrm{lt_{solar\,th.\,system}}}{\mathrm{lt_{hcl}}}$	kg
Water, completely softened	$15.4 \cdot \frac{\mathrm{lt_{solar\,th.\,system}}}{\mathrm{lt_{hcl}}}$	kg
Processes:		
Sheet rolling, aluminium	14	kg
OUTPUT		
Final disposal:		
PU/PIR to municipal incineration	100	%
PVC sheet to municipal incineration	100	%
Heat carrier liquid to waste water treatment	100	%
Recycling:		
Stainless steel	100	%
Aluminium	100	%

Table B.6: Infrastructure - waste water storage 130 liter

Waste water storage 130 l		p
INPUT		
Basic materials:		
Stainless steel pipes	26.6	kg
Polyethylene	24.5	kg
Propylene glycol	$2.4 \cdot \frac{\mathrm{lt_{wwhr}}}{\mathrm{lt_{hcl}}}$	kg
Water, completely softened	$4.6 \cdot \frac{\mathrm{lt_{wwhr}}}{\mathrm{lt_{hcl}}}$	kg
Processes:		
Stetch blow moulding	24.5	kg
OUTPUT		
Final disposal:		
Polyethylene to municipal incineration	100	%
Heat carrier liquid to waste water treatment	100	%
Recycling:		
Stainless steel	100	%

Table B.7: Heat - solar-ice system

Heat - solar-ice system		MJ
INPUT		
Infrastructure:		
Ice storage - Casing	$1/(\mathrm{lt_{ice\,stor.}} \cdot \mathrm{heat_{year}})$	p
Ice storage - Heat exchanger	# heat exchangers$/(\mathrm{lt_{ice\,stor.}} \cdot \mathrm{heat_{year}})$	p
Ice storage - Piping	$1/(\mathrm{lt_{ice\,stor.}} \cdot \mathrm{heat_{year}})$	p
Heat pump, brine-water, 8 kW, incl. circulating pumps	$1/(\mathrm{lt_{hp}} \cdot \mathrm{heat_{year}})$	p
Solar thermal system	$1/(\mathrm{lt_{solar\,th.\,system}} \cdot \mathrm{heat_{year}})$	p
Waste heat recovery device 130 l	$(1 \text{ or } 0)/(\mathrm{lt_{wwhr}} \cdot \mathrm{heat_{year}})$	p
Use:		
Electricity, low voltage, CH grid	$1/\mathrm{SPF}$	MJ
Refrigerant, R134a	2.5E-6	kg
Maintenance transport, van < 3.5 t	$175/(5 \cdot \mathrm{heat_{year}})$	tkm
OUTPUT		
Refrigerant, R134a	2.5E-6	kg